

## REVIEW ARTICLE

# Design and development of photoanodes for water-splitting dye-sensitized photoelectrochemical cells†

Cite this: *Chem. Soc. Rev.*, 2013, **42**, 2357

John R. Swierk and Thomas E. Mallouk\*

Dye sensitized solar cells (DSSCs) use low-cost materials, feature tunable molecular sensitizers, and exhibit quantum efficiencies near unity. These advantageous features can be exploited in the context of solar water splitting by functionalizing DSSCs with catalysts for water oxidation and reduction. This article will cover the development of photoanodes for water splitting DSSCs from the perspective of water oxidation catalysts, sensitizers, electron transfer mediators, photoanode materials, and system level design. Within each section we will endeavor to highlight critical design elements and how they can affect the efficiency of the overall system.

Received 8th July 2012

DOI: 10.1039/c2cs35246j

[www.rsc.org/csr](http://www.rsc.org/csr)

## 1. Introduction

Dihydrogen, the smallest and simplest molecule, plays an increasingly important role in the global energy economy. In 2010, over 40 million tons of hydrogen were produced globally, the vast majority used in the production of petrochemicals and ammonia.<sup>1</sup> Beyond these industrial applications, the demand for hydrogen is expected to rise as it finds greater use as an energy carrier. Unlike hydrocarbons, hydrogen gas produces only water as a combustion product and can readily run any system currently using natural gas. The stored chemical energy in hydrogen can be efficiently converted to electricity

by air-breathing fuel cells.<sup>2</sup> In applications that require carbon-based fuels, hydrogen can be used to form methane *via* the Sabatier reaction, combined with carbon monoxide to make hydrocarbon fuels by the Fischer–Tropsch process, catalytically reacted with carbon dioxide to make methanol, or added to liquefied coal to make synthetic gasoline.<sup>3</sup>

Enabling a fuel economy based on hydrogen is however a major challenge. Currently, hydrogen is produced directly from methane or indirectly *via* electrolysis using electricity from non-renewable resources.<sup>1</sup> A more sustainable approach would be to produce hydrogen from renewable energy sources.<sup>4</sup> Of the renewable energy sources, sunlight has enormous potential. Its power density is 1 kW m<sup>-2</sup> on a clear day and the global potential of solar power is approximately 10 000 greater than the current primary power use (16 TW) of the entire world.<sup>4</sup> In

*Department of Chemistry, The Pennsylvania State University, University Park, Pennsylvania 16802, USA. E-mail: tem5@psu.edu*

† Part of the solar fuels themed issue.



John R. Swierk

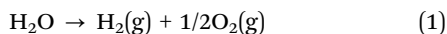
*John R. Swierk received his BS in Chemistry and BSE in Materials Science & Engineering from the University of Pennsylvania. In 2008, he began his PhD at Penn State under the supervision of Professor Thomas E. Mallouk studying electron transfer in water splitting systems.*



Thomas E. Mallouk

*Thomas E. Mallouk received his ScB degree from Brown University (1977) and his PhD in Chemistry from the University of California, Berkeley (1983). He was a postdoctoral fellow at MIT (1983–1985). His research focuses on the synthesis, assembly, and applications of nanoscale inorganic materials.*

this context, hydrogen can be liberated by splitting water into molecular hydrogen and oxygen, either directly by photocatalysis or in a photoelectrochemical process:



The basic thermodynamic requirements for splitting water are modest. It is an uphill reaction, requiring the input of energy, with a Gibbs free energy of  $237.178 \text{ kJ mol}^{-1}$ . Considered as an electrochemical potential, a minimum potential of  $1.229 \text{ V}$  is required at  $298 \text{ K}$ . In principle any wavelength of light shorter than  $1 \mu\text{m}$  has enough energy to split the water molecule, allowing for the use of the entire visible solar spectrum and much of the near-infrared, which together comprise  $\sim 80\%$  of the total solar irradiance.<sup>5</sup>

How well photochemical water splitting transitions to real world systems hinges on how efficiently photons are absorbed and used to form hydrogen. In real systems not all of the solar energy available can be converted into a chemical fuel. Detailed balance calculations can be used to calculate a maximum theoretical efficiency by considering various loss processes. Shockley and Queisser<sup>6</sup> first developed this type of analysis for single junction silicon solar cells with many other authors extending it to multiple junction cells<sup>7</sup> and photochemical processes.<sup>5,8,9</sup> All treatments begin by assuming an ideal absorber, a material with a single bandgap or absorption threshold ( $U_g$ ) that absorbs all photons with energy greater than  $U_g$  and absorbs no photons with energy less than  $U_g$ . As a consequence, some fraction of the solar spectrum with energy less than  $U_g$  is not used by the photochemical system. It is also assumed that excited electrons rapidly lose energy in excess of  $U_g$  by thermalization and relax back to the bandgap or absorption edge. Thus much of the energy from photons with energy greater than  $U_g$  is lost to the system as heat. Considering only these two loss mechanisms would mean that at most an ideal system could convert  $\sim 50\%$  of incident solar energy into a chemical fuel. However a third loss mechanism is introduced because the maximum extractable work from a photovoltaic or photochemical system is always less than  $U_g$ . This is because a sea of electrons in the ground state surrounds each electron in an excited state, creating significant entropy of mixing and introducing an unavoidable thermodynamic loss parameter. Finally, a small fraction of excited states must decay radiatively in order to maintain a high chemical potential. When these loss mechanisms are taken together, a single absorber with  $U_g = 1.59 \text{ eV}$  has a maximum efficiency of  $30.6\%$  under ideal conditions. Multiple absorber systems can exceed this limit, though the theoretical efficiency depends on how many absorbers are used. Realistically attainable efficiencies are well below these theoretical limits due to electron transfer losses, catalyst overpotentials, and reflection losses. Fig. 1 demonstrates how additional processes can contribute to energy loss.

## 2. Water splitting systems

Nature provided an enduring blueprint for photochemical water splitting with the evolution of photosynthesis 2.4–3 billion years

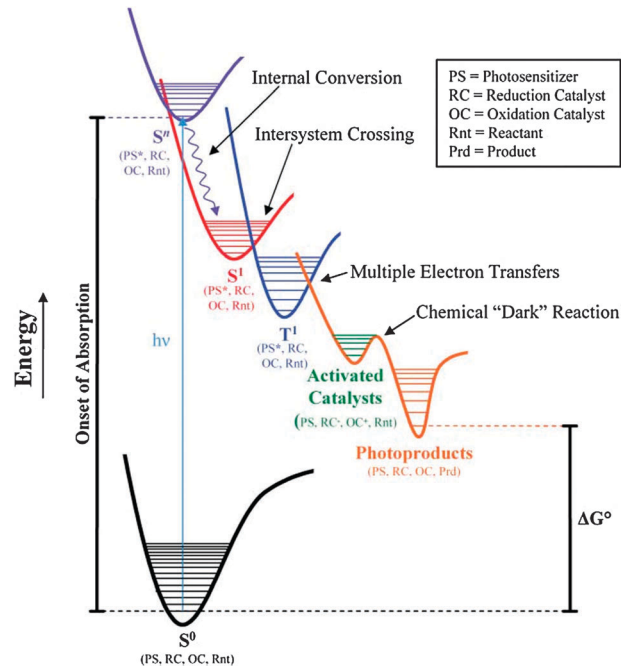


**Fig. 1** Energy diagram demonstrating energy losses in a water splitting system sensitized by a molecular dye. Reproduced from ref. 5 with permission from The Royal Society of Chemistry.

ago.<sup>10</sup> Algae and higher green plants use two coupled photosystems, photosystem II and photosystem I, to absorb light and split water into oxygen and NADPH. Briefly, a series of light harvesting pigments absorb visible light and within one picosecond funnel the excitation energy to a P680 chlorophyll dimer located within the reaction center protein of photosystem II. The excited P680 passes an electron to a nearby pheophytin, a chlorophyll molecule lacking a  $\text{Mg}^{2+}$  ion, which is then followed by rapid electron transfer to a plastoquinone.<sup>11</sup> Within 200 ps, the electron is physically separated from the oxidized  $\text{P680}^+$  by a distance of about  $26 \text{ \AA}$  giving a charge-separated state stable for hundreds of microseconds.<sup>12</sup> A redox active tyrosine group is oxidized by  $\text{P680}^+$  and mediates the rapid charge transfer steps at P680 with the slow oxidation of the oxygen-evolving complex (OEC). At the heart of the OEC lies an oxo-bridged cluster of one calcium and four manganese ions. The OEC accumulates four oxidizing equivalents before releasing oxygen and being regenerated to its reduced resting state.<sup>13</sup> As the OEC is being oxidized, the electrons from P680 leave photosystem II *via* another plastoquinone and cytochrome  $b_6/f$  molecule to make their way to photosystem I. Here another chlorophyll, P700, is excited and oxidized, with electrons being funneled down a charge transfer chain until they are used to reduce  $\text{NADP}^+$  to NADPH. The electrons from photosystem II regenerate the oxidized P700. Overall, two photons are required for every electron transferred (Fig. 2).<sup>14</sup>

Despite all of the exquisite complexity and sophistication of natural photosynthesis, plants are optimized for reproductive success and not efficient energy conversion. For example, P680 and P700 have significant spectral overlap, meaning that a large portion of the usable solar spectrum is wasted. Likewise, plants

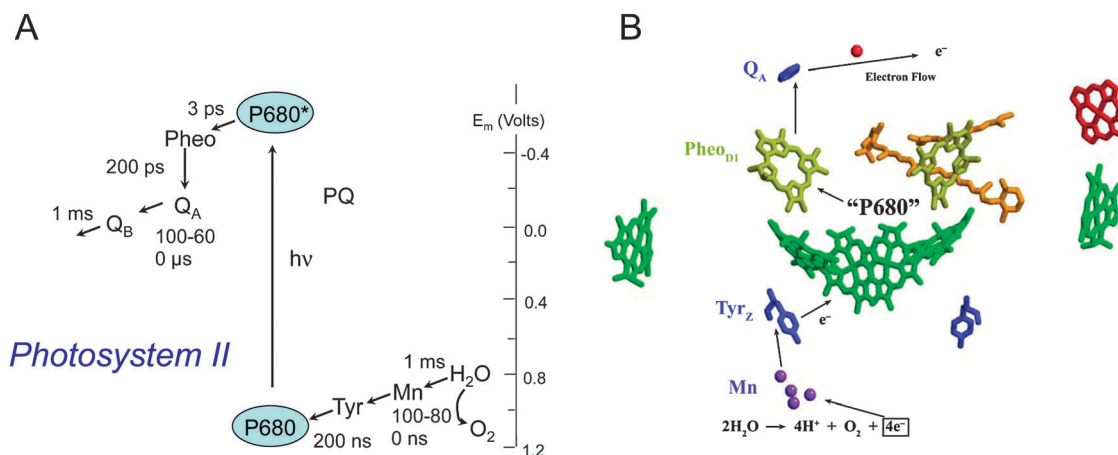


**Fig. 2** (A) Redox potentials with photosystem II reaction center. (B) Photosystem II reaction complex after light excitation with surrounding protein structure removed. Reproduced from ref. 15 with permission from The Royal Society of Chemistry.

absorb more light energy than they are able to process with up to 80% of absorbed energy being discarded.<sup>16</sup> Additionally, photorespiration can be responsible for a loss of up to 25% of the stored energy in plants.<sup>17</sup> These factors limit the overall efficiency of photosynthesis to less than 10% at low light levels, and 1–3% in full sunlight.<sup>18–21</sup> While the natural photosynthetic apparatus provides inspiration for the design of efficient biomimetic systems, plant photosynthesis itself is unlikely to be bioengineered to the level where it can be competitive with other commodity fuel sources (including photovoltaics coupled to electrolyzers).<sup>22</sup> Among the major impediments to such improvement is the mass transport limit of atmospheric  $CO_2$ . Because of the low concentration of  $CO_2$  in the atmosphere (390 ppm), photosynthesis is forced to operate at low concentrations of  $CO_2$ . The equivalent current density that a photosynthetic system can provide in atmospheric  $CO_2$  can be calculated from the large-area, boundary-layer mass-transport limit for atmospheric  $CO_2$  capture (400 tC per ha year).<sup>23</sup> This mass-transport limit translates to an equivalent current density of  $3.7 \text{ mA cm}^{-2}$ , assuming that the reduction of  $CO_2$  to carbohydrates involves four electrons per carbon atom. The free energy stored per mole of carbon is  $-480 \text{ kJ}$  in glucose, a representative carbohydrate product. It follows that the power that can be stored in carbohydrates at the mass transport limit is  $4.6 \text{ mW cm}^{-2}$ , which corresponds to a maximum power conversion efficiency of 4.6% (the power input from the sun being  $\sim 100 \text{ mW cm}^{-2}$ ). However, like any other energy conversion system, photosynthesis cannot operate efficiently at the mass transport limit because of concentration polarization of  $CO_2$ . Some of the stored energy is also needed for respiration in living plants.<sup>24</sup> Considering these loss mechanisms, the  $CO_2$  mass-transport limit corresponds closely to the  $\sim 1$ –3% efficiency of plant photosynthesis in full sun. In contrast, efficient solar energy conversion devices such as crystalline silicon cells, which operate at quantum yields (electrons generated per photon absorbed) near unity, have power conversion efficiencies and current densities that are approximately one order of magnitude higher than photosynthesis. For example, the short-circuit current density at a 24.4% efficient silicon solar cell in full sun

is  $42.0 \text{ mA cm}^{-2}$ .<sup>25</sup> It follows that artificial photosynthetic systems will need to be more like the latter kind of device, ultimately operating near unit quantum efficiency, in order to be competitive with other forms of commodity energy.

The development of artificial photosynthetic systems can roughly be divided into two general approaches, photocatalysis and photoelectrochemical cells (PEC). Any material that can both absorb light and perform water oxidation or reduction can be considered a photocatalyst, though in the context of photochemical water splitting the term is more narrowly applied. Overall water splitting by a photocatalyst typically refers to a photoactive colloidal suspension, which produces hydrogen and oxygen in close proximity to each other. PECs can perform a variety of electrochemical half-reactions, and in regenerative cells (like the DSSC), the anode reaction is simply the reverse of the cathode reaction and the cell generates electricity. Water-splitting PECs are a special case where hydrogen is made at the cathode and oxygen at the anode. These electrodes are physically well separated from each other, in contrast to the situation in photocatalysis. Many of the materials that are used as photocatalysts are also employed as photoelectrodes in PECs. This approach is reminiscent of the compartmentalization of oxygen and NADPH production in natural photosynthesis.

More than 130 inorganic materials have been identified as possible photocatalysts for water splitting.<sup>26</sup> Early work on photocatalysts focused on titanium dioxide and demonstrated the production of hydrogen and oxygen using UV light and a co-catalyst.<sup>27,28</sup> Photocatalysts with enhanced visible light absorption, such as  $BiVO_4$ , produce oxygen photochemically with visible light, but require the use of a sacrificial  $Ag^+$  electron acceptor because the conduction band potential is too positive for hydrogen evolution.<sup>29,30</sup> Overall water splitting using a  $(Ga_{1-x}Zn_x)(N_{1-x}O_x)$  photocatalyst modified with rhodium and chromium mixed oxide was achieved by Domen and co-workers.<sup>31,32</sup> An early version of this system had a quantum yield of 2.5% with 420 nm excitation,<sup>33</sup> which was later improved to 5.9%.<sup>33</sup> In general though, these materials have relatively wide bandgaps and poor absorption characteristics. For example the onset of absorption in

(Ga<sub>1-x</sub>Zn<sub>x</sub>)(N<sub>1-x</sub>O<sub>x</sub>) is 510 nm, and the quantum yield is low due to electron–hole recombination, another problem typical of photocatalytic systems.

The first demonstration of photoelectrochemical water splitting used an oxygen-evolving rutile TiO<sub>2</sub> photoanode and hydrogen evolving platinum cathode.<sup>34</sup> Rutile has a bandgap (3.0 eV) that limits light absorption to the ultraviolet, so the quantum yield of water splitting in sunlight is typically below 2%. Many groups have worked to extend the visible absorption of TiO<sub>2</sub> *via* doping with transition metal<sup>35,36</sup> and main group elements.<sup>37,38</sup> While dopants do increase visible light absorption by introducing localized color centers, or in some cases by shifting the valence and/or conduction band edges, doping also introduces a high density of trap states and can decrease hole mobility leading to increased electron–hole recombination.<sup>39</sup> Other metal oxides such as WO<sub>3</sub>,<sup>40</sup> BiVO<sub>4</sub>,<sup>41</sup> and Fe<sub>2</sub>O<sub>3</sub><sup>42</sup> have also been investigated as possible visible light absorbing photoanodes, but are generally limited to wavelengths shorter than 500 nm, exhibit poor hole transport properties, and require large bias voltages. Some recent work has focused on the development of metal oxide heterostructures as a route to improving the performance of these photoanode materials.<sup>43</sup>

Oxynitrides photoanodes offer an alternative strategy for visible light absorption. Introduction of nitrogen atoms into oxygen sites shifts the valence band edge to more negative potentials through hybridization of N 2p and O 2p orbitals. Domen and co-workers have demonstrated high quantum efficiency (IPCE = ~76% at 400 nm) with TaON based photoanodes, though the application of an external bias and a co-catalyst were required.<sup>44,45</sup> Other oxynitrides such as LaTiO<sub>2</sub>N<sup>46</sup> and SrNbO<sub>2</sub>N<sup>47</sup> have similarly been studied as photoanodes.

An alternative strategy for PECs is to decouple the light absorption and catalytic functions of the electrode. In the simplest form of this concept, a semiconductor photovoltaic is coupled to oxygen- and hydrogen-evolving catalysts. An early demonstration of this approach was photolysis of HBr and HI on a silicon p–n junction coated with aluminum. This system, developed in the 1970's by Texas Instruments, used concentrically doped silicon microspheres. Because of the small size of these spheres, inexpensive metallurgical silicon could be used.<sup>48–50</sup> Bipolar series arrays of TiO<sub>2</sub><sup>51</sup> and CdSe/CoS<sup>52</sup> photoelectrochemical cells were subsequently demonstrated to drive overall water splitting, although in both cases efficiency was low (≤1%). The CdSe/CoS-based array was designed to avoid the well-known stability problem of oxygen-evolving photoanodes based on semiconductors with visible light bandgaps. In the bipolar CdSe/CoS cell, the chalcogenide portion of the cell was in contact with a stabilizing polysulfide solution and prevented from contacting the aqueous side of the cell. Khaselev and Turner<sup>53</sup> later developed a monolithic system with an overall water splitting efficiency of 12.4% by combining an oxidatively unstable GaAs p–n junction with a cathodically protecting p-type GaInP<sub>2</sub> layer connected through a tunnel junction. Licht and co-workers<sup>54</sup> achieved the highest reported water splitting efficiency, 18.3%, by extending this multijunction approach to include as many as 10 components. More recently, arrays of

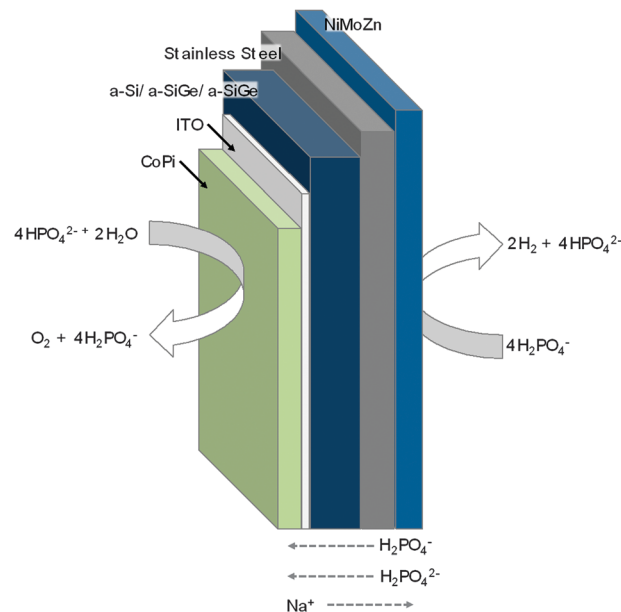


**Fig. 3** Monolithic wireless water splitting device developed by Nocera and co-workers. Migration of anions and cations occurs in the direction shown at the bottom of the figure.

silicon microwires have been used to drive the hydrogen-evolving half cell of a water splitting system,<sup>55,56</sup> although as single-junction devices they lacked the photovoltage needed for unassisted water splitting. Multijunction wires<sup>57</sup> coupled to electrocatalysts could in principle provide a sufficient photovoltage to drive the overall reaction. In related work, Nocera and coworkers<sup>58</sup> recently demonstrated a 4.7% efficient water-splitting PEC by coupling a monolithic three-junction amorphous silicon–germanium photovoltaic cell to a cobalt phosphate oxygen evolving catalyst and a Ni–Zn–Mo hydrogen evolving catalyst (Fig. 3). This system is interesting because it uses only abundant elements and because the cathode catalyst, unlike the noble metals used in many water-splitting systems, is relatively insensitive to impurities in the water.

An ideal photoelectrochemical water splitting cell would combine the low cost of terrestrially abundant materials with the high quantum efficiency of a photovoltaic cell. In addition, tunability of the absorption characteristics and the use of multiple absorbers is desirable in order to “evolve” towards a system that can use the solar spectrum efficiently. Dye sensitized solar cells (DSSCs) are made from inexpensive TiO<sub>2</sub> anodes sensitized with visible light absorbing dyes.<sup>59</sup> The latter are tunable by molecular design to cover different parts of the solar spectrum, and tandem arrangements with multiple dyes<sup>60,61</sup> and dyes combined with semiconductor absorbers have been demonstrated.<sup>62–66</sup> The quantum efficiency of DSSCs is near unity for charge injection into the semiconductor electrode.

When employed as photovoltaics, DSSCs use a redox shuttle to complete the photoelectrochemical circuit. If the dye is instead coupled to a water oxidation catalyst, water can serve as an electron source for regenerating the oxidized dye.<sup>67</sup> In this arrangement, the photoanode of the dye cell oxidizes water,

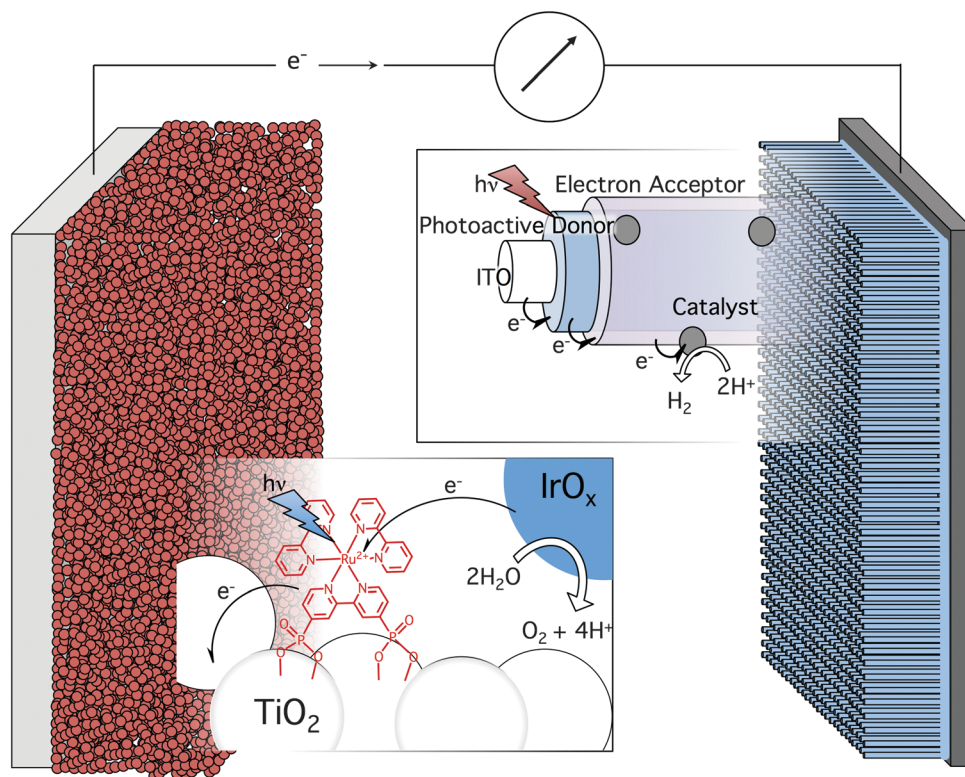


Fig. 4 Scheme of an 8-photon, 4-electron water splitting system.

and proton reduction to hydrogen occurs at that cathode. So far such systems employ only one light absorber and an external bias voltage must be applied because the photovoltage generated by the dye is not sufficient to drive overall water splitting. In principle, these dye-sensitized photoanodes could be coupled to complementary photocathodes to effect water splitting in an eight-photon, four-electron process that is mimetic of the two coupled photosystems in plant photosynthesis. For example, Kaschak *et al.* demonstrated photoinduced electron transfer from a porphyrin to polyviologen electron acceptor using a semiconducting nanosheet to mediate the forward charge transfer.<sup>68</sup> Though not explored in the paper, the potential of the polyviologen is sufficiently negative to drive hydrogen evolution. In principle this system, or one similar, could be grown upon a conductive support to prepare a photocathode. A possible dual absorbing photoelectrochemical cell is sketched in Fig. 4. This review will focus on the recent design and development of the dye-sensitized photoanodes of such water splitting systems.

### 3. Dye-sensitized photoanodes

Dye-sensitized water splitting cells are comprised of four major components: visible light-absorbing sensitizer, water oxidation catalyst (WOC), water reduction catalyst, and semiconductor anode. Electron transfer mediators can be added and choice of pH and buffer must be considered. Here, we will focus on the design of WOCs, sensitizers, mediators, and electrodes and review examples that have been shown to participate in water

oxidation reactions either with sacrificial reagents or under electrochemical/photoelectrochemical conditions. Because the major bottleneck in the design of efficient and durable water splitting cells is the catalytic four-electron oxidation of water, we do not discuss here the rapidly developing science of catalysts and sensitizers for water reduction and refer the interested reader to several recent reviews of that topic<sup>69,70</sup>

#### 3.1 Water oxidation catalysts

An ideal WOC must collect four oxidizing equivalents per oxygen molecule generated, facilitate the formation of dioxygen, and be chemically stable; for practical use over a 20–30 year system life, the catalyst should be active for approximately  $10^9$  cycles or self-repairing. Catalysts are classified as either molecular or particle-based. Molecular WOCs, which are often studied in solution as homogeneous catalysts, can be more readily characterized structurally and are amenable to detailed kinetic/mechanistic studies. These benefits of molecular catalysts come with a price, namely synthetic complexity and often a lack of stability. Conversely, heterogeneous, nanoparticle-based catalysts are simpler to prepare and are more chemically robust, but their structural and mechanistic characterization is more challenging.

The utility of WOCs can be quantified by three parameters: the turnover number (TON), turnover frequency (TOF), and overpotential at the desired TOF. The TON of a catalyst describes how many cycles it is able to cycle through before becoming inactive. TOF is the number of cycles a catalyst undergoes per unit time. Ideally the TOF of the catalyst should

substantially exceed the flux of photons in full sun in order to obtain a high quantum yield. Following the analysis of Frei and Jiao,<sup>71</sup> a lower limit for TOF can be calculated. Integrating the solar photon flux over wavelengths shorter than 1000 nm gives approximately  $4290 \mu\text{E m}^{-2} \text{s}^{-1}$  or  $2600 \text{ photons nm}^{-2} \text{s}^{-1}$ .<sup>5</sup> Assuming a dual absorber system, eight photons must be absorbed for each molecule of oxygen produced. At a catalyst coverage of one site per nanometer squared, this gives a minimum TOF of  $325 \text{ s}^{-1}$ . Complete light absorption by dyes, which usually have extinction coefficients in the range of  $10^4$ – $10^5 \text{ M}^{-1}\text{cm}^{-1}$  ( $\sim 10^{-3}$ – $10^{-2} \text{ cm}^{-2}$  at a coverage of  $1 \times 10^{-10} \text{ mol cm}^{-2}$ ) typically requires porous electrodes with surface areas that are hundreds of times larger than their geometrical area, relaxing the TOF requirement for the dye–catalyst dyad to approximately  $3 \text{ s}^{-1}$ . However, as detailed below, artificial photosynthetic systems generally require very fast electron transfer from the WOC in order to compete with faster back electron transfer processes, so in practice much higher TOFs are needed.

The overpotential is the excess energy per unit charge that must be added to drive the process as the catalyst cycles. In practice this is often measured as the difference between the onset of water oxidation and the formal potential for water oxidation at the pH where the cell is operated. Common overpotentials for WOCs are 0.3 to 0.7 V, though WOCs with lower overpotentials exist.<sup>72</sup> The high overpotential of the four-electron water oxidation reaction is one of the major reasons why real system efficiencies cannot meet theoretical efficiency and much work is being devoted to developing catalysts with lower overpotentials at adequate TOFs.

Rationally designing catalysts with lower overpotentials and TOFs requires understanding the catalytic mechanism and identifying rate limiting steps. Much of the detailed mechanistic work on water oxidation has used homogeneous catalysts. In these systems two mechanisms of oxygen bond formation have been identified: nucleophilic attack of water on a high oxidation state M–O group and O–O bond formation by two catalytic M–O units. In the first mechanism, a water molecule attacks a bound oxygen atom to form a hydroperoxide intermediate. This is the likely mechanism of the OEC in photosystem II. In the second mechanism, two adjacent M–O bonds form a metal peroxo intermediate that then breaks down into M–OH and M–OOH groups by addition of water.<sup>73</sup> Studies of  $\text{TiO}_2$  photocatalysts have identified a mechanism with both features. Water attacks a bridging oxo group to give a surface hydroxyl and an oxygen radical, which then couple to form a peroxo bond between two adjacent Ti atoms. Subsequent water attack forms hydroperoxo and surface hydroxyl groups that then collapse to form dioxygen.<sup>74</sup> A hydroperoxide surface intermediate has also been observed on iridium oxide nanoparticles,<sup>75</sup> suggesting that this species is common to heterogeneous WOCs (Fig. 5).

In both natural and artificial photosynthetic systems, proton coupled electron transfer (PCET) has been identified as part of the multi-electron catalysis cycle. In PCET, the movement of electrons and protons is concerted in a process that has a lower energy barrier than sequential transfer. This process can be understood within the conceptual framework of semi-classical

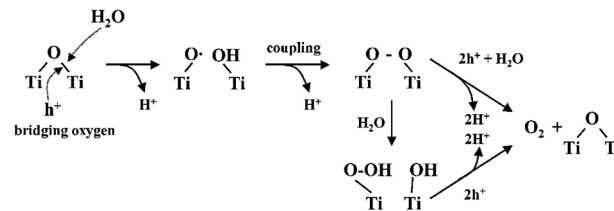


**Fig. 5** Reaction scheme for the photochemical formation of oxygen on  $\text{TiO}_2$ . Reprinted with permission from ref. 74. Copyright 2004 American Chemical Society.

Marcus theory in the limit of weak coupling between the reactant and product potential surfaces. Solvent fluctuations occasionally make the energy of the donor and acceptor states equal, at which point protons and electrons can cross isoenergetically between the reactant and the product potential surfaces. Quantum mechanical tunneling of protons can contribute to the kinetics of PCET.<sup>76</sup> In photosystem II, the redox mediator tyrosine in the OEC uses PCET to simultaneously transfer an electron to  $\text{P680}^+$  and a proton to a nearby histidine residue. This avoids the formation of a charged tyrosine, which is unfavorable in the low dielectric medium of the protein, and thus proton and electron transfer occur together in a single, lower energy step.<sup>77</sup> In mutants that lack the histidine proton acceptor, the quantum yield of water oxidation drops dramatically to zero, illustrating the importance of the PCET mechanism.<sup>78,79</sup> PCET has also been identified in many artificial photosynthetic systems. Because water oxidation catalysts must manage the transfer of four protons and electrons for each molecule of oxygen generated, efficient proton management is a key for a good WOC.<sup>80</sup>

Four types of WOCs have so far been integrated into dye-sensitized photoanodes: molecular catalysts, cubanes, polyoxometalates, and heterogeneous catalysts. As a starting point for comparison across different classes of catalysts, we review TOF, TON, and overpotential data for representative catalysts. Wherever possible we have presented numbers given by the authors but in some instances we have calculated the values from published data. In general, TOF and TON are calculated assuming every metal center is catalytically active. Overpotential is taken at the initial onset of catalytic water oxidation current.

**3.1.1 Molecular water oxidation catalysts.** One attractive feature of the OEC in PSII is its remarkable level of structural organization. Essential amino acid functional groups are precisely arranged around the  $\text{CaMn}_4$  cluster that is the heart of the OEC. A logical starting point for the development of WOCs is a molecular design that finely tunes atomic positions through synthetic chemistry. Many examples of molecular WOCs have been developed,<sup>81–83</sup> of which we will highlight some notable examples.

Meyer and co-workers reported the first molecular WOC in the early 1980s, *cis,cis*- $[\text{Ru}(\text{bpy})_2(\text{H}_2\text{O})]_2(\mu\text{-O})^{4+}$  also known as the blue dimer (Fig. 6, #1 Table 1).<sup>84,85</sup> This catalyst features many of the points common to molecular catalysts. It uses two transition metal atoms connected by a bridging ligand, and exploits polypyridyl chemistry to tune the redox properties of the catalyst as well as to satisfy ruthenium's coordination

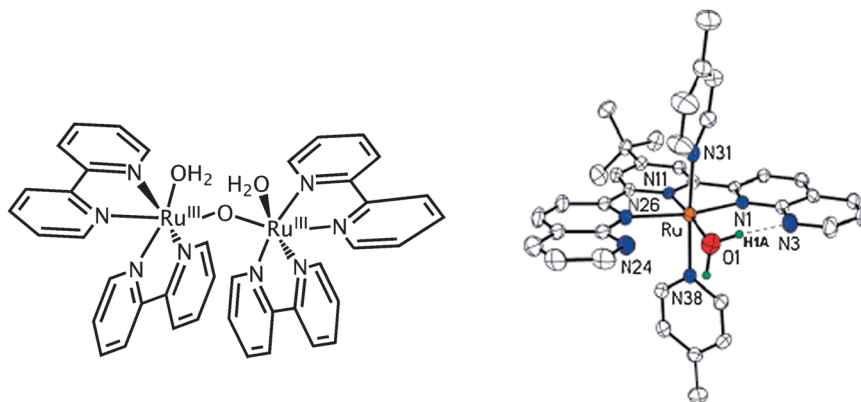


**Fig. 6** (Left) Blue dimer developed by Meyer and co-workers; (Right) single site ruthenium WOC developed by Thummel. Reprinted with permission from ref. 90. Copyright 2005 American Chemical Society.

sphere. The blue dimer has an overpotential of  $\sim 470$  mV, demonstrating the moderate overpotentials typical of ruthenium dimers. Through its easily cleaved bridging oxo group, it also exemplifies a major pitfall of molecular catalysts, instability. With this unstable oxo group, a TON of  $\sim 13$  and TOF of  $0.004 \text{ s}^{-1}$  were obtained.<sup>86,87</sup> If a rigid bridging ligand is used instead of oxygen the TON can surpass 10 000 (#5 Table 1).<sup>88</sup> It is important to note that molecular catalysts are often studied not under photochemical or electrochemical conditions but using a chemical oxidant, such as Ce(IV), to drive the water oxidation reaction. Chemical oxidants avoid the complication of competing forward and back electron transfer pathways as well as direct water oxidation at electrode surfaces. While these reagents simplify the kinetics of water oxidation, the concentration of the oxidant can be significantly higher than in experiments in which the reaction is driven electrochemically or photochemically, leading to artificially high TOFs and TONs. Additionally, sacrificial reagents can generate highly oxidizing species, in some cases in excess of 3.45 V vs. NHE.<sup>89</sup> These species can lead to undesirable side reactions and complicate the overall kinetics.

In parallel with dinuclear catalysts, single-site catalysts have also been developed. Single-site catalysts avoid some of the stability issues encountered with binuclear catalysts, though their ligands are still susceptible to oxidative degradation. Thummel and co-workers developed the first mononuclear ruthenium complexes with high turnover rates as WOCs (Fig. 6).<sup>90</sup> Initially, the ruthenium center is in the +2 oxidation state with a coordination number of 6 and a total electron count of 18. Two oxidizing equivalents increase the oxidation state of ruthenium to +4, leaving the highly electrophilic metal open to attack by water. Two more oxidizing equivalents give a Ru(VI) doubly bound to an oxygen atom. This complex undergoes water nucleophilic attack to produce a peroxo intermediate that then loses a proton to oxygen.<sup>91</sup> An interesting feature of the complex that is reminiscent of the OEC in PSII is hydrogen bonding between a bound water molecule and a free nitrogen atom in the naphthyridine ring, which helps stabilize the complex (Scheme 1).

Single site ruthenium catalysts<sup>92,92</sup> developed by the Meyer group have likewise exploited polypyridyl chemistry to operate

at lower overpotentials than dinuclear catalysts (280–377 mV vs. NHE) and with oxidant-limited TONs (#9–10 Table 1). A single site ruthenium(II) complex was suspended in Nafion and used as a WOC in a dye sensitized PEC (#11 Table 1).<sup>93</sup> A relatively low TON of 16 and TOF of  $27 \text{ h}^{-1}$  were measured for this system at neutral pH. Recently, a single site ruthenium catalyst with a TOF of greater than  $300 \text{ s}^{-1}$  was reported.<sup>94</sup> This TOF was achieved at very high molar concentrations of Ce(IV) and is probably not representative of the catalyst performance under photochemical conditions.

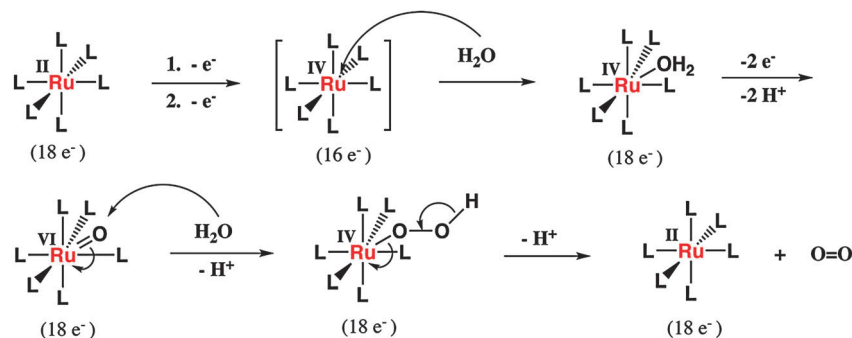
In 2008, a new class of molecular iridium WOCs was introduced. The first of these WOCs, a family of cyclometalated iridium complexes, was synthesized by Bernhard and coworkers (#12 Table 1).<sup>95</sup> These catalysts are synthetically simple, easily tunable, highly soluble in water, and chemically robust due to strong carbon–iridium bonding. An extension of this approach uses electron-donating Cp\* ligands to stabilize high oxidation state Ir centers.<sup>96,97</sup> Of particular relevance to dye sensitized photoanodes, Cp\*–Ir complexes can be functionalized with carboxylic acids and other ligating groups for attachment to metal oxide surfaces.<sup>98</sup>

Some success with molecular manganese WOCs has been achieved. Limburg, Brudvig, and Crabtree<sup>106</sup> prepared Mn complexes with dipicolinate and 2,2':6',2''-terpyridine ligands that generated oxygen when exposed to oxone. It was proposed that these complexes initially formed an oxo-linked dimer before decomposing to form permanganate (Fig. 7). A subsequent study<sup>108</sup> examined the behavior of the terpyridine dimer in sodium hypochlorite and found that a  $\text{Mn}^{\text{V}}=\text{O}$  species was the key intermediate in the formation of oxygen. Stoichiometric oxygen evolution from a  $\text{Mn}^{\text{III}}$  porphyrin dimer was observed by Naruta and co-workers.<sup>109,110</sup> Individually, the  $\text{Mn}^{\text{III}}$  porphyrins were not able to generate oxygen, but when held in a fixed geometry by a 1,2-substituted phenyl ring, oxygen evolution was observed. They also identified a  $\text{Mn}^{\text{V}}=\text{O}$  intermediate and postulated that the O–O bond was formed either by nucleophilic attack on this species or *via* a coupling of two oxo groups. Recently, a tetra-sulfonic acid functionalized  $\text{Mn}^{\text{III}}$  porphyrin was incorporated into a poly(terthiophene) film and demonstrated catalytic behavior

**Table 1** Comparison of selected molecular water oxidation catalysts

Catalyst	Oxidant	TOF (s <sup>-1</sup> )	TON	Overpotential (mV vs. NHE)	Ref.
1 <i>cis,cis</i> -[Ru(bpy) <sub>2</sub> (H <sub>2</sub> O)] <sub>2</sub> (μ-O) <sup>4+</sup>	Ce(IV)	0.004	13	474	84, 85
2 <i>in,in</i> -[(Ru(tpy)(H <sub>2</sub> O)] <sub>2</sub> (μ-bpp) <sup>3+</sup>	Ce(IV)	0.86	512		99
3 <i>trans,trans</i> -[Ru <sub>2</sub> (L1)(4-CH <sub>3</sub> O-py) <sub>4</sub> Cl] <sup>3+</sup>	Ce(IV)	3.8 × 10 <sup>-5</sup>	689		100
4 [Ru <sub>2</sub> (L2)(4-CH <sub>3</sub> -py) <sub>6</sub> ] <sup>1+</sup>	Ce(IV)	0.24	1690	424	101
5 [Ru <sub>2</sub> (L3)(4-CH <sub>3</sub> -py) <sub>4</sub> Cl] <sup>1+</sup>	Ce(IV)	1.2	10 400	330	88
6 [Ru(tpy-PO <sub>3</sub> H <sub>2</sub> )(H <sub>2</sub> O) <sub>2</sub> ] <sup>4+</sup>	1.25–1.5 V vs. Ag/AgCl		1.8	414	102
7 [Ru <sub>2</sub> (OH)(3,6- <sup>t</sup> Bu <sub>2</sub> qui) <sub>2</sub> (btpyan)] <sup>2+</sup>	1.7 V vs. Ag/AgCl	0.232	33 500	405	103
8 <i>trans</i> -[Ru(L4)(4-CH <sub>3</sub> -py) <sub>2</sub> (H <sub>2</sub> O)] <sup>2+</sup>	Ce(IV)	0.0028	260		90
9 [Ru(tpy)(bpm)(OH <sub>2</sub> )] <sup>2+</sup>	Ce(IV)	0.019	7.5	377	92
10 [Ru(Mebimpy)(bpy)(OH <sub>2</sub> )] <sup>2+</sup>	Ce(IV)	0.0067	7.5	280	104
11 Ru(6,6'-dcbpy)(pic) <sub>2</sub>	RuP	0.0069	15	330	105
12 [Ir(ppy) <sub>2</sub> (OH <sub>2</sub> ) <sub>2</sub> ] <sup>+</sup>	Ce(IV)	0.004	2490	185	95
13 Cp*Ir(ppy)Cl	Ce(IV)	0.167	>1500	585	96
14 Cp*Ir(3'-ppy)Cl	ZnCCPP	0.001	0.066	185	98
15 [Mn(dpa) <sub>2</sub> ] <sup>3+</sup>	Oxone	8.3 × 10 <sup>-6</sup>	0.6		106
16 [Mn(tpy)] <sup>3+</sup>	Oxone	0.00014	>50		106
17 [Fe(OTf) <sub>2</sub> (mcp)] <sup>2+</sup>	Ce(IV)/NaIO <sub>4</sub>	0.23	>1050		107

1. bpy = 2,2'-bipyridine; 2. tpy = 2,2':6',2''-terpyridine, bpp = bis(2-pyridyl)-3,5-pyrazolate; 3. L1 = 3,6-bis[6'-(1'',8''-naphthrid-2''-yl)pyrid-2'-yl]-pyridazine, 4-CH<sub>3</sub>O-py = 4-methoxypyridine; 4. L2 = 3,6-bis-(6'-carboxypyrid-2'-yl)-pyridazine, 4-CH<sub>3</sub>-py = 4-methylpyridine, TOF calculated using initial rate of oxygen evolution; 5. L3 = 1,4-bis(6'-COOH-pyrid-2'-yl)phthalazine; 6. tpy-PO<sub>3</sub>H<sub>2</sub> = 4'-phosphonato-2,2':6'',2''-terpyridine; 7. 3,6-<sup>t</sup>Bu<sub>2</sub>qui = 3,6-di-*tert*-butyl-1,2-semiquinone, btpyan = 1,8-bis(2,2':6',2''-terpyridyl)anthracene, TOF represents a lower limit; 8. L4 = 4-*tert*-Butyl-2,6-di([1',8']-naphthrid-2'-yl)pyridine; 9. bpm = 2,2'-bipyrimidine, TOF calculated from initial O<sub>2</sub> evolution rate; 10. Mebimpy = 2,6-bis(1-methylbenimidazol-2-yl)pyridine, TOF calculated from initial O<sub>2</sub> evolution rate; 11. 6,6'-dcbpy = 6,6'-dicarboxylic acid-2,2'-bipyridine, pic = 4-picoline, RuP = [Ru(bpy)<sub>2</sub>(4,4'-diphosphonic acid-2,2'-bipyridine)]<sup>3+</sup> photoelectrochemically generated; 12. ppy = 2-phenylpyridine; 13. Cp\* = pentamethylcyclopentadienyl, TON is number of turnovers in 5.5 hours; 14. 3'-ppy = 3'-carboxy-2-phenylpyridine, ZnCCPP = Zinc 5-(4-carbomethoxyphenyl)-15-(4-carboxyphenyl)-10,20-bis(pentafluorophenyl) photoelectrochemically generated; 15. dpa = dipicolinate; 17. OTf = trifluoromethanesulfonate, mcp = (*N,N'*-dimethyl-*N,N'*-bis(2-pyridylmethyl)-cyclohexane-1,2-diamine).

**Scheme 1** Mechanism for water oxidation by single site ruthenium WOC. Reprinted with permission from ref. 91. Copyright 2008 American Chemical Society.

with an apparently low overpotential at pH = 7 (~90 mV).<sup>111</sup> The authors postulated that catalytic behavior comes from the fraction of porphyrin molecules in the film that are in close enough proximity to mimic the behavior of the Naruta dimer. Detailed reviews on molecular Mn WOCs<sup>112,113</sup> and on the Mn-based<sup>15</sup> OEC in PSII have recently been published.

Tetraamido iron-centered molecular WOCs were recently introduced by Ellis *et al.*<sup>114</sup> Using Ce(IV) as a chemical oxidant, they observed biphasic behavior with an initial rapid release of oxygen, followed by steady oxygen evolution over the course of hours. Building upon those initial findings, Fillol *et al.* studied a series of iron coordination complexes for oxygen evolution activity.<sup>107</sup> When two adjacent, labile sites were present in the catalyst, oxygen evolution was observed. With *trans* sites or a single site, there was no activity. They also proposed a catalytic cycle that involves water nucleophilic attack on an Fe(V) oxo group to give a peroxo intermediate that releases oxygen upon subsequent oxidation.

A molecular cobalt catalyst, [Co<sup>II</sup>(qpy)(OH<sub>2</sub>)<sub>2</sub>]<sup>2+</sup> (qpy = 2,2':6',2'':6'',2''-quaterpyridine), was shown by Leung *et al.* to undergo chemical and photochemical water oxidation at pH > 8 in the presence of [Ru(bpy)<sub>3</sub>]<sup>2+</sup>/S<sub>2</sub>O<sub>8</sub><sup>2-</sup>. The complex exhibited more than 330 turnovers and using [Ru(bpy)<sub>3</sub>]<sup>3+</sup> as a chemical oxidant, a TOF of 4 s<sup>-1</sup>. The onset of water oxidation occurred at an overpotential of ~250 mV.<sup>115</sup>

One of the most advantageous aspects of molecular WOCs is the ability to add specific functionality to the catalyst. Wada *et al.*<sup>103</sup> developed a ruthenium dimer bridged with an anthracene backbone functionalized with two terpyridines to bind the ruthenium atoms (Fig. 8, #7 Table 1). Notably, this catalyst used 3,6-di-*tert*-butyl-1,2-benzoquinone a ligand on the ruthenium to introduce quinone functionality. As the SbF<sub>6</sub> salt, this catalyst could be deposited onto an ITO substrate and catalyze 30 000+ turnovers of water electrolysis at the mildly acidic pH of 4 with a moderate overpotential (~400 mV). The quinones play an active role in the

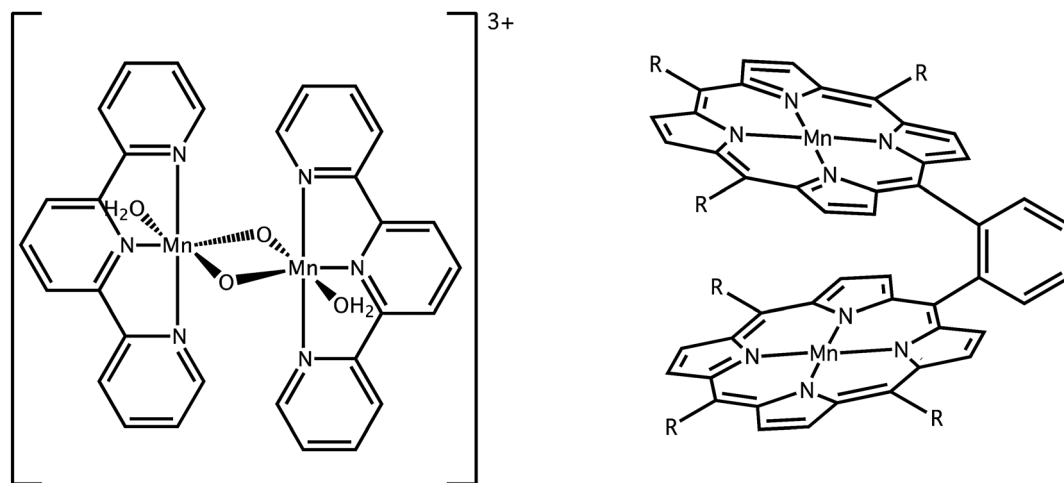


Fig. 7 (Left) Manganese terpyridine dimer introduced by Limburg *et al.*, (Right) Naruta's porphyrin dimer catalyst.

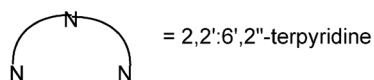
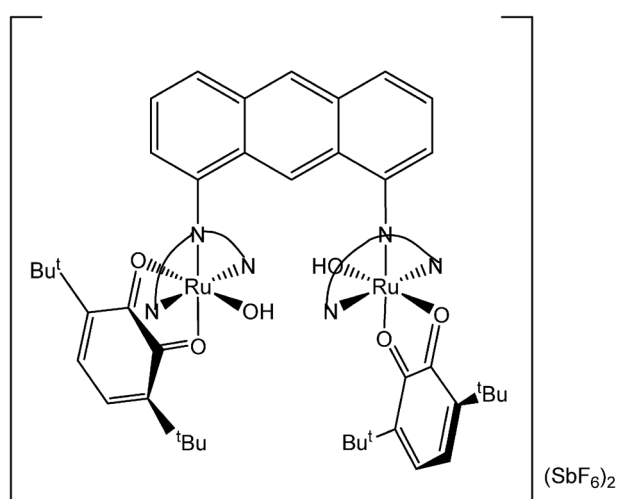


Fig. 8  $[\text{Ru}_2(\text{OH})(3,6\text{-}^t\text{Bu}_2\text{qui})_2(\text{btpyan})](\text{SbF}_6)_2$  where 3,6- $^t\text{Bu}_2\text{qui}$  = 3,6-di-tert-butyl-1,2-semiquinone and btpyan = 1,8-bis(2,2':6',2''-terpyridyl)anthracene.

catalytic cycle, switching between quinone and semiquinone oxidation states, providing a pathway for proton coupled electron transfer, and allowing the ruthenium centers to stay in the low Ru(II)/Ru(III) oxidation states. Interestingly, the monoruthenium analog does not show activity nor does an analog in which the benzoquinone ligand has been replaced with 2,2'-bipyridine. This demonstrates that the ruthenium centers act in concert with the quinone ligands to split water.

Before leaving the topic of molecular WOCs, it is important to note that in the study of these catalysts, care must be taken to identify the active catalytic species. Decomposition of the molecular species to form an active heterogeneous catalyst is a common issue with molecular WOCs.<sup>116–119</sup> A detailed

discussion of the techniques used to identify the active form of the catalyst is beyond the scope of this review, but the interested reader is directed to a detailed review by Widegren and Finke<sup>120</sup> as well as a recent article by Schley *et al.*<sup>121</sup>

**3.1.2 Cubanes.** Over the last decade a class of homogeneous catalysts based on the cuboidal structure of the active  $\text{CaMn}_4$  core in photosystem has been developed. Generally cubanes have the core structure  $[\text{M}_4\text{O}_4]^{6+}$  or  $4+$  with six to eight bidentate ligands helping to hold it together. Dismukes and coworkers first demonstrated gas phase photochemical oxygen evolution from  $\text{Mn}_4\text{O}_4(\text{PPh}_2)_6$  (**1**, Fig. 9) under UV

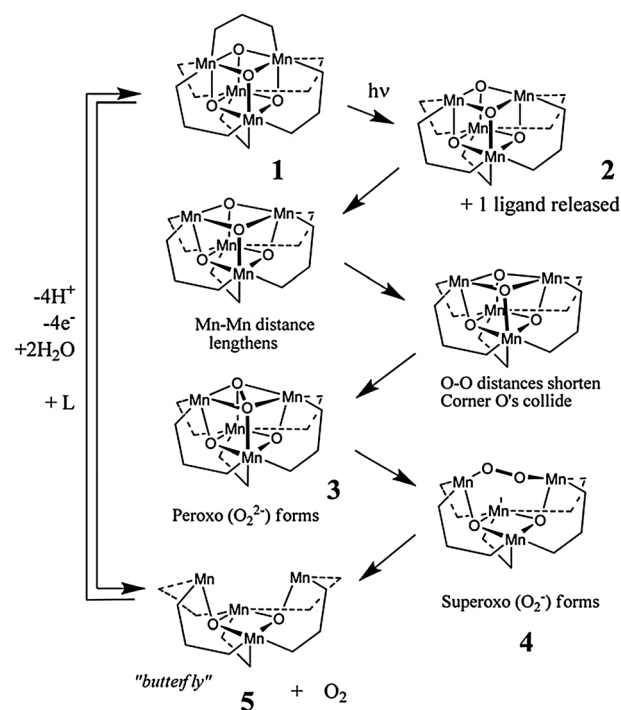


Fig. 9 Mechanism of photochemical  $\text{O}_2$  formation and release ( $\lambda = 350$  nm) in the gas phase. Reproduced from ref. 124 with permission from The Royal Society of Chemistry.

**Table 2** Comparison of cubane catalysts

Catalyst	Oxidant	TOF (s <sup>-1</sup> )	TON	Overpotential (mV vs. NHE)	Ref.
<b>18</b> [Mn <sub>4</sub> O <sub>4</sub> L <sub>6</sub> ] <sup>+</sup>	1 V vs. Ag/AgCl	0.075–0.005	>1000	380	125
<b>19</b> Co <sub>4</sub> O <sub>4</sub> (OAc) <sub>4</sub> (py) <sub>4</sub>	[Ru(bpy) <sub>3</sub> ] <sup>2+</sup> /S <sub>2</sub> O <sub>8</sub> <sup>2-</sup>	0.02	40	332	129

**18.** L = di-(*p*-methoxyphenyl)-phosphine; **19.** OAc = acetate, py = pyridine, TON given after 60 min.

illumination.<sup>122,123</sup> It was proposed that a cationic species, [Mn<sub>4</sub>O<sub>4</sub>(PPh<sub>2</sub>)<sub>5</sub>]<sup>+</sup> (**2**), is initially formed. The flexibility of **2** allows the two manganese atoms on the open face to move apart due to repulsion. As the distance between the two manganese atoms increases, the pair of oxygens bridging between the two are brought into contact. This allows a peroxo species (**3**) to develop as a bond between the two oxygen atoms is formed. Moving from species **2** to **3** is the rate-limiting step in the formation of dioxygen because of the strain introduced in flexing the structure. Following the formation of **3** a superoxo species (**4**) forms, which releases O<sub>2</sub> to give the open “butterfly” (**5**) conformation. *Via* the uptake of two new water molecules and proton coupled electron transfer, **5** is regenerated to the starting state.

Using Nafion as a support, a PEC with Mn<sub>4</sub>O<sub>4</sub>((*p*-OMe-C<sub>6</sub>H<sub>4</sub>)PO<sub>2</sub>)<sub>6</sub> as the WOC was developed and showed sustained water oxidation photocurrent over a period of 10 hours under UV illumination. Based on the total photocurrent, a TON of greater than 1000 turnovers was reported, with TOFs from 0.014 s<sup>-1</sup> to 0.075 s<sup>-1</sup> (Table 2).<sup>125</sup> This approach was extended to use visible light by the addition of ruthenium sensitizer<sup>126</sup> and by coupling to two DSSCs in series.<sup>127</sup> With the Nafion support, water oxidation by the Mn cubane was possible in the condensed solution phase. The authors postulated that the Nafion may have provided a stabilizing, protecting influence on the oxidized cubane. This conclusion was recently challenged by Hocking *et al.*<sup>128</sup> They reported that in the Nafion membrane, the tetramanganese cubane dissociates into Mn(II) compounds, which are then reoxidized to form a mixed(III/IV) disordered heterogeneous phase similar to birnessite.

A novel cobalt cubane, Co<sub>4</sub>O<sub>4</sub>(OCMe)<sub>4</sub>(py)<sub>4</sub> (py = pyridine), was recently reported by McCool *et al.*<sup>129</sup> They observed a TON greater than 40 with a TOF of 0.02 s<sup>-1</sup> at a pH of 7. Working with the same compound, La Ganga *et al.*<sup>130</sup> measured a quantum yield of 30%, though they noted that pH and catalyst concentration played a major role in determining the quantum yield. A recent review detailing the function of the cubane structure in enzymatic, homogeneous, and heterogeneous catalysis is available.<sup>124</sup>

**3.1.3 Polyoxometalates.** Good WOCs must have oxidative, hydrolytic, and thermal stability; which are the major issues for molecular WOCs. Molecular WOCs typically fail on oxidative stability due to the presence of carbon–hydrogen bonds in the ligands. Polyoxometalates (POM) are entirely inorganic and so avoid the problem of carbon-containing bonds. POMs are formed by condensing small oxometalate clusters around templating anions such as SO<sub>4</sub><sup>2-</sup>, SiO<sub>4</sub><sup>4-</sup>, or PO<sub>4</sub><sup>3-</sup>. Most often the oxometalate clusters are vanadates, molybdates, and tungstates. Molybdate and tungstate POMs can incorporate up to hundreds of octahedrally coordinated metal centers whereas

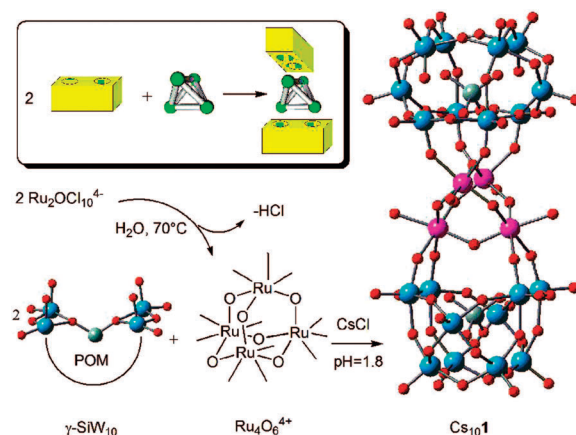


**Fig. 10** Synthesis of Ru<sub>4</sub>SiPOM by metalation of SiW<sub>10</sub> by [Ru<sub>4</sub>O<sub>6</sub>(H<sub>2</sub>O)<sub>*n*</sub>]<sup>4+</sup>. Reprinted with permission from ref. 132. Copyright 2008 American Chemical Society.

vanadate POMs are much smaller, between 4 and 30 vanadium centers, and are structurally more diverse.<sup>131</sup>

Recently much effort been devoted to the development of POMs as WOCs. In 2008, [Ru<sub>4</sub>(μ-O)<sub>4</sub>(μ-OH)<sub>2</sub>(H<sub>2</sub>O)<sub>4</sub>(γ-SiW<sub>10</sub>O<sub>36</sub>)<sub>2</sub>]<sup>10-</sup> (Ru<sub>4</sub>SiPOM) was simultaneously reported by two groups as the Cs<sub>10</sub> salt<sup>132</sup> and Rb<sub>8</sub>K<sub>2</sub> salt.<sup>133</sup> Ru<sub>4</sub>SiPOM is based around a tetraruthenium core that is prepared by *in situ* decomposition of Ru<sub>2</sub>OCl<sub>10</sub><sup>4-</sup> to generate [Ru<sub>4</sub>O<sub>6</sub>(H<sub>2</sub>O)<sub>*n*</sub>]<sup>4+</sup> (Fig. 10).

Catalytic activity for water splitting was initially tested using Ce(IV) as a chemical oxidant. The TON was limited by the amount of oxidant added and over 500 turnovers were demonstrated with no apparent loss of catalytic activity and an O<sub>2</sub> yield of 90%. A maximum TOF of >0.125 s<sup>-1</sup> was observed. Photochemical experiments using [Ru(bpy)<sub>3</sub>]<sup>2+</sup> and S<sub>2</sub>O<sub>8</sub><sup>2-</sup> resulted in persulfate-limited TONs up to 350 and initial an TOF of 0.08 s<sup>-1</sup>.<sup>134</sup> The phosphorous-containing analog [Ru<sub>4</sub>(μ-O)<sub>5</sub>(μ-OH)(H<sub>2</sub>O)<sub>4</sub>(γ-PW<sub>10</sub>O<sub>36</sub>)<sub>2</sub>]<sup>9-</sup> (Ru<sub>4</sub>PPOM) was prepared and the catalytic activity investigated. While Ru<sub>4</sub>PPOM proved capable of oxidizing water, the rate of photodriven water oxidation was approximately 20% lower than with Ru<sub>4</sub>SiPOM.<sup>135</sup> In an effort to integrate Ru<sub>4</sub>SiPOM into a PEC, Ru<sub>4</sub>SiPOM was attached to a TiO<sub>2</sub> nanocrystalline film *via* ruthenium(II) tris(4,4'-dicarboxylic-2,2'-bipyridine).<sup>136</sup> This assembly was investigated spectroscopically and showed that electron transfer between Ru<sub>4</sub>SiPOM and the ruthenium dye was on the order of a few microseconds and competitive with back electron transfer from the TiO<sub>2</sub> electrode. An electrochemical oxygen-evolving electrode prepared from Ru<sub>4</sub>SiPOM attached to multiwalled carbon nanotubes by dendrimers was demonstrated and operated at modest overpotentials ( $\eta = 0.35$  V).<sup>137</sup> Single site ruthenium

POMs  $[\text{Ru}(\text{H}_2\text{O})\text{SiW}_{11}\text{O}_{39}]^{5-}$  and  $[\text{Ru}(\text{H}_2\text{O})\text{GeW}_{11}\text{O}_{39}]^{5-}$  demonstrate catalytic water oxidation when treated with  $\text{Ce}(\text{iv})$ .<sup>138</sup>

A breakthrough in using POMs for water oxidation came with the development of  $[\text{Co}_4(\text{H}_2\text{O})_2(\text{PW}_9\text{O}_{34})_2]^{10-}$  (Co4PPOM)<sup>139,140</sup> and more recently  $[\text{Co}_4(\mu\text{-OH})(\text{H}_2\text{O})_3(\text{SiW}_{19}\text{O}_{70})_2]^{11-}$  (Co4SiPOM),<sup>141</sup>  $[\text{Co}_2\text{Mo}_{10}\text{O}_{38}\text{H}_4]^{6-}$ , and  $[\text{CoMo}_6\text{O}_{24}\text{H}_6]^{3-}$ .<sup>142</sup> These WOCs have the advantage of containing only earth abundant elements, which makes them especially attractive compared to noble metal-containing catalysts. The proposed active WOC in Co4PPOM and possibly in all cobalt polyoxometalates has recently been called into question by Stracke and Finke.<sup>119</sup> Under electrochemical conditions, they determined that Co4PPOM was actually a pre-catalyst for the formation of a heterogeneous  $\text{CoO}_x$  film. This film was examined with a scanning electron microscope and found to have a different morphology than an authentic Co4PPOM film. Furthermore, as the solution was aged for several hours in a pH 8 sodium phosphate buffer, the oxidation current increased indicating the formation of a new species different from Co4PPOM. Finally, the authors noted that cobalt dissociation constants had been measured for other cobalt-containing POMs and that the electrochemical activity of an aged Co4PPOM could be completely accounted for by authentic  $\text{Co}(\text{ii})$  at a level equivalent to the level of leached cobalt. Stracke and Finke do note that Co4PPOM may actually function as a WOC with use of a chemical or photochemical oxidant, but their results suggest more detailed study into the true nature of WOC by cobalt-containing POMs under a variety of conditions is warranted.

The question of heterogeneous *versus* homogeneous catalysis in polyoxometalates is an interesting one. An iridium(III) containing POM,  $\text{IrCl}_4\text{PPOM}$ , demonstrates water oxidation at a rate two orders of magnitude faster than  $\text{IrO}_x \cdot n\text{H}_2\text{O}$ , a known and highly efficient WOC, before hydrolytically breaking down to form  $\text{IrO}_x \cdot n\text{H}_2\text{O}$ .<sup>143</sup> It is an interesting observation that TOFs of Co4PPOM and  $\text{IrCl}_4\text{PPOM}$  are noticeably lower when compared to other WOC POMs (Table 3). The TOF for Co4PPOM is also comparable with other examples of heterogeneous cobalt WOCs discussed in the next section (Table 4). It should be noted that while  $[\text{Ru}(\text{H}_2\text{O})\text{SiW}_{11}\text{O}_{39}]^{5-}$  also exhibits a low TOF, the value of  $0.003 \text{ s}^{-1}$  represents a lower limit since oxygen evolution data was not presented in the paper.

**3.1.4 Heterogeneous metal oxides.** Compared to molecular catalysts, heterogeneous WOCs have the major advantage of being synthetically simple to prepare. Typically heterogeneous WOCs either refer to colloidal suspensions of nanoparticles or electrochemically deposited catalytic films.

The most successful WOCs to date have been based on noble metal oxides, with ruthenium and iridium oxides receiving the most attention. Both oxides have a long history as anode materials in water and chloride electrolyzers.<sup>144–146</sup> These catalysts can access high oxidation states, stabilizing the highly electrophilic intermediates in the water oxidation process.  $\text{RuO}_2$  received a great deal of early attention as a heterogeneous WOC for photocatalysis. Those studies<sup>147–149</sup> identified colloidal  $\text{RuO}_2$  as a WOC that could be driven with a chemical oxidant,  $\text{Ce}(\text{iv})$  or  $[\text{Ru}(\text{bpy})_3]^{3+}$ , or photochemically with  $[\text{Ru}(\text{bpy})_3]^{2+}/\text{S}_2\text{O}_8^{2-}$  or  $[\text{Co}(\text{NH}_3)_5\text{Cl}]^{2+}$ . The major attraction for  $\text{RuO}_2$  is a low overpotential and high TOF. Unfortunately,  $\text{RuO}_2$  also corrodes under oxidizing conditions, which limits its utility. In recent years, work on  $\text{RuO}_2$  as a WOC has slowed, though a recent study of rutile  $\text{RuO}_2$  has suggested that it may be a more active WOC than previously thought.<sup>150</sup> Although it corrodes under anodic conditions, under cathodic conditions it shows better chemical stability and can function as a hydrogen evolution catalyst.<sup>151</sup>

Iridium oxide ( $\text{IrO}_x \cdot n\text{H}_2\text{O}$ ) is unfortunately prepared from the least abundant stable element in the periodic table, but it is so far unparalleled as a WOC across a wide range of pH values. Initially used to catalyze water oxidation by  $\text{Ce}(\text{iv})$  and  $[\text{Ru}(\text{bpy})_3]^{3+}$  by Kiwi and Grätzel,<sup>152</sup> crystalline  $\text{IrO}_2$  and amorphous colloidal  $\text{IrO}_x \cdot n\text{H}_2\text{O}$  were soon found to be highly active WOCs.<sup>153,154</sup>  $\text{IrO}_x \cdot n\text{H}_2\text{O}$  exhibits a low overpotential,  $\sim 200\text{--}300 \text{ mV}$ , for water oxidation and is active over a wide pH range.<sup>155</sup> TOFs for surface atoms in colloidal suspensions of  $\text{IrO}_x \cdot n\text{H}_2\text{O}$  are as high as  $40 \text{ s}^{-1}$ .<sup>156</sup>

Iridium oxide has played a major role in the development of dye-sensitized photoanodes for water oxidation. Our group developed chemistry for capping iridium oxide with dicarboxylate ligands.<sup>156,157</sup> Using this chemistry, colloidal iridium oxide has been covalently coupled to a variety of ruthenium poly(pyridyl) dyes that contain malonate or succinate linkers. Functionalizing the ruthenium dye with both malonate and phosphonate groups allows for adsorption of the dye-  $\text{IrO}_x \cdot n\text{H}_2\text{O}$  dyad to a nanocrystalline  $\text{TiO}_2$

**Table 3** Comparison of polyoxometalates active for water oxidation

Catalyst	Oxidant	TOF ( $\text{s}^{-1}$ )	TON	Overpotential (mV vs. NHE)	Ref.
20 $[\text{Ru}_4(\mu\text{-O})_4(\mu\text{-OH})_2(\text{H}_2\text{O})_4(\gamma\text{-SiW}_{10}\text{O}_{36})_2]^{10-}$	$\text{Ce}(\text{iv})$	0.131	488	246	133, 132
21 $[\text{Ru}_4(\mu\text{-O})_4(\mu\text{-OH})_2(\text{H}_2\text{O})_4(\gamma\text{-SiW}_{10}\text{O}_{36})_2]^{10-}$	$[\text{Ru}(\text{bpy})_3]^{2+}/\text{S}_2\text{O}_8^{2-}$	0.08	35		134
22 $[\text{Ru}_4(\mu\text{-O})_5(\mu\text{-OH})(\text{H}_2\text{O})_4(\gamma\text{-PW}_{10}\text{O}_{36})_2]^{9-}$	$[\text{Ru}(\text{bpy})_3]^{2+}/\text{S}_2\text{O}_8^{2-}$	0.13	120	248	135
23 $[\text{Co}_4(\text{H}_2\text{O})_2(\text{PW}_9\text{O}_{34})_2]^{10-}$	$[\text{Ru}(\text{bpy})_3]^{2+}/\text{S}_2\text{O}_8^{2-}$	0.0013	224	441	140
24 $[\text{Co}_4(\mu\text{-OH})(\text{H}_2\text{O})_3(\text{SiW}_{19}\text{O}_{70})_2]^{11-}$	$[\text{Ru}(\text{bpy})_3]^{2+}/\text{S}_2\text{O}_8^{2-}$	0.1	80		141
25 $[(\text{IrCl}_4)\text{KP}_2\text{W}_{20}\text{O}_{72}]^{14-}$	$[\text{Ru}(\text{bpy})_3]^{3+}$	0.0292	5.25	215	143
26 $[\text{Ru}(\text{H}_2\text{O})\text{SiW}_{11}\text{O}_{39}]^{5-}$	$\text{Ce}(\text{iv})$	0.003	20	188	138
27 $[\text{Co}_2\text{Mo}_{10}\text{O}_{38}\text{H}_4]^{6-}$	$[\text{Ru}(\text{bpy})_3]^{2+}/\text{S}_2\text{O}_8^{2-}$	0.171	154	350	142
28 $[\text{CoMo}_6\text{O}_{24}\text{H}_6]^{3-}$	$[\text{Ru}(\text{bpy})_3]^{2+}/\text{S}_2\text{O}_8^{2-}$	0.119	107	420	142

21. 20 mM pH 7.2 sodium phosphate buffer, turnover number persulfate limited; 22. pH 5.8  $\text{NaSiF}_6$  buffer; 23. 80 mM pH 8 sodium borate buffer; 24. 25 mM sodium borate pH 9 buffer; 25. 20 mM sodium phosphate pH 7.2 buffer, TOF represents a lower limit TOF based on complete reduction of  $\text{Ru}(\text{iii})$  within 3 minutes; 26. 0.1 M  $\text{HNO}_3$ , TOF calculated based on number of turnovers after 20 minutes; 27. and 28. overpotential represents upper limit.

**Table 4** Comparison of heterogeneous WOCs

Catalyst	Oxidant	TOF (s <sup>-1</sup> )	TON	Overpotential (mV vs. NHE)	Ref.
29 RuO <sub>2</sub>	[Ru(bpy) <sub>3</sub> ] <sup>2+</sup> /[Co(NH <sub>3</sub> ) <sub>5</sub> Cl] <sup>2+</sup>	0.052	68	310	148
30 RuO <sub>2</sub> (5 nm)	[Ru(bpy) <sub>3</sub> ] <sup>2+</sup> /S <sub>2</sub> O <sub>8</sub> <sup>2-</sup>	0.0045	19.2	310	149
31 RuO <sub>2</sub> (10 nm)	[Ru(bpy) <sub>3</sub> ] <sup>2+</sup> /S <sub>2</sub> O <sub>8</sub> <sup>2-</sup>	0.089	2.7	310	149
32 rutile RuO <sub>2</sub> (6 ± 2 nm)	1.48 V vs. RHE	≥ 0.000069		280	150
33 IrO <sub>x</sub> · <i>n</i> H <sub>2</sub> O	[Ru(bpy) <sub>3</sub> ] <sup>2+</sup> /S <sub>2</sub> O <sub>8</sub> <sup>2-</sup>	0.0004	3	310	153
34 citrate-IrO <sub>x</sub> · <i>n</i> H <sub>2</sub> O (20 nm)	[Ru(bpy) <sub>3</sub> ] <sup>2+</sup> /S <sub>2</sub> O <sub>8</sub> <sup>2-</sup>	0.05	80	330	156
35 succinate-IrO <sub>x</sub> · <i>n</i> H <sub>2</sub> O	[Ru(bpy) <sub>3</sub> ] <sup>2+</sup> (PF <sub>6</sub> ) <sub>2</sub> /S <sub>2</sub> O <sub>8</sub> <sup>2-</sup>	0.049	28	330	157
36 IrO <sub>x</sub> · <i>n</i> H <sub>2</sub> O	1.4 V vs. Ag/AgCl	4.71		220	176
37 IrO <sub>x</sub> · <i>n</i> H <sub>2</sub> O	1.3 V vs. Ag/AgCl	0.64		330	177
38 Co <sub>3</sub> O <sub>4</sub>	[Ru(bpy) <sub>3</sub> ] <sup>2+</sup> /S <sub>2</sub> O <sub>8</sub> <sup>2-</sup>	0.035		325	158
39 Co <sub>3</sub> O <sub>4</sub>		≥ 0.0025		350	158
40 Co <sub>3</sub> O <sub>4</sub>		≥ 0.020		295	158
41 Co <sub>3</sub> O <sub>4</sub>		≥ 0.0008		414	158
42 Co <sub>3</sub> O <sub>4</sub>		≥ 0.006		235	158
43 SBA-15/Co <sub>3</sub> O <sub>4</sub> (4%)	[Ru(bpy) <sub>3</sub> ] <sup>2+</sup> /S <sub>2</sub> O <sub>8</sub> <sup>2-</sup>	0.01		350	158
44 Co <sub>3</sub> O <sub>4</sub> (5.9 ± 1.1 nm)	0.534 V vs. Ag/AgCl	0.0187		328	159
45 CoPi	1.29 V vs. NHE	≥ 0.0007		410	158
46 MnO <sub>2</sub>		≥ 0.013		440	158
47 Mn <sub>2</sub> O <sub>3</sub>	[Ru(bpy) <sub>3</sub> ] <sup>2+</sup> /S <sub>2</sub> O <sub>8</sub> <sup>2-</sup>	0.055		325	158
48 CaMn <sub>1.6</sub> <sup>IV</sup> Mn <sub>0.4</sub> <sup>III</sup> O <sub>4.5</sub> (OH) <sub>0.5</sub> · <i>z</i> H <sub>2</sub> O	Ce(IV)	0.002			169
49 λ-MnO <sub>2</sub> (~20 nm)	[Ru(bpy) <sub>3</sub> ] <sup>2+</sup> /S <sub>2</sub> O <sub>8</sub> <sup>2-</sup>	3 × 10 <sup>-5</sup>		370	175

electrode. In principle, direct coupling of the sensitizer to the WOC should facilitate rapid electron transfer and enhance efficiency. Actual quantum yields are low due to two factors. First, the covalently attached IrO<sub>x</sub>·*n*H<sub>2</sub>O colloids can rapidly quench the excited state of the dye. Second, multiple sensitizer molecules were bound to each colloidal particle with the result that some of the bound sensitizers were unable to inject into the TiO<sub>2</sub> electrode.

Despite the success of noble metal oxides as WOCs, it would be desirable to develop alternative catalysts based on terrestrially abundant materials. To this end a great deal of recent attention has been paid to cobalt oxide structures as WOCs. Early work on Co<sub>3</sub>O<sub>4</sub> demonstrated TOFs between 0.0008 to 0.035 s<sup>-1</sup> at overpotentials between 235 and 414 mV.<sup>71</sup> Jiao and Frei grew clusters of Co<sub>3</sub>O<sub>4</sub> in the pores of mesoporous silica and observed TOFs of 0.5 s<sup>-1</sup> nm<sup>-2</sup> at an overpotential of 350 mV.<sup>158</sup> A subsequent study established that the smaller the Co<sub>3</sub>O<sub>4</sub> particle, the lower the overpotential and the higher the activity of the catalyst.<sup>159</sup> The dramatic difference between the activity of unsupported and silica-supported Co<sub>3</sub>O<sub>4</sub> may arise from a buffering effect of the support near neutral pH.

Nocera and Kanan reported the anodic deposition of a catalytically active, amorphous cobalt phosphate (CoPi) film on ITO from a solution of Co(II) in neutral potassium phosphate buffer.<sup>161</sup> Subsequent work demonstrated that use of a proton accepting buffer was critical in depositing active, stable films<sup>162</sup> and that the films were self-healing through a cycle of dissolution and re-deposition.<sup>163</sup> Gerken *et al.* extended this work by depositing from a fluoride buffer, allowing the electrodeposited catalyst to function at mildly acidic pHs.<sup>160</sup> They also reported detailed mechanistic studies on water oxidation from pH 0 to 14 (Fig. 11). Above pH 3.5, heterogeneous CoO<sub>x</sub> is the active electrocatalyst. Below pH 3.5, homogeneous catalysis dominates and oxygen is formed *via* a hydrogen peroxide intermediate. Most recently, photoelectrochemical activity was observed with a heterogeneous cobalt aluminophosphate (CoAPO5) photocatalyst doped into a Nafion-coated electrode.<sup>164</sup>

A photocurrent was observed at bias voltages greater than 0.8 V vs. Ag/AgCl.

Keeping with the idea of using abundant first row transition elements as WOCs, heterogeneous Mn WOCs have been studied. MnO<sub>x</sub> was investigated in the 1970's as an anode material for electrochemical water oxidation.<sup>165</sup> A later study identified colloidal MnO<sub>2</sub> as active for water oxidation using [Ru(bpy)<sub>3</sub>]<sup>3+</sup> as a chemical oxidant.<sup>166</sup> Harriman also identified Mn<sub>2</sub>O<sub>3</sub> as one of the more active WOCs within a series of heterogeneous metal oxides.<sup>153</sup> In the past few years there has been a resurgence of interest in manganese oxides as WOCs. Using a strategy previously applied to Co<sub>3</sub>O<sub>4</sub>, Jiao and Frei deposited manganese oxide into the pores of a mesoporous silica support and observed efficient photochemical oxygen evolution.<sup>167</sup> Jiao later examined different polymorphs of nanostructured MnO<sub>2</sub> and observed TOFs on the order of 10<sup>-5</sup> s<sup>-1</sup> per Mn with little difference between crystal structure and morphology.<sup>168</sup> A biomimetic calcium manganese oxide, CaMn<sub>1.6</sub><sup>IV</sup>Mn<sub>0.4</sub><sup>III</sup>O<sub>4.5</sub>(OH)<sub>0.5</sub>·*z*H<sub>2</sub>O, demonstrated water oxidation activity under chemical and photochemical oxidation.<sup>169,170</sup> Though an amorphous material, XAS analysis showed a layered oxide similar to birnessite with disordered cuboidal Mn<sub>3</sub>CaO<sub>4</sub> and Mn<sub>4</sub>O<sub>4</sub> units throughout the layers.<sup>171</sup> As noted above, manganese cubanes form a heterogeneous oxide when supported by nafion.<sup>128</sup> Nanoscale (<50 nm) particles of calcium manganese oxide showed a relatively high TOF (~0.002 s<sup>-1</sup>) using Ce(IV) as a chemical oxidant.<sup>172</sup> Replacement of the Ca(II) with Zn(II) and Al(III) led to efficient oxygen evolution with Ce(IV).<sup>173</sup> Inspired by studies of electrodeposited cobalt oxide films, Zaharieva *et al.* electrodeposited a manganese oxide by voltage cycling.<sup>174</sup> At a potential of 1.35 V vs. NHE at neutral pH, they obtained a TOF comparable to Nocera's cobalt phosphate films (0.01 s<sup>-1</sup> vs. 0.017 s<sup>-1</sup>). Treatment of nanocrystalline LiMn<sub>2</sub>O<sub>4</sub> with nitric acid delithiates the material while leaving the λ-MnO<sub>2</sub> spinel structure intact.<sup>175</sup> The delithiated spinel structure is cuboidal with open sites for water oxidation at the lithium vacancies. Oxygen evolution was

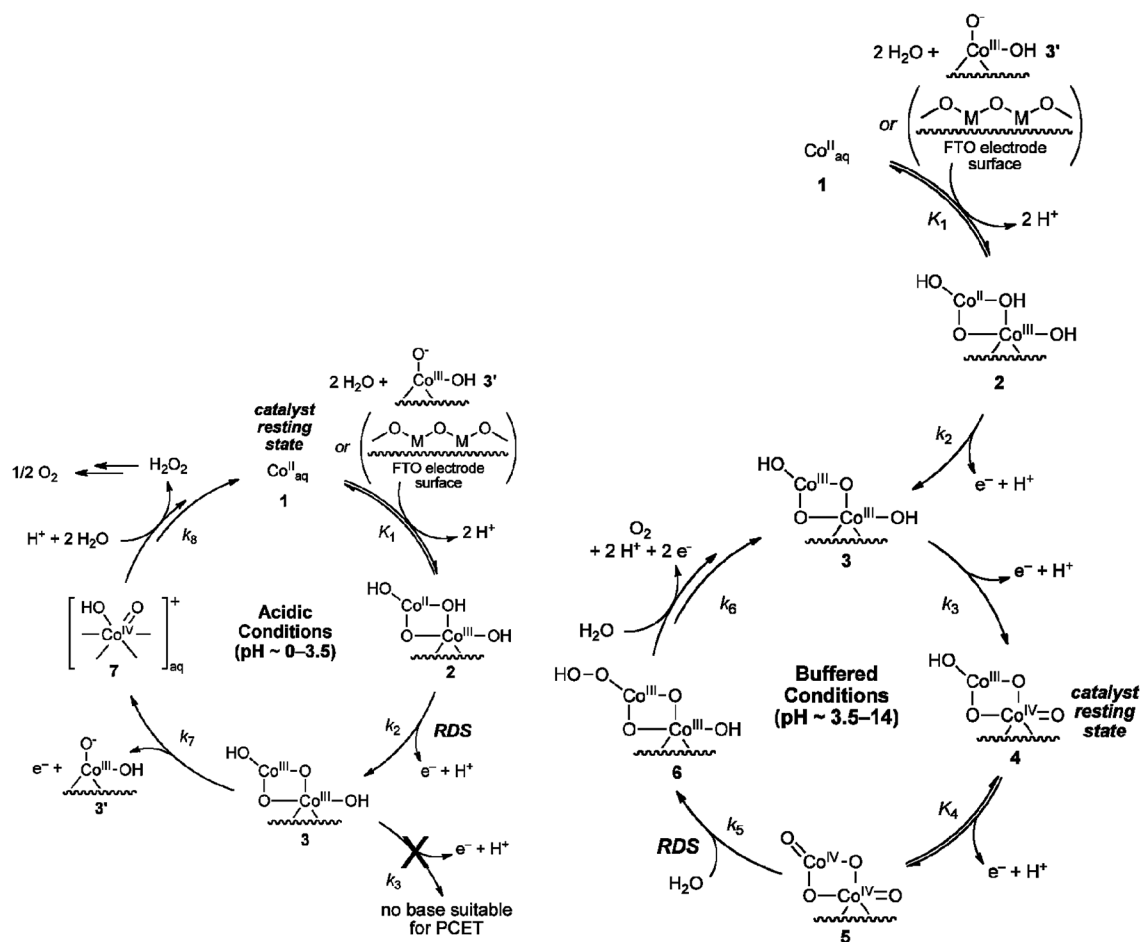


**Fig. 11** Scheme for the electrodeposition of CoO<sub>x</sub> films and water oxidation in the pH range of 0–3.5 (left) and 3.5–14 (right). Reprinted with permission from ref. 160. Copyright 2011 American Chemical Society.

limited to surface sites which could be accessed by photo-generated  $[\text{Ru}(\text{bpy})_3]^{3+}$  making the TOF strongly dependent on particle size.

### 3.2 Dyes

Efficiently converting light energy into chemical energy requires that light be absorbed to create excited states that have sufficient oxidizing or reducing power to drive at least one of the half-cell reactions of water splitting. At a dye-sensitized photoanode, this role falls to a dye molecule (also called a sensitizer) adsorbed at the solid–liquid interface. The ideal dye should absorb a significant fraction of visible spectrum, convert all absorbed photons to electron–hole pairs, bind persistently to the surface, and have the appropriate redox potential to drive the catalytic oxidation of water at a WOC. Most molecules fail to meet these stringent requirements. New photosensitizers continue to be developed, although much of the current emphasis is on the hydrogen-evolving half-cell reaction.<sup>178–180</sup> To date, most studies of dye-sensitized photoanodes have employed  $[\text{Ru}(\text{bpy})_3]^{2+}$  derivatives or high potential porphyrins, which have a long history in studies of light-driven electron transfer reactions and in conventional dye-sensitized solar cells.<sup>181–184</sup>

As noted above, functional water-splitting systems require more energy than the 1.23 V stored in the products (Fig. 1). Most of the dyes that have sufficiently negative excited state redox potentials to transfer an electron to TiO<sub>2</sub> and are sufficiently oxidizing to accept electrons from water absorb in the blue part of the visible spectrum. In  $[\text{Ru}(\text{bpy})_3]^{2+}$  derivatives, the major visible absorption is a metal-to-ligand charge transfer (MLCT) band with an absorbance maximum around 450–470 nm (454 nm = 2.7 eV). Absorption of a photon initially produces a singlet state, which undergoes intersystem crossing within 300 fs to give a predominantly triplet MLCT state.<sup>185</sup> This rapid decay to the triplet state, which is several hundred mV lower in energy than the singlet state, is the first energy loss within the cell.<sup>186</sup> As the return of the excited electron to the ground state is spin-forbidden, the triplet MLCT state lifetime is relatively long (~600 ns) for  $[\text{Ru}(\text{bpy})_3]^{2+}$  and many of its derivatives. The electrochemical potential of the triplet MLCT state is typically reported as the oxidation potential of the photoexcited dye, although there is evidence that ultrafast hot electron injection into TiO<sub>2</sub> occurs with ruthenium polypyridyl sensitizers.<sup>187,188</sup> In the lowest triplet excited state of the dye, the metal center is oxidized and one of the bipyridine ligands is reduced.<sup>189</sup>

For a dye-sensitized photoanode to operate efficiently, the excited electron must be transferred before the molecule can relax back to the ground state. This is accomplished by one of two means, transferring an electron to a metal oxide electrode or to a sacrificial reagent. Model systems typically use sacrificial oxidants, commonly sodium persulfate ( $\text{Na}_2\text{S}_2\text{O}_8$ ) or  $\text{Co}(\text{NH}_3)_5\text{Cl}$ , as these reagents irreversibly oxidize the dye and simplify the kinetic analysis of subsequent steps in water oxidation catalysis by eliminating back electron transfer. When the photoanode is operated without sacrificial reagents (*i.e.*, as a water-splitting cell), the excited dye injects an electron into the conduction band of a metal oxide semiconductor, usually titanium dioxide. The electron then percolates through the semiconductor films until it finds its way into an external circuit before being used to reduce protons to hydrogen at a counter-electrode.<sup>190</sup> If the oxidized dye is not rapidly reduced by the WOC, the electrons injected into semiconductor can be transferred back to the oxidized dye, regenerating the reduced form of the dye in its ground state. Rapid back electron transfer is the dominant kinetic pathway in dye-sensitized photoanodes and is the primary reason for their low quantum yield. Dye stability is also a significant problem. Ruthenium based sensitizers are unstable in the 3+ oxidation state and susceptible to nucleophilic attack by water and buffer anions on a timescale of tens of seconds.<sup>191</sup> Fast electron transfer between the WOC and the oxidized sensitizer is thus critical to both the efficiency and stability of the water-splitting dye cell.

The chemical attachment of the dye to the high surface area oxide semiconductor is an important and subtle issue. Carboxylic acids are the most frequently used linking groups in dye-sensitized solar cells (DSSCs), and provide strong electronic coupling for ultra-fast electron injection from the dye excited state. However, photoanodes for water splitting necessarily operate in solutions that contain water, and are often used with aqueous buffer solutions, making hydrolysis of the carboxylic acid-metal bond a significant problem. Under the aqueous conditions, phosphonate linkers provide a more robust linkage to the oxide surface. The performance of phosphonate-functionalized dyes is generally comparable or better than that of carboxylate analogues under non-aqueous conditions because of reduced dye desorption.<sup>192–194</sup> Recent work by Hanson *et al.*<sup>195,196</sup> has shown that the photodesorption of phosphonate-bound dyes in water is accelerated in the presence of oxygen, possibly because of the generation of superoxide ions by back electron transfer from  $\text{TiO}_2$ . However, dye desorption can be hindered with by having multiple ligands with phosphonic acid functionalities. Unfortunately, the electron injection efficiency of dye molecules decreases with increasing number of phosphonic acid groups,<sup>196</sup> suggesting that further work on optimizing dye attachment and electron injection efficiency is needed.

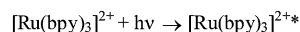
**3.2.1 Ruthenium polypyridyl sensitizers.** Ruthenium(II) tris(bipyridine) figures prominently in early studies of sensitized hydrogen<sup>197,198</sup> and oxygen<sup>199–201</sup> production from water. As a model sensitizer,  $[\text{Ru}(\text{bpy})_3]^{2+}$  has many attractive features. It absorbs strongly below 500 nm ( $\epsilon_{450\text{nm}} = 14\,400 \text{ M}^{-1} \text{ cm}^{-1}$ ) and has a sufficiently long-lived excited state lifetime ( $\sim 600 \text{ ns}$ ) for a

diffusional encounter with an electron donor or acceptor in solution.<sup>202</sup> Perhaps most importantly, the internal quantum yield for formation of the MLCT excited state is nearly unity, meaning that virtually all excited sensitizer molecules can participate in electron transfer reactions.<sup>203</sup> Thermodynamically, the redox potential of the excited state is sufficiently negative ( $-0.66 \text{ V vs. NHE}$ ) to form hydrogen from water below pH 10. The Ru(III)/Ru(II) reduction potential is sufficiently positive at 1.26 V vs. NHE to drive the water oxidation process, even in acidic solutions (Fig. 14).<sup>202</sup> However if an overpotential of 300 mV is needed to drive electron transfer from the WOC at a rate that can compete with back electron transfer, then  $[\text{Ru}(\text{bpy})_3]^{2+}$  cannot be used below pH  $\sim 4.5$  as a sensitizer for water splitting.

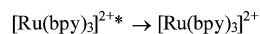
Because both its oxidized and reduced forms are relatively stable in water, the photocatalytic reactions of  $[\text{Ru}(\text{bpy})_3]^{2+}$  have been well studied using sacrificial reagents. Of particular interest in the context of water oxidation is the reaction of  $[\text{Ru}(\text{bpy})_3]^{2+}$  and a sacrificial oxidant, most commonly persulfate,  $\text{S}_2\text{O}_8^{2-}$ . The generally accepted mechanism for oxidation of  $[\text{Ru}(\text{bpy})_3]^{2+}$  by persulfate.<sup>204,205</sup> begins with the initial excitation of  $[\text{Ru}(\text{bpy})_3]^{2+}$  (Scheme 2, eqn (1)). From a precursor complex,  $\text{S}_2\text{O}_8^{2-}-[\text{Ru}(\text{bpy})_3]^{2+*}$ , an electron is rapidly transferred with a bimolecular rate constant on the order  $10^8 \text{ M}^{-1} \text{ s}^{-1}$ .<sup>206</sup> If the persulfate ion is in excess at concentrations on the order of millimolar or higher, the reaction between  $[\text{Ru}(\text{bpy})_3]^{2+*}$  and persulfate is essentially diffusion controlled, with nearly all  $[\text{Ru}(\text{bpy})_3]^{2+*}$  oxidized as in eqn (3). At lower persulfate concentration, some excited sensitizer molecules decay *via* eqn (2). Upon receiving an electron,  $\text{S}_2\text{O}_8^{2-}$  irreversibly decomposes into one molecule of sulfate,  $\text{SO}_4^{2-}$ , and one sulfate radical anion,  $\text{SO}_4^{\bullet-}$ . Sulfate radical anion is a powerful oxidizing agent,  $>3.45 \text{ V vs. NHE}$ , and rapidly reacts with any ground state sensitizer molecules it encounters (eqn (4)) to generate a second molecule of  $[\text{Ru}(\text{bpy})_3]^{3+}$ .<sup>89</sup>

As noted above, derivatives of  $[\text{Ru}(\text{bpy})_3]^{2+}$  functionalized with carboxylic acid or phosphonic acid groups can be directly coupled to a metal oxide semiconductor electrode and from their excited state can inject an electron directly into the electrode. The kinetic theory of electron transfer from an excited sensitizer to a nanocrystalline electrode follows from

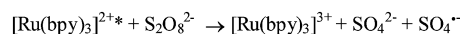
(1) Excitation



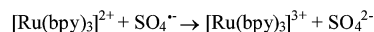
(2) Intramolecular deactivation



(3) Oxidative Quenching



(4) Thermal Oxidation



Scheme 2

semi-classical Marcus theory and has been reviewed in detail.<sup>207,208</sup> Using the Franck–Condon principle that nuclear coordinates do not change during electron transfer, a distribution of donor energy states for the excited sensitizer molecule can be calculated. The width of this distribution depends on the free energy of the excited state as well as the reorganization energy required for the change in oxidation state of the sensitizer. For reorganization energies between 0.3 and 0.8 eV the width of distribution is approximately equal to the reorganization energy, and for larger reorganization energies, the width of the distribution is less. If the width of the donor distribution is equal to the reorganization energy then the maximum rate of electron transfer occurs when the free energy of an electron in the semiconductor conduction band ( $G_c$ ) is lower than or equal to the free energy of the ground state ( $G^0$ ) plus the difference in free energy between the ground and excited states ( $G_{00}$ ) minus twice the reorganization energy ( $\lambda$ ) (eqn (2)).

$$G_c \leq G^0 + G_{00} - 2\lambda \quad (2)$$

Eqn (2) describes the situation shown on the left in Fig. 12 where the entirety of the distribution of donor states lies above the conduction band edge potential. When considering real sensitizers, this means that the maximum rate of electron transfer will occur when the quantity,  $-(G^0 + G_{00} - 2\lambda) \text{ nF}^{-1}$ , is more negative than the conduction band edge potential of the electrode. For  $[\text{Ru}(\text{bpy})_3]^{2+}$ , the potential of the excited state,  $-(G^0 + G_{00}) \text{ nF}^{-1}$ , is  $-0.84 \text{ V}$  vs. NHE and the reorganization energy for the excited state is approximately 0.35 eV.<sup>209</sup> Using these values, the maximum rate of electron injection into  $\text{TiO}_2$  will occur when the potential of the conduction band edge is more positive than  $-0.14 \text{ V}$  vs. NHE. The conduction band edge potential of anatase  $\text{TiO}_2$  is 0 V vs. NHE at pH = 0 but decreases by 55 mV per pH unit. Thus it is expected that at low pH there is a significant overlap between unoccupied states in the conduction band and the distribution of donor states in the excited sensitizer. As the pH increases, the overlap decreases as the potential of the conduction edge band becomes more negative than  $-0.14 \text{ V}$

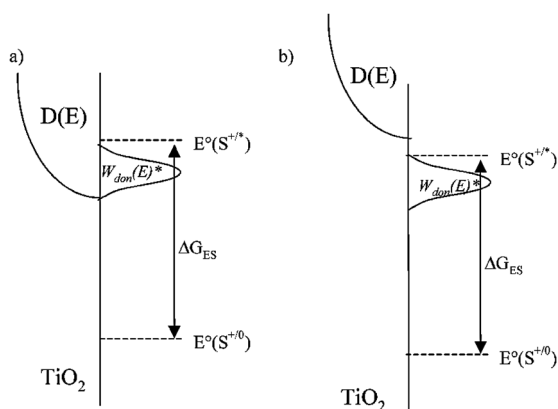


**Fig. 12** Diagram of donor distribution functions,  $W_{\text{don}}(G)$ , and the density of states within the semiconductor electrode,  $D(E)$  at (a) low pH and (b) high pH. Reprinted with permission from ref. 183. Copyright 2005 American Chemical Society.

vs. NHE and the rate of electron transfer falls off (Fig. 12). In the case of  $\text{TiO}_2$ , this model is insufficient to explain the experimental behavior. As we shall discuss in the photoanode section, the high density of conduction band states allows for injection from excited states higher in energy than the lowest MLCT excited state.

One attractive quality of ruthenium tris(bipyridyl) derivatives and related complexes is the possibility of including multiple functionalities into the three ligands. In addition to phosphonic and carboxylic acid attachment functionalities,<sup>192–194</sup> bipyridine ligands can be modified to act as linkage units to catalysts. Hoertz *et al.* functionalized 2,2'-bipyridine with dicarboxylic acid units in the 4,4' positions.<sup>157</sup> These dicarboxylic acid groups were used as capping agents for the controlled hydrolysis of  $\text{IrCl}_6^{2-}$  to form  $\text{IrO}_x \cdot n\text{H}_2\text{O}$  with sensitizers directly coupled to the WOC particle. In an extension of that work, Youngblood *et al.* prepared a sensitizer containing a malonic acid functionality, which was used to cap an  $\text{IrO}_x \cdot n\text{H}_2\text{O}$  nanoparticle, as well as a 4,4'-diphosphonic-2,2'-bipyridine ligand for attachment to the nanocrystalline electrode (Fig. 13).<sup>67</sup>

Beyond attachment functionality, ligand modification can be used to tune the redox and spectroscopic properties of the sensitizer.<sup>210,211</sup> The lowest excited state of a ruthenium tris(bipyridyl) sensitizer,  $\text{Ru}^{\text{II}}\text{L}_3$ , is best described in terms of a ligand-localized state,  $\text{Ru}^{\text{III}}\text{L}_2(\text{L}^-)$ . Because the electron localizes on one bipyridine ligand, the excited state of the sensitizer mirrors the electrochemical and spectroscopic properties of the free reduced ligand. Upon excitation, the excited electron hops rapidly ( $<15 \text{ ps}$ )<sup>212</sup> between ligands and thermally equilibrates to reside primarily on the most readily reduced, that is the most electron-deficient, ligand. The excited state oxidation potential can be made more positive by adding an electron-deficient ligand or more negative by adding electron-rich ligands.<sup>210</sup> By using a combination of  $\sigma$ -donor and  $\pi$ -acceptor effects, the ground state oxidation potential can also be shifted. Broadly considered, a more electron-deficient ligand donates less electron density *via*  $\sigma$ -donation giving a higher nuclear charge on the metal center and as a consequence, stabilizing the  $d\pi$  orbitals. Back-bonding between the  $d\pi$  and  $\pi^*$  orbitals of the ligands results in further stabilization of the  $d\pi$  orbitals. The net effect is that complexes with ligands that are more readily reduced exhibit more positive oxidation potentials.<sup>189,213</sup> In the context of water-splitting, electron injection into a semiconductor electrode can be accelerated by making the ligand bound to the electrode the most electron-withdrawing. Along the same lines, an increased reduction potential to drive a WOC can be generated by using more easily reduced ligands. Of course, this strategy also leads to more positive excited state potentials, which can affect the efficiency of electron injection.

Multinuclear dendrimer sensitizers present an interesting pathway towards enhanced light harvesting in water-splitting dye cells. By coupling multiple photoactive metal centers, dendritic sensitizers show both extended and increased absorption in the visible region relative to mononuclear sensitizers. Through careful selection of the core and branching metal ions

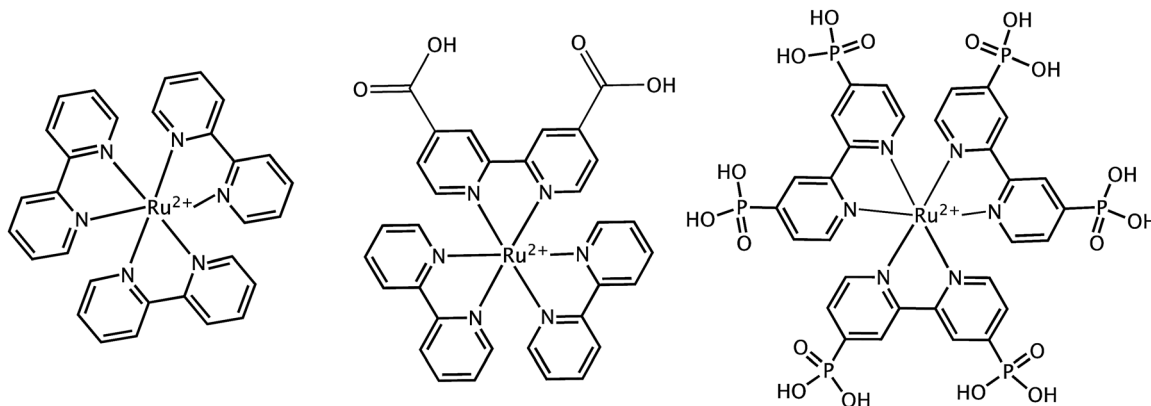


Fig. 13 Structure of  $[\text{Ru}(\text{bpy})_3]^{2+}$  (Left),  $[\text{Ru}(\text{dcbpy})(\text{bpy})_2]^{2+}$  (Middle), and  $[\text{Ru}(\text{dpbpy})_3]^{2+}$  (Right).

and ligands, a directed energy cascade reminiscent of photosynthesis can be designed.<sup>214,215</sup> Recently the tetra-ruthenium sensitizer,  $[\text{Ru}\{\mu\text{-dpp}\}\text{Ru}(\text{bpy})_2]_3(\text{PF}_6)_8$  (dpp = -2,3'-bis(2'-pyridyl)-pyrazine) was shown to drive water oxidation under sacrificial conditions.<sup>216,217</sup> Notably, this complex drove water oxidation under illumination with light  $>700$  nm using  $\text{IrO}_x \cdot n\text{H}_2\text{O}$  as the WOC. Extended light absorption comes with a price, namely that the excited state redox potential is roughly 0.4 V vs. NHE (Fig. 14) limiting the use of this complex to sacrificial systems. In principle, such a sensitizer could function at a water-splitting photoanode

using a semiconductor such as  $\text{SnO}_2$  or  $\text{In}_2\text{O}_3$ , which have more positive conduction band edge potentials than  $\text{TiO}_2$ .<sup>218</sup>

**3.2.2 Porphyrin sensitizers.** Porphyrins and related macrocyclic chromophores have been studied as sensitizers for water splitting reactions for nearly three decades.<sup>222,223</sup> Porphyrins are strongly absorbing with intense Soret bands ( $\epsilon \sim 10^5 \text{ M}^{-1} \text{ cm}^{-1}$ ) in the blue part of the visible spectrum and Q-bands ( $\epsilon \sim 10^4$ ) in the green to red.<sup>224</sup> In recent years attention has returned to high potential porphyrins as sensitizers for both DSSCs and water-splitting photoanodes. A malonate substituted

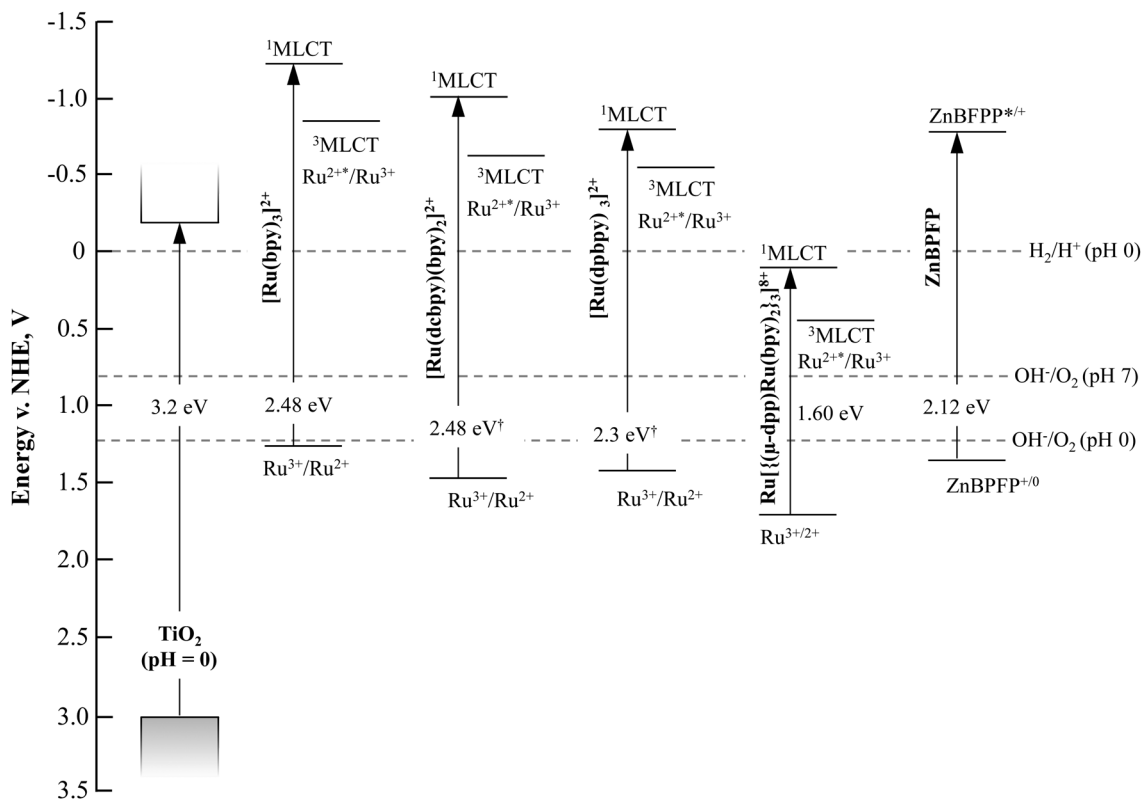
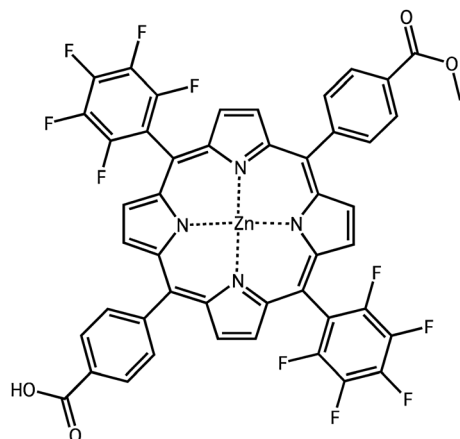


Fig. 14 Plot of ground state, singlet, and triplet redox potentials versus the conduction and valence bands of  $\text{TiO}_2$ . The difference in water oxidation potential at pH 0 and 7 is shown. **1.**  $[\text{Ru}(\text{bpy})_3]^{2+}$  (bpy = 2,2'-bipyridine);<sup>186,196,211</sup> **2.**  $[\text{Ru}(\text{dcbpy})(\text{bpy})_2]^{2+}$  (dcbpy = 4,4'-dicarboxy-2,2'-bipyridine);<sup>219</sup> **3.**  $[\text{Ru}(\text{dpbpy})_3]^{2+}$  (dpbpy = 4,4'-diphosphonic-2,2'-bipyridine);<sup>196</sup> **4.**  $\text{Ru}\{[\mu\text{-dpp}]\text{Ru}(\text{bpy})_2\}_3^{18+}$  (dpp = -2,3'-bis(2'-pyridyl)pyrazine)<sup>220</sup> **5.** ZnBPFP (BPFP = 5-(4-carbomethoxyphenyl)-15-(4-carboxyphenyl)-10,20-bis(pentafluorophenyl)porphyrin).<sup>221</sup> <sup>†</sup> Singlet-triplet state splitting estimated via the method of Vlcek *et al.*<sup>211</sup>



**Fig. 15** Zinc 5-(4-carbomethoxyphenyl)-15-(4-carboxyphenyl)-10,20-bis-(pentafluorophenyl)porphyrin (ZnBPFP).

5,10,15,20-tetrakis(4-bromomethylphenyl)porphyrin was used to cap  $\text{IrO}_x \cdot n\text{H}_2\text{O}$  nanoparticles.<sup>225</sup> The porphyrin-capped particles demonstrated strong electronic coupling and sustained catalytic activity when poised at a potential of 1.4 V vs. Ag/AgCl. Moore *et al.* demonstrated visible light water-splitting *via* the co-deposition of a high potential porphyrin zinc 5-(4-carbomethoxyphenyl)-15-(4-carboxyphenyl)-10,20-bis-(pentafluorophenyl)porphyrin (ZnBPFP) and a  $\text{Cp}^*$  iridium WOC onto a  $\text{TiO}_2$  electrode.<sup>98</sup> A subsequent study considered photoanodes prepared from ZnBPFP as well as the free base version and palladium analogue.<sup>221</sup> While no water oxidation catalyst was present, each porphyrin demonstrated sufficient oxidizing potential for water oxidation, however, only ZnBPFP had an excited state sufficiently negative to inject an electron into the  $\text{TiO}_2$  anode (Fig. 15).

**3.2.3 Sensitizer-catalyst dyads.** Direct coupling of the sensitizer and WOC should lead to faster electron transfer rates and in principle to higher overall efficiency. As noted above, Youngblood *et al.*<sup>67</sup> coupled a ruthenium sensitizer directly to an  $\text{IrO}_x \cdot x\text{H}_2\text{O}$  nanoparticle. Unfortunately, rapid quenching of the excited state by  $\text{IrO}_x \cdot x\text{H}_2\text{O}$  limited any gains from faster electron transfer. Since the publication of that work several groups have adopted a coupled sensitizer-catalyst dyad strategy to address this problem.

Kaveevitchai and co-workers coupled a ruthenium polypyridyl sensitizer to a single-site ruthenium WOC (Fig. 16).<sup>226</sup> Under photochemical conditions with  $\text{S}_2\text{O}_8^{2-}$  as sacrificial

electron acceptor they observed a TOF of  $\sim 0.005 \text{ s}^{-1}$  and a TON of 134 over six hours. While low, the TON for the uncoupled system at higher concentrations was only 6. Furthermore, the  $[\text{Ru}(\text{bpy})_2(\text{pynap})]^{2+}$  (pynap = 2-(pyrid-2'-yl)-1,8-naphthyridine) sensitizer upon which the dyad is based was shown to be an ineffective sensitizer.

A similar system built around a single site  $[\text{RuL}(\text{pic})_2]$  ( $\text{L}$  = 6,6'-dicarboxy-2,2'-bipyridine; pic = 4-picoline) complex was introduced by Li *et al.*<sup>227</sup> This system coupled a modified ruthenium trisbipyridine sensitizer through each picoline ligand. As above, under photochemical conditions, a significantly higher TON was observed for the coupled system than for the analogous uncoupled system, 38 vs. 8 turnovers.

Ashford and coworkers introduced a general approach for coupling chromophores and molecular WOCs.<sup>228</sup> *Via* an amide linkage formed at elevated temperatures, they coupled an amine functionalized ruthenium trisbipyridyl sensitizer to a single site, ruthenium terpyridyl catalyst. Although they did not report photochemical water oxidation, electrochemical and chemical water oxidation was found with oxygen yields of  $\sim 70\%$  relative to initial  $\text{Ce}(\text{IV})$  concentrations. Transient spectroscopy showed rapid intrasubassembly energy transfer. This followed work by the same group on coupled a sensitizer-catalyst dyad absorbed on a  $\text{TiO}_2$  electrode.<sup>229</sup> Rapid injection into  $\text{TiO}_2$  and electron transfer from the catalyst to the sensitizer were observed. Back electron transfer to the oxidized catalyst was observed on the microsecond time scale. Injection yields into  $\text{TiO}_2$  were low, possibly due to unfavorable energetics. Steady state photolysis data was not reported, but electrochemical water oxidation current was observed.

Ultrafast flash photolysis studies of perylene derivatives coupled to a  $\text{Cp}^*$  molecular Ir WOC revealed ultrafast electron transfer ( $< 10 \text{ ps}$ ) from the WOC to the excited perylene.<sup>230</sup> Unfortunately back electron transfer was also rapid and occurred within several nanoseconds. While photocatalytic activity was not observed due to the short charge separation lifetime, catalytic activity was retained and demonstrated electrochemically.

### 3.3 Electron transfer mediators

The photochemical systems we have described thus far generally involve a direct electron transfer between an oxidized sensitizer molecule and the WOC. As noted above, direct

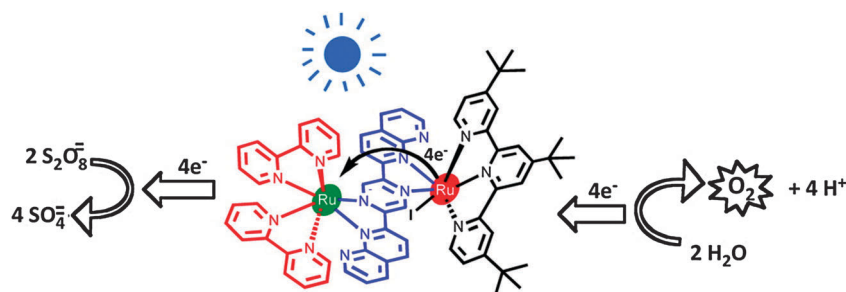


**Fig. 16** Photochemical water oxidation by a ruthenium bipyrindyl sensitizer (red) coupled to a single site ruthenium WOC (black) through a 2,6-di-(1',8'-naphthyrid-2'-yl)pyrazine (blue). Reprinted with permission from ref. 226. Copyright 2012 American Chemical Society.

electron transfer between  $\text{P680}^+$  and the OEC does not occur in photosystem II, instead the tyrosine–histidine mediator between them is an essential component of the electron transport chain. The mediator couples the fast electron transfer necessary to regenerate  $\text{P680}^+$  with the slower electron transfer from the OEC. By analogy, incorporating a mediator between an oxidized, unstable sensitizer and WOC is a promising strategy for use in a water-splitting DSSC.

Use of mediators in artificial photosynthesis has been pursued for some time. Molecular triads used in electron transfer studies represent the early examples of mediator-like systems. The initial example featured a carotenoporphyrin–quinone triad which underwent rapid ( $<100$  ps) initial charge separation to yield a long-lived charge separated state ( $t_{1/2} = 170$  ns).<sup>231</sup> In the context of water splitting, triads have been designed to closely mimic some of the structural and functional features of photosystem II. Johansson *et al.* prepared triads containing a  $[\text{Ru}(\text{bpy})_3]^{2+}$  core, a tyrosine ethyl ester, and a variety of electron acceptors.<sup>232</sup> They observed a charge separation yield of  $\sim 10\%$  with a fraction of the charge separated states persisting for microseconds. Extending the triad concept to a tyrosine-modified ruthenium trisbipyridyl complex adsorbed to the nanocrystalline  $\text{TiO}_2$  film, Pan *et al.* noted ultrafast electron injection into the  $\text{TiO}_2$  and  $\sim 90\%$  internal quantum yield for transfer of an electron from the tyrosine.<sup>233</sup> A multiexponential charge recombination process was observed with a component on the millisecond time scale.

Though it was not used to drive photochemical water splitting, a molecular triad containing a high potential porphyrin bearing two pentafluorophenyl groups demonstrated a charge separated state that was thermodynamically capable of water oxidation.<sup>234</sup> This triad featured a benzimidazole–phenol (BiP) electron donor, which mimics the tyrosine–histidine mediator found in the OEC. Unlike most phenols, which undergo irreversible oxidation, hydrogen bonding between the histidine in BiP and the phenolic proton allows for the proton to be shuttled upon oxidation of the phenol.<sup>235</sup> An ionizable proton controls the electrochemical potential of the mediator, with the potential 1.19 V vs. SCE in acidic conditions and 0.21 V vs. SCE under basic conditions (Fig. 17).<sup>236</sup>

Recently Zhao *et al.* coupled the BiP mediator to an  $\text{IrO}_x \cdot n\text{H}_2\text{O}$  colloid and co-absorbed a ruthenium polypyridine

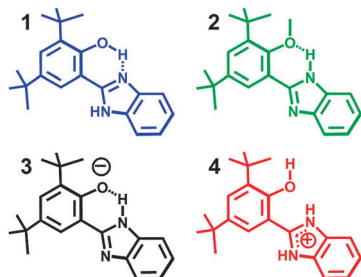


**Fig. 17** Benzimidazole–phenol (BiP) mediator at neutral conditions (1), basic conditions (3), and acidic conditions (4). Also shown is a methoxy derivative (2) that does not undergo reversible oxidation. Reprinted with permission from ref. 236. Copyright 2010 American Chemical Society.

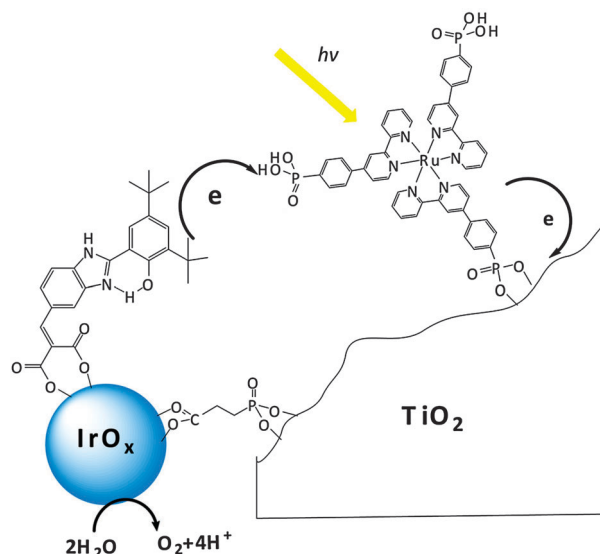


**Fig. 18** Electron transfer reactions of mediator-decorated iridium oxide and dye sensitized  $\text{TiO}_2$  anode. Reprinted with permission from ref. 237.

sensitizer onto a  $\text{TiO}_2$  electrode (Fig. 18).<sup>237</sup> With the mediator-capped catalyst, substantially higher and sustained photocurrent was measured compared to mediator free catalyst. It is important to note that in this system there was no direct linkage between the sensitizer and the mediator, which were separately adsorbed onto the high surface area  $\text{TiO}_2$  electrode. The kinetics of bleaching recovery of the sensitizer, studied by nanosecond flash photolysis, were multi-exponential as expected for a kinetically complex system with a range of distances between the electron donor and acceptor. Using a Pt collector electrode, they verified that the Faradaic efficiency (percentage of charge passed converted to oxygen) was close to unity, *i.e.*, that the observed photocurrent corresponded to water oxidation.

As an alternative to using tyrosine derived mediators, the Meyer group has focused on the use of ruthenium polypyridyls as electron transfer mediators. The rate limiting step in  $\text{Ce}(\text{IV})$  driven catalytic water oxidation by the blue dimer is oxidation of a  $\text{Ru}^{\text{IV}}=\text{O}$  to  $\text{Ru}^{\text{V}}$  or oxidation of terminal peroxido group  $\text{Ru}^{\text{IV}}-\text{OOH}$  to give oxygen. In either case, these steps are rate-limiting due to slow  $\text{Ce}(\text{IV})$  electron transfer. Ruthenium polypyridyls, for example  $[\text{Ru}(\text{bpy})_3]^{2+}$  or  $[\text{Ru}(\text{bpy})_2(\text{bpm})]^{2+}$ , can be added to function as redox mediators, undergoing rapid oxidation by  $\text{Ce}(\text{IV})$  and increasing the rate of water oxidation by 30-fold in the case of  $[\text{Ru}(\text{bpy})_2(\text{bpm})]^{2+}$ .<sup>238</sup> To extend this work to electrochemical systems, they adsorbed  $[\text{Ru}(\text{bmbppy})_2(\text{bpy})]^{2+}$  ( $\text{bmbppy} = 4,4'$ -bis-(methyl)phosphonato-2,2'-bipyridine) onto an ITO electrode and left the blue dimer in solution. Without surface modification, a  $3e^-/3\text{H}^+$  oxidation wave corresponding to oxidation of  $\text{Ru}^{\text{IV}}-\text{OH}$  and  $\text{Ru}^{\text{III}}-\text{OH}_2$  to  $\text{Ru}^{\text{V}}=\text{O}$  is not present. When the surface is modified by  $[\text{Ru}(\text{bmbppy})_2(\text{bpy})]^{2+}$ , this wave appears. Sustained electrocatalysis at 1.46 V vs. NHE resulted in 17 500 turnovers of  $[\text{Ru}(\text{bmbppy})_2(\text{bpy})]^{2+}$  and 1.25 turnovers of the blue dimer at a Faradaic efficiency of 95%. Higher turnovers of the blue dimer were limited by precipitation of the catalyst onto the electrode surface.<sup>239</sup> The issue of catalyst precipitation

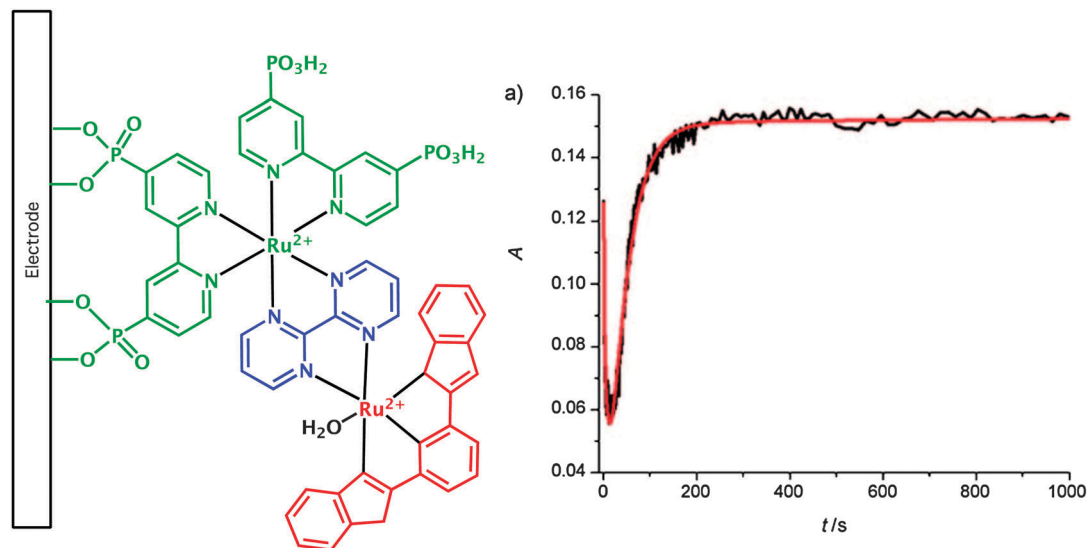


**Fig. 19** (Left) Combination electron transfer mediator (green) and water oxidation catalyst (red)  $[(\text{bmpbpy})_2\text{Ru}^{\text{II}}(\text{bpm})-\text{Ru}^{\text{II}}(\text{tpy})(\text{OH}_2)]^{4+}$  adsorbed to ITO electrode. (Right) Electrolysis at 1.8 V vs. NHE in 1.0 M  $\text{HClO}_4$ ,  $\sim 28\,000$  turnovers,  $0.6\text{ s}^{-1}$ . Reprinted with permission from ref. 240. Copyright 2009 Wiley-VCH Verlag GmbH & Co.

was circumvented by preparing a single site ruthenium catalyst directly coupled to the phosphonate-modified electron transfer mediator through a 2,2'-bipyrimidine. When attached to an ITO electrode held at 1.8 V vs. NHE, more than 28 000 turnovers could be observed with a TOF of  $0.6\text{ s}^{-1}$  and no loss of catalytic activity (Fig. 19). On a nanocrystalline  $\text{TiO}_2$  electrode, a Faradaic efficiency of 98% for oxygen production was obtained.<sup>240</sup>

### 3.4 Photoanode materials

The anode in a dye-sensitized solar cell serves two major functions, to facilitate light absorption and effectively collect electrons. Efficient light absorption with ruthenium-based sensitizers requires electrodes with surface areas hundreds of times greater than the geometric area of the cell. Also, the framework that supports the sensitizer must be transparent in the visible region. The most common photoanode in dye cells is a mesoporous film of sintered  $\text{TiO}_2$  nanocrystals prepared on top of a transparent conducting oxide (TCO) such as fluorine doped tin oxide. A secondary benefit is that the high surface area structure relaxes the minimum TOF required for the WOC in full sun. As noted above, the minimum TOF for a catalyst adsorbed on a high surface area electrode is on the order of  $\sim 3\text{ s}^{-1}\text{ nm}^{-2}$ .

Once a reasonably high fraction of the light can be absorbed and utilized, electron collection becomes critical. An efficient photoanode must accept an electron rapidly from the excited state of the sensitizer before intramolecular relaxation can occur. Once injected, the electron should rapidly move through the film until it reaches the TCO. The collection efficiency is a measure of how effectively the semiconductor film transports electrons, and is defined as the fraction of injected electrons that exit the photoanode to the external circuit. Electron generation, diffusion, and interception govern the collection

efficiency, which can be described by the continuity equation:

$$\frac{\partial n}{\partial t} = \eta_{\text{inj}} I_0 \alpha e^{-\alpha x} + D_n \frac{\partial^2 n}{\partial x^2} - \frac{n(x)}{\tau_n} = 0 \quad (3)$$

Here  $n$ ,  $\eta_{\text{inj}}$ ,  $I_0$ ,  $\alpha$ , and  $D_n$  are the free electron concentration in the film, charge injection efficiency, photon flux, absorption coefficient of the film, and apparent diffusion coefficient, respectively.  $\tau_n$  is the free electron lifetime and in a DSSC describes the rate of interception by triiodide electron acceptors in the electrolyte. If boundary conditions are applied, the current at a given voltage can be found by solving steady-state equation for a film of thickness  $x$ . Generally this equation shows that maximizing any of those values can increase efficiency in a DSSC. As we discussed in the section on sensitizers, injection efficiency ( $\eta_{\text{inj}}$ ) is a function of the overlap of excited donor states on the molecule and density of states on the semiconductor. The photon flux and absorption coefficient are controlled by transparency of the semiconductor framework and the concentration of the sensitizer within the film. Theoretically, the apparent diffusion coefficient is dependent upon the mobility of the electron within the semiconductor. Likewise,  $\tau_n$  should only depend on electron density under illumination and by extension the Fermi level of the electrons in the film. As we shall discuss, both parameters are controlled by charge trapping (Fig. 20).

Trap states play a significant role in controlling the apparent diffusion coefficient and lifetime of electrons in the semiconductor film. Electrons are initially injected from the excited sensitizer to the conduction band of the  $\text{TiO}_2$  electrode. Once in the conduction band, the electrons rapidly relax into an exponential distribution of band gap trap states.<sup>241,242</sup> Energetically deep trap states lie far below the conduction band and result in electrolyte recombination in the DSSC, determining  $\tau_n$ .<sup>243</sup> Shallow trap states provide the dominant pathway for charge transport in nanocrystalline  $\text{TiO}_2$  films.<sup>244</sup> Electrons hop from trap to trap in a thermally activated

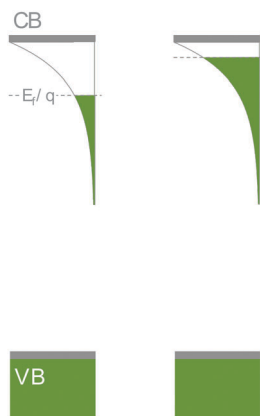


Fig. 20 Effect of Fermi level on trap filling.

process described by a continuous random walk model. Because the process is thermally activated the probability of an electron hopping from a trap state depends on the depth of the trap.<sup>245</sup> Transport through a nanocrystalline film involves  $\sim 10^7$  trapping/detrapping events.<sup>246</sup> The apparent diffusion coefficient,  $D_n$ , depends heavily on the density and depth of trap states.<sup>247</sup> Biasing the electrode in the forward direction, *i.e.* shifting the potential towards the open circuit value, raises the Fermi level of the electrons in the film and fills the deeper traps before filling the shallower traps (Fig. 21).<sup>244</sup>

Applying the above analysis to oxygen-evolving dye-sensitized photoanodes is not straightforward. Little work has been done to understand the dynamic processes that limit collection efficiencies in such cells, although some analogies can be drawn. In DSSCs, regeneration of the oxidized sensitizer by  $I^-$  (or other donors such as  $Co^{2+}$  complexes<sup>248,249</sup>) is fast so the major recombination pathway is with the oxidized donor in the electrolyte. In contrast, water is a slow electron donor at oxygen-evolving photoanodes and electron scavenging by photogenerated oxygen is not a major kinetic pathway. Instead, the recombination kinetics are dominated by back electron transfer to oxidized sensitizer molecules at the  $TiO_2$ /solution interface, and this process is about one order of magnitude faster than electron transfer from the catalyst to the oxidized sensitizer.<sup>67,250</sup> It is likely that deep traps favor recombination relative to current collection as they do in conventional DSSCs, but the details are unknown at this time. The recombination kinetics are non-exponential, implying multiple processes with

multiple activation energies.<sup>193,251</sup> This suggests that recombination involves a range of trap states, but further work is needed to better understand this process.

In the following sections we will discuss three oxide semiconductors,  $TiO_2$ ,  $SnO_2$ , and  $ZnO$ , which have been well studied in DSSCs and how they apply to oxygen-evolving photoanodes. We will also discuss electrode-related routes to increase overall efficiency.

**3.4.1  $TiO_2$  electrodes.** To date, all water-splitting dye cells have been based upon nanocrystalline  $TiO_2$ . This is not surprising as  $TiO_2$  was the first photoanode material used in DSSCs and remains the most common today. Titania has three common crystal polymorphs, rutile, anatase, and brookite.<sup>252</sup> Phase pure brookite is difficult to obtain and is the least studied of the three. Rutile is composed of  $TiO_6$  octahedra that share opposite edges to form linear chains along the [001] direction. These chains are connected by three-coordinate oxygen atoms to make the three-dimensional lattice. In DSSCs, anatase is typically the crystal polymorph of choice. The major reasons for the use of anatase are its superior electron transport properties relative to rutile and its conduction band edge potential, which is  $\sim 200$  mV more negative than rutile. Anatase also has a slightly more open structure than rutile because the  $TiO_6$  octahedra share only four edges, leading to higher dye loading.<sup>252</sup>

Electron transport in  $TiO_2$  takes place in surface mid-bandgap trap states.<sup>253</sup> Under-coordinated  $Ti^{3+}$  centers on the (001) and possibly (101) surfaces of the nanoparticles are thought to be responsible for these trap states.<sup>254</sup> As a result of these surface trap states, diffusion coefficients of nanocrystalline  $TiO_2$  electrodes are roughly 3 orders of magnitude lower than in single crystal anatase.<sup>255,256</sup> Lattice mismatches at grain boundaries can also create diffusion limiting trap states.<sup>257</sup>

Compared to other nanocrystalline oxide semiconductors, electron injection into  $TiO_2$  is unusually fast ( $< 100$  fs) in the DSSC. As we discussed in sensitizer section, classical electron transfer theory states that an electron from the sensitizer is transferred from a distribution of donor states below the excited state redox potential. In this model, electron injection should not be possible when the excited state potential of the dye lies below the conduction band edge. Experimental studies by Asbury *et al.* demonstrate that sensitizers with excited state potentials below the conduction band edge of  $TiO_2$  are able to inject electrons into the semiconductor.<sup>179,182</sup> Their results

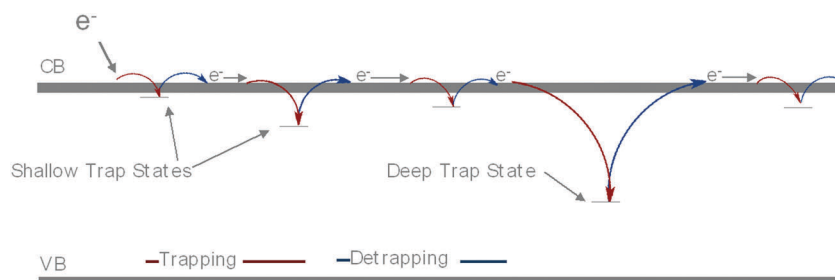
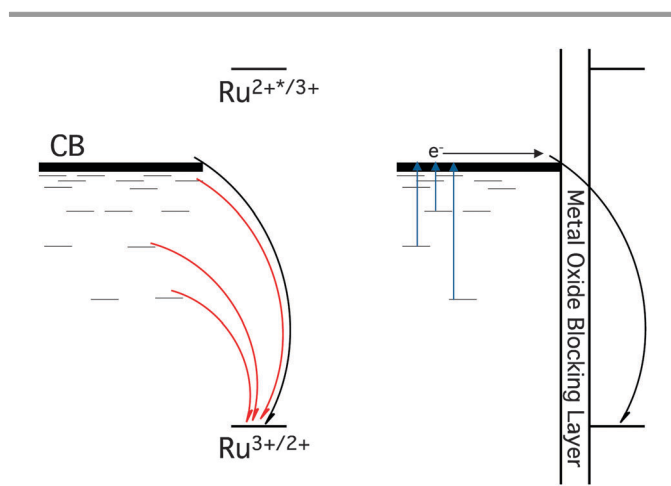


Fig. 21 Trapping/detrapping transport through semiconductor.

show that electron injection occurs from a vibrationally hot state, *i.e.* an excited molecule that has not relaxed to the bottom of the  $^3\text{MLCT}$  state, into a high density of conduction band states. This behavior is not observed with ZnO or SnO<sub>2</sub> and it was postulated that differences in the conduction band density of states could explain this behavior. The conduction band in TiO<sub>2</sub> is formed from empty 3d orbitals, whereas in ZnO and SnO<sub>2</sub> the conduction bands are respectively comprised of 4s and 5s/5p orbitals.

Ultrafast injection kinetics of TiO<sub>2</sub> could be utilized for higher efficiency water splitting cells. Charge injection in the DSSC only needs to be fast compared to dye relaxation. In anatase, charge injection is typically 3 orders of magnitude faster than relaxation,<sup>258</sup> and this provides some design flexibility to engineer slower recombination rates. Thin metal oxide blocking layers, such as Al<sub>2</sub>O<sub>3</sub>,<sup>259</sup> Nb<sub>2</sub>O<sub>5</sub>,<sup>260</sup> ZrO<sub>2</sub>,<sup>261</sup> MgO, and Y<sub>2</sub>O<sub>3</sub>,<sup>262</sup> can be inserted between the sensitizer and the TiO<sub>2</sub> to increase the physical separation and passivate surface traps. At an uncoated TiO<sub>2</sub> electrode, recombination can occur directly from trap states at the surface or *via* thermal detrapping from interior trap states.<sup>190,251,263</sup> With the surface states passivated, recombination can only occur from interior trap states, which must undergo thermal detrapping into the conduction band. The recombination kinetics are roughly a factor of three slower and dominated by the rate of tunneling from the conduction band through the barrier (Fig. 22).<sup>264</sup> Charge injection through the barrier is also slowed, but as long as the barrier layers are thin, unit injection yields are still observed because the rate can be slowed by two orders of magnitude and still be fast compared to relaxation. Lee *et al.* introduced the blocking layer strategy for oxygen-evolving photoanodes by coating a TiO<sub>2</sub> electrode with 1–2 nm thick layers of ZrO<sub>2</sub> or Nb<sub>2</sub>O<sub>5</sub>. Tests in a DSSC configuration showed injection yields remained high with 1–2 nm thick coatings but fell off as the coating thickness increased. With the introduction of the blocking layer, the recombination rate slows by a factor of 2–3 and a fast component of charge recombination disappears.



**Fig. 22** Recombination of an injected electron to the oxidized sensitizer without a blocking layer (Left) and with a blocking layer (Right). Red arrows denote recombination from surface trap states.

Photoelectrochemical tests with the Nb<sub>2</sub>O<sub>5</sub> coated electrodes showed higher peak and sustained photocurrent when compared to the bare TiO<sub>2</sub> and a Faradic efficiency of  $\sim 100\%$  for oxygen evolution.<sup>265</sup> These results strongly suggest that blocking layers are a promising avenue for improvement. However, more studies both on layer composition and thickness are needed to deliver on this promise.

As we noted earlier, diffusion in nanocrystalline films is slow compared to single crystals. Besides surface trap states, grain boundaries between particles contribute to poor diffusion in conventional TiO<sub>2</sub> nanocrystalline films. In principle, eliminating or minimizing grain boundaries should lead to enhanced diffusion and increased carrier lifetime. One-dimensional nanostructures offer moderately high surface area for light harvesting, while eliminating deleterious interparticle connections. Electrodes prepared from films<sup>266–268</sup> and oriented arrays of TiO<sub>2</sub><sup>269–274</sup> nanotubes and nanowires have received a great deal of attention as a method for improving electron transport. Generally speaking, the charge collection efficiencies in these geometries are somewhat higher than with nanoparticulate electrodes. For nanotubes, this is more a function of slow recombination as transport times *versus* nanoparticle electrodes are roughly the same, possibly due to similarities in crystallite size.<sup>270,275</sup> Feng *et al.* recently reported that crystalline rutile nanowires also show slow recombination and exhibit a diffusion coefficient  $\sim 200$  times higher than polycrystalline rutile films.<sup>276</sup> TiO<sub>2</sub> coated nanotubes of indium tin oxide (ITO) grown within the pores of a high surface area membrane demonstrated enhanced current density due to efficient radial collection of electrons by the conductive ITO layer.<sup>277</sup> At this time, no examples of dye-sensitized water splitting cells exploiting 1-D electrode morphologies have been published.

Introduction of dopants into the TiO<sub>2</sub> crystal structure represents a third significant avenue towards improved electron transport. A rapidly growing list of dopants added to TiO<sub>2</sub> in DSSCs include cations Li<sup>+</sup>,<sup>278</sup> Nb<sup>5+</sup>,<sup>279,280</sup> Ta<sup>5+</sup>,<sup>281</sup> Zn<sup>2+</sup>,<sup>282</sup> Al<sup>3+</sup>,<sup>283</sup> Mg<sup>2+</sup>,<sup>284</sup> W<sup>6+</sup>,<sup>285</sup> Ga<sup>3+</sup>, B<sup>3+</sup>,<sup>286</sup> and Y<sup>3+</sup>,<sup>287</sup> as well as the N<sup>3-</sup> anion<sup>288</sup> and B<sup>3+</sup>/N<sup>3-</sup>-co-dopants.<sup>289</sup> Despite the wide variety of dopants, several points are common across the various reports. First, high dopant levels generally lead to degradation in the device performance. Second, charge collection is generally enhanced by a suppression of recombination rates. Third, conduction band potentials shift, while valence band potentials are unaffected. Fourth, electron transport and diffusion rates are generally slowed. An interesting exception to this rule is Zn<sup>2+</sup>, which shows faster transit times through the film. The authors posit that the intrinsically high donor density of Zn<sup>2+</sup> leads to fewer unfilled trap states and increased electron mobility.<sup>282</sup> Theoretical work on the effect of dopants has been undertaken. Morgan *et al.* considered Nb- and Ta-doped TiO<sub>2</sub><sup>290</sup> and observed that both dopants created similar small polarons localized on Ti<sup>3+</sup> sites, leading to similar performance. This agrees with the conclusions of Dy *et al.*<sup>291</sup> who reported that addition of tantalum and niobium shifted the Fermi level towards otherwise unoccupied conduction band states. By contrast, ruthenium doping created mid-gap states and only slightly shifted the

Fermi level. The model suggests that ruthenium does not incorporate readily into anatase so that the mid-bandgap states are a result of formation of new electronic states within the material. Tantalum, and to a lesser extent niobium, readily incorporate into the lattice and perturb largely surface states. An important caveat is that this work has been done entirely in the context of DSSCs, where recombination with the triiodide is the main challenge. To the best of our knowledge, doped-TiO<sub>2</sub> has not been considered in the context of dye-sensitized water splitting cells.

**3.4.2 SnO<sub>2</sub> electrodes.** As noted above in the context of dendrimer based sensitizers, increasing utilization of the solar spectrum while maintaining sufficient oxidizing power to drive water oxidation results in excited state redox potentials that are too positive for electron injection into TiO<sub>2</sub>. Substituting a semiconductor with a more positive conduction band potential for TiO<sub>2</sub> would allow for the use of less reducing dyes. While this would reduce the photovoltage of the cell, it would also lower the driving force for back electron transfer and possibly slow the rate of that process. The conduction band edge of rutile SnO<sub>2</sub> is ~500 mV more positive than that of anatase TiO<sub>2</sub>. Bergeron *et al.* have demonstrated the viability of this approach using ruthenium sensitizers on SnO<sub>2</sub> with excited state potentials too positive for electron injection into TiO<sub>2</sub>.<sup>292</sup>

Numerous examples of SnO<sub>2</sub>-based DSSCs appear in the literature.<sup>293–299</sup> Generally, unmodified SnO<sub>2</sub> DSSCs exhibit poor solar cell characteristics compared to TiO<sub>2</sub>: lower open circuit voltage, lower current density, and poorer fill factors. Kay and Grätzel demonstrated that better performing SnO<sub>2</sub> electrodes could be made by adding a thin insulating shell. They attributed the improvement to enhanced dye loading and inhibition of back electron transfer to I<sub>3</sub><sup>-</sup>.<sup>262</sup> SnO<sub>2</sub> has higher electrical conductivity<sup>300</sup> and mobility<sup>301</sup> than TiO<sub>2</sub>, but the higher electron mobility of SnO<sub>2</sub> was recognized by Green *et al.* as a contributor to its poor performance in DSSCs.<sup>302</sup> Like TiO<sub>2</sub>, electron transport in SnO<sub>2</sub> is controlled by thermal trapping/detrapping. Unlike TiO<sub>2</sub>, however, the density of trap states in SnO<sub>2</sub> is significantly lower, resulting in an electron diffusion coefficient 2 orders of magnitude greater than in TiO<sub>2</sub>. The rate of electron transport in SnO<sub>2</sub> is rapid enough that in DSSCs it competes with the fast reduction of the oxidized sensitizer by I<sup>-</sup>. SnO<sub>2</sub> also exhibits slower injection dynamics when compared to TiO<sub>2</sub>.<sup>188</sup> Ai *et al.* suggested this difference may be due to differences in the conduction band densities of states of the two semiconductors. In TiO<sub>2</sub> the conduction band is primarily composed of relatively localized d-orbitals, which give a narrow distribution of states of much higher density than the sp-orbital conduction band of SnO<sub>2</sub>.<sup>303</sup>

**3.4.3 ZnO core-shell electrodes.** Although the bandgap and conduction band edge potential of ZnO are similar to those of TiO<sub>2</sub>,<sup>304</sup> the carrier lifetime in ZnO is higher.<sup>305</sup> Electron diffusivity in crystalline ZnO nanowires is hundreds of times faster than in TiO<sub>2</sub> nanoparticle films.<sup>306</sup> Despite these desirable properties, ZnO is not likely to be a good photoanode for water splitting cells because of its instability in acidic conditions.<sup>307</sup> However, it may be possible to stabilize ZnO in

core-shell structures. ZnO nanowires coated with a TiO<sub>2</sub> shell showed a decrease in the recombination rate, which was attributed to a radial surface field caused by the TiO<sub>2</sub> coating.<sup>308</sup> A similar strategy was used to coat a quasi-1D silica aerogel with coaxial layers of ZnO and TiO<sub>2</sub>. Electron transport in the construct was ~2 orders of magnitude faster than in aerogels coated with only TiO<sub>2</sub>, suggesting that the ZnO layer acts as a rapid conduit for electron transport.<sup>309</sup>

### 3.5 System-level design

**3.5.1 Overall cell efficiency.** While water splitting DSSCs operate with low quantum yield (2–3%) because of the fast kinetics of back electron transfer, it is important to consider how they might function as energy conversion systems if this kinetic problem could be solved. In a water splitting cell containing a single light absorber (*e.g.*, [Ru(dppp)<sub>3</sub>]<sup>2+</sup>) sensitizing a TiO<sub>2</sub> anode, the maximum photovoltage or open circuit voltage can be estimated from the potentials of the O<sub>2</sub>/H<sub>2</sub>O couple and the Fermi level of the semiconductor, which at low trap density and high levels of illumination should be close to the conduction band potential. A common misconception is that the photovoltage should be calculated as the difference between the Fermi level and the potential of the H<sub>2</sub>/H<sup>+</sup> couple. The maximum photovoltage will be obtained when the cathode reaction is the reverse of the anode reaction, *i.e.*, reduction of oxygen. At a pH of 5.8 the thermodynamic potential for water splitting is 0.89 V *vs.* NHE and the conduction band edge of TiO<sub>2</sub> is -0.54 V *vs.* NHE, meaning that the maximum photovoltage that could be generated by the cell is 1.43 V. In practice, however, the open circuit voltage of the best dye-sensitized photoanodes is ~1.0 V and a bias of several hundred mV is needed to reach the maximum power point. This implies that a second, complementary absorber should be added to the cathode side of the cell to provide additional photovoltage to drive overall water splitting. Connolly and coworkers performed a detailed analysis of the efficiency limits of solar water splitting.<sup>8</sup> They determined that dual absorber “Z-schemes,” which like plant photosynthesis use two photons per electron, are more forgiving than single-absorber systems. If operated near unit quantum efficiency, photoelectrochemical Z-schemes could achieve overall efficiencies in the 10–15% range, assuming quantum yields near unity and reasonable total losses (~700–800 mV) for series resistance and catalyst overpotentials.

Because dye-sensitized water splitting cells operate near neutral pH in buffered aqueous solutions, Hernández-Pagán *et al.* considered the inherent potential losses in such systems when the anode and cathode separated by an ion exchange membrane to facilitate separation of hydrogen and oxygen.<sup>310</sup> They gave the total potential loss in the cell as:

$$E = \eta_{\text{anode}} + \eta_{\text{cathode}} + iR_{\text{sol}} + E_{\text{M}} + E_{\text{pH}} \quad (4)$$

where  $\eta_{\text{anode}}$  and  $\eta_{\text{cathode}}$  represent the overpotentials of the anode and cathode,  $iR_{\text{sol}}$  is the resistance of the solution,  $E_{\text{M}}$  is the membrane resistance, and  $E_{\text{pH}}$  is the potential loss associated with the pH gradient. Resistance losses due to charge transport through TiO<sub>2</sub> are typically low and therefore

not considered. In acetate and phosphate buffers, overpotential losses were between 400–650 mV depending on the concentration of the buffer. This implies that the remaining potential losses in equation should be  $\sim 200$  mV or less to achieve reasonably efficient water splitting. In concentrated buffers, the losses from solution resistance ( $iR_{\text{sol}}$ ) and membrane resistance ( $E_M$ ) were typically small, provided that the solution path length was kept short. However, the potential drop due to the formation of a pH gradient across the membrane could be as large as several hundred millivolts at current densities typical of efficient photoelectrochemical cells.

The formation of the pH gradient could be understood by considering migration of buffer ions through the membrane. With an anionic membrane and phosphate buffer, the only charge carriers that can migrate through the membrane are  $\text{HPO}_4^{2-}$  and  $\text{H}_2\text{PO}_4^-$ . This process depletes the buffer on the cathode side of the cell, where the reduction of protons causes the pH to increase substantially there. In order for  $E_{\text{pH}}$  to remain low, the diffusional flux of the neutral form of the buffer,  $J_D$ , must be equal and opposite to the migrational flux of the charged form of the buffer,  $J_M$ . With 200  $\mu\text{m}$  thick membranes,  $J_M$  was much larger than  $J_D$  leading to membrane polarization. The conclusion of the study was that thinner, more permeable membranes would need to be developed and used in conjunction with very concentrated buffers in order for photoelectrochemical water splitting cells to operate efficiently.

**3.5.2 Buffer selection.** The choice of buffer can have a substantial and largely uninvestigated effect on the efficiency of water oxidation. Using a  $[\text{Ru}(\text{bpy})_3]^{2+}\text{-S}_2\text{O}_8^{2-}\text{-IrO}_x$  model system, Hara *et al.* demonstrated a three-fold enhancement in the TON for oxygen evolution when a  $\text{Na}_2\text{SiF}_6\text{-NaHCO}_3$  buffer was used instead of  $\text{KH}_2\text{PO}_4\text{-Na}_2\text{B}_4\text{O}_7$  buffer.<sup>156</sup> Slower decomposition of the oxidized sensitizer was suggested as the reason for improvement, but the authors conceded that the complex overall decomposition pathway made it difficult to quantify the kinetics. An interesting observation is that phosphate deactivation of metal oxide catalysts in other oxidation reactions is well known.<sup>311–314</sup> Deactivation of surface sites by phosphate exchange<sup>315</sup> as well as scavenging of hydroxyl radicals<sup>316</sup> is generally accepted as the reason for decreased catalytic activity. More work is needed to elucidate the role that the buffer plays in catalysis and in the decomposition of sensitizer molecules.

The silicate buffer derived from  $\text{Na}_2\text{SiF}_6\text{-NaHCO}_3$  is unstable, decomposing to colloidal silica over a period of days. It is likely that the actual buffer in this system is an oligomeric silicate. The silicate buffer has been useful for testing many WOCs under photocatalytic conditions, and a study by Morris and Mallouk optimized the buffer composition and pH in the  $[\text{Ru}(\text{bpy})_3]^{2+}\text{-S}_2\text{O}_8^{2-}\text{-IrO}_x$  system by a factorial design-of-experiment method.<sup>317</sup> In a photoelectrochemical cell however, this oligomeric buffer may be problematic because it may not be able to access all of the pore volume of the nanocrystalline  $\text{TiO}_2$  electrode. Inefficient buffering may explain the anode polarization effect that has been observed in almost all water-splitting dye cell experiments to date. This is illustrated in Fig. 23, and is also evident in Fig. 19. When the cell is held at a potential at which water splitting can occur and the

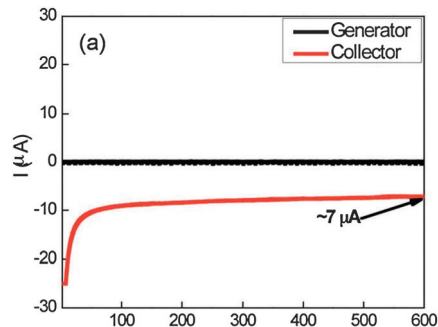


**Fig. 23** Generator–collector measurements indicating polarization for a  $\text{TiO}_2\text{-dye-IrO}_x$  photoanode. The black trace corresponds to the photocurrent from the electrode, while the red trace corresponds to current from the catalytic reduction of evolved oxygen. Reproduced from ref. 265 with permission from The Royal Society of Chemistry.

light is switched on, the initial photocurrent is typically in the range of  $0.2\text{--}0.3\text{ mA cm}^{-2}$ , corresponding to a quantum yield (per absorbed photon) on the order of 20%. The steady state photocurrent decays over tens of seconds, reaching a plateau that is 10–20% of the initial value. The oxygen evolved can be quantified by using a dark Pt electrode near the photoanode. This experiment reveals that oxygen is produced with high current efficiency during the photocurrent decay. Switching the light off for tens of seconds restores the initial photocurrent, and this cycle can be repeated hundreds of times. There are two possible causes of this polarization effect. One is that electron transfer between catalyst and oxidized sensitizer becomes slower as the catalyst is oxidized, and the other is that the solution becomes locally more acidic because the water oxidation reaction generates four protons per  $\text{O}_2$  molecule. In the latter case, the overpotential for catalytic water oxidation, and thus the catalytic rate, would decrease as the pH is driven down by the reaction. Experiments with buffers that can penetrate the pore volume of the  $\text{TiO}_2$  electrode are clearly needed to address this question and to minimize electrode polarization.

**3.5.3 Z-schemes.** All of the photochemical and photoelectrochemical systems we have discussed to this point utilize a single absorber, and as noted above dual-absorber systems are likely to be more effective in utilizing the solar spectrum to drive unassisted water splitting. However, for a two-absorber system to work efficiently, the photoredox levels of the two parts of the electron transport chain must be properly aligned (Fig. 24). The first oxidized absorber drives water oxidation, while the second reduced absorber drives water reduction. Both absorbers could both be on the same electrode or split to give a photoanode and photocathode. In either configuration, two photons are absorbed to generate one electron for water reduction and one hole for water oxidation. As we noted earlier, this is the basic design of plant photosynthesis.

Z-schemes have been demonstrated with photocatalysts,<sup>318</sup> but only with low ( $\sim 1\%$ ) quantum yields. The kinetic optimization of Z-schemes is difficult because of the requirement for current matching and because of the increased possibilities for

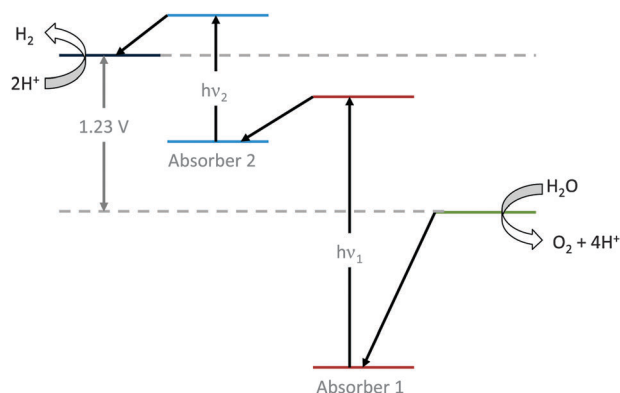


Fig. 24 Two absorber Z-scheme for overall water splitting.

charge recombination in more complex photosystems. The concept is so far largely untested in dye-sensitized water splitting cells. Fukuzumi and co-workers showed dual absorber behavior with a photochemical system based on ruthenium sensitizers and  $\text{BiVO}_4$ .<sup>319</sup> Using  $[\text{Co}(\text{NH}_3)_5\text{Cl}]^{2+}$  as a sacrificial reagent, they demonstrated a five-fold enhancement of photochemical oxygen evolution with the addition of  $[\text{Ru}(\text{bpy})_3]^{2+}$ . They speculated that  $[\text{Ru}(\text{bpy})_3]^{2+}$  was oxidized by the sacrificial cobalt complex and reduced *via* electron transfer of an electron from the conduction band of  $\text{BiVO}_4$ . The thermodynamics of the system would support this conclusion, as the driving force for electron transfer to  $[\text{Co}(\text{NH}_3)_5\text{Cl}]^{2+}$  is much larger with  $[\text{Ru}(\text{bpy})_3]^{2+}$  than  $\text{BiVO}_4$  and  $[\text{Ru}(\text{bpy})_3]^{3+}$  is not sufficiently oxidizing to drive water oxidation with  $\text{BiVO}_4$  as the catalyst. While this is an interesting proof of concept, the absorption bands of  $[\text{Ru}(\text{bpy})_3]^{2+}$  and  $\text{BiVO}_4$  overlap and are confined to the blue part of the spectrum. Brillet *et al.* demonstrated a multiple absorber water splitting cell using hematite as a photoanode in series with two DSSCs to produce sufficiently high voltage for water reduction.<sup>320</sup> The photon to hydrogen conversion efficiency was low ( $\sim 1.36\%$ ) due to poor light harvesting.

## 4. Conclusions

Water splitting using dye sensitized electrodes is a relatively new area of research that has significant promise for the development of efficient solar fuel systems. Although the current performance of these systems is very poor – with steady state photocurrents corresponding to only 2–3% quantum yield in visible light – most of the problems with these cells are understood and in principle addressable by using well-established principles of electron transfer kinetics and molecular design. At the photoanode, the key problem is to control the relative rates of forward and back electron transfer at the sensitizer molecule. Because back electron transfer occurs on the timescale of hundreds of microseconds, the system needs to be designed to regenerate the reduced sensitizer on the microsecond (or faster) timescale. Experiments with electron transfer mediators (Fig. 18 and 19) are beginning to attack this problem. In this context, it should be possible to utilize some of the design principles of electron transfer supermolecules (dyads, triads, tetrads, *etc.*) that have been engineered to give long-lived

charge-separated states by controlling the distance between redox-active components.<sup>68</sup> A related problem is to synthesize water oxidation catalysts, preferably from abundant elements, that can be used in water-splitting photoanodes at modest overpotentials. While the absolute requirement for these catalysts is a site turnover frequency on the order of  $3 \text{ s}^{-1}$ , to keep up with the flux of solar photons, in practice much faster turnover is needed to compete with back electron transfer. The turnover frequencies of the best synthetic and colloidal WOCs are already approaching that of the OEC in photosystem II, which generates oxygen in high quantum yield thanks to fast electron transfer between the tyrosine–histidine mediator and  $\text{P680}^+$ . It is not unreasonable to expect that synthetic systems could soon be engineered with similar kinetics and high quantum yields.

Beyond the photoanode, system-level problems need to be addressed in order to achieve efficient photoelectrochemical water splitting. It seems clear that a two-absorber Z-scheme will be needed in order to use the visible and near-infrared parts of the spectrum effectively. Placing one photosystem at the anode and the other at the cathode, as shown in Fig. 4, avoids some of the possible short-circuiting reactions of colloidal Z-schemes and would allow for the use of two different sensitizers, perhaps with energy transfer cascades at the anode or cathode or both to improve light harvesting. Along these lines, we were able to construct, using layer-by-layer assembly of polyelectrolytes and oxide semiconductor nanosheets, a porphyrin-based energy/electron transfer cascade that separated charge across a semiconductor nanosheet.<sup>68</sup> Although that system was not coupled to catalysts for hydrogen evolution, the viologen electron acceptor that was used is capable of reducing water to  $\text{H}_2$  at neutral pH. Subsequent experiments have shown that it is possible to use light driven charge separation across nanosheets to generate  $\text{H}_2$  in high quantum yield in sacrificial systems.<sup>321</sup> The challenge is to construct systems like this on high surface area electrodes where the photogenerated holes can be carried away to the external circuit. Some progress has recently been made in synthesizing arrays of (ITO) nanotubes,<sup>322</sup> as well as high surface area porous ITO electrodes,<sup>323</sup> which might be used for this purpose.

Beyond the challenge of demonstrating an efficient water splitting system at the proof-of-concept level using dye-sensitized electrodes, it will be important to engineer such systems for durability. In practical terms, this implies sensitizer and catalyst TONs approaching  $10^9$ . Photoredox molecules are notoriously unstable in water at the potential of water oxidation and it is well known that even photosystem II is subject to oxidative damage on a timescale of tens of minutes in full sun. Two possible strategies for addressing this problem are repair and protection, both of which are used effectively in natural photosynthesis. In an engineered photoelectrochemical system, it is difficult to imagine such a repair mechanism, especially for organic dyes and redox molecules that are degraded by reactive oxygen species generated at the photoanode. However, protection of the photoredox assembly, *e.g.*, by encapsulation in silica, is a strategy that is already beginning to be explored for molecule-catalyst dyads.<sup>324</sup>

## Acknowledgements

We gratefully acknowledge the efforts of our Penn State coworkers in the water splitting project, Paul Hoertz, Justin Youngblood, Anna Lee, Yixin Zhao, Dongdong Qin, Nella Vargas-Barbosa, Emil Hernández-Pagán, Nina Kovtyukhova, Nick McCool, Timothy Saunders, Landy Blasdel, and Deanna Lentz, as well as our Arizona State collaborators Jackson Megiatto, Ana Moore, Tom Moore, and Devens Gust. This work was supported by the Office of Basic Energy Sciences, Division of Chemical Sciences, Geosciences, and Energy Biosciences, Department of Energy under contract DE-FG02-07ER15911.

## References

- 1 T. Lipman, *An Overview of Hydrogen Production and Storage Systems with Renewable Hydrogen Case Studies*, Clean Energy States Alliance, Oakland, CA, 2011.
- 2 C. A. Grimes, O. K. Varghese and S. Ranjan, *In Light, Water, Hydrogen: The Solar Generation of Hydrogen by Water Photolysis*, Springer Science, New York, 1st edn, 2008, pp. 1–33.
- 3 L. Vernon, *Fuel*, 1980, **59**, 102–106.
- 4 R. B. Alley, *Earth The Operators Manual*, W.W. Norton & Co., New York, 2011, pp. 239–251.
- 5 N. D. McDaniel and S. Bernhard, *Dalton Trans.*, 2010, **39**, 10021–10030.
- 6 W. Shockley and H. J. Queisser, *J. Appl. Phys.*, 1961, **32**, 510–519.
- 7 M. C. Hanna and A. J. Nozik, *J. Appl. Phys.*, 2006, **100**, 074510.
- 8 J. R. Bolton, S. J. Strickler and J. S. Connolly, *Nature*, 1985, **316**, 495–500.
- 9 M. D. Archer and J. R. Bolton, *J. Phys. Chem.*, 1990, **94**, 8028–8036.
- 10 H. D. Holland, *Philos. Trans. R. Soc., B*, 2006, **361**, 903–915.
- 11 M. Grabolle and H. Dau, *Biochim. Biophys. Acta*, 2005, **1708**, 209–218.
- 12 H. J. van Gorkom and R. de Wijn, *Biochim. Biophys. Acta*, 2002, **1553**, 302–308.
- 13 J. McEvoy and G. Brudvig, *Chem. Rev.*, 2006, **106**, 4455–4483.
- 14 I. McConnell, G. Li and G. W. Brudvig, *Chem. Biol.*, 2010, **17**, 434–447.
- 15 R. J. Pace, R. Stranger and S. Petrie, *Dalton Trans.*, 2012, **41**, 7179–7189.
- 16 A. Melis, *Plant Sci.*, 2009, **177**, 272–280.
- 17 X.-G. Zhu, S. P. Long and D. R. Ort, *Annu. Rev. Plant Biol.*, 2010, **61**, 235–261.
- 18 N. Nelson and C. F. Yocum, *Annu. Rev. Plant Biol.*, 2006, **57**, 521–565.
- 19 C. Beadle and S. P. Long, *Biomass*, 1985, **8**, 119–168.
- 20 C. Beale and S. P. Long, *Plant, Cell Environ.*, 1995, **18**, 641–650.
- 21 D. R. Ort and S. P. Long, in *Plants, Genes, and Crop Biotechnology*, ed. M. Chrispeels and D. Sadvada, Jones and Bartlett Publishers International, 2003, pp. 240–269.
- 22 H. Michel, *Angew. Chem., Int. Ed.*, 2012, **51**, 2516–2518.
- 23 S. Elliott, K. S. Lackner, H. J. Ziock, M. K. Dubey, H. P. Hanson, S. Barr, N. A. Ciszowski and D. R. Blake, *Geophys. Res. Lett.*, 2001, **28**, 1235–1238.
- 24 X.-G. Zhu, S. P. Long and D. R. Ort, *Curr. Opin. Biotechnol.*, 2008, **19**, 153–159.
- 25 J. Zhao, A. Wang, M. A. Green and F. Ferrazza, *Appl. Phys. Lett.*, 1998, **73**, 1991.
- 26 F. E. Osterloh, *Chem. Mater.*, 2008, **20**, 35–54.
- 27 G. Schrauzer and T. Guth, *J. Am. Chem. Soc.*, 1977, **99**, 7189–7193.
- 28 K. Yamaguti and S. Sato, *J. Chem. Soc., Faraday Trans. 1*, 1985, **81**, 1237–1247.
- 29 A. Kudo, K. Ueda, H. Kato and I. Mikami, *Catal. Lett.*, 1998, **53**, 229–230.
- 30 A. Kudo, K. Omori and H. Kato, *J. Am. Chem. Soc.*, 1999, **121**, 11459–11467.
- 31 K. Maeda, K. Teramura, D. Lu, T. Takata, N. Saito, Y. Inoue and K. Domen, *Nature*, 2006, **440**, 295.
- 32 K. Maeda, K. Teramura, T. Takata, M. Hara, N. Saito, K. Toda, Y. Inoue, H. Kobayashi and K. Domen, *J. Phys. Chem. B*, 2005, **109**, 20504–20510.
- 33 K. Maeda, K. Teramura and K. Domen, *J. Catal.*, 2008, **254**, 198–204.
- 34 A. Fujishima and K. Honda, *Nature*, 1972, **238**, 37–38.
- 35 M. R. Hoffmann, S. T. Martin, W. Choi and D. W. Bahnemann, *Chem. Rev.*, 1995, **95**, 69–96.
- 36 A. Linsebigler, G. Lu and J. T. Yates, *Chem. Rev.*, 1995, **95**, 735–758.
- 37 R. Asahi, T. Morikawa, T. Ohwaki, K. Aoki and Y. Taga, *Science*, 2001, **293**, 269–271.
- 38 G. R. Torres, T. Lindgren, J. Lu, C. G. Granqvist and S. E. Lindquist, *J. Phys. Chem. B*, 2004, **108**, 5995–6003.
- 39 J. Augustyński, B. D. Alexander and R. Solarska, *Top. Curr. Chem.*, 2011, **303**, 1–38.
- 40 X. Liu, F. Wang and Q. Wang, *Phys. Chem. Chem. Phys.*, 2012, **14**, 7894–7911.
- 41 F. F. Abdi and R. van de Krol, *J. Phys. Chem. C*, 2012, **116**, 9398–9404.
- 42 K. Sivula, F. Le Formal and M. Grätzel, *ChemSusChem*, 2011, **4**, 432–449.
- 43 C. X. Kronawitter, L. Vayssieres, S. Shen, L. Guo, D. A. Wheeler, J. Z. Zhang, B. R. Antoun and S. S. Mao, *Energy Environ. Sci.*, 2011, **4**, 3889–3899.
- 44 R. Abe, M. Higashi and K. Domen, *J. Am. Chem. Soc.*, 2010, **132**, 11828–11829.
- 45 M. Higashi, K. Domen and R. Abe, *J. Am. Chem. Soc.*, 2012, **134**, 6968–6971.
- 46 C. M. Leroy, A. E. Maegli, K. Sivula, T. Hisatomi, N. Xanthopoulos, E. H. Otal, S. Yoon, A. Weidenkaff, R. Sanjines and M. Grätzel, *Chem. Commun.*, 2012, **48**, 820–822.
- 47 K. Maeda, M. Higashi, B. Siritanaratkul, R. Abe and K. Domen, *J. Am. Chem. Soc.*, 2011, **133**, 12334–12337.
- 48 J. S. Kilby, *US Pat.*, 4 021 323, 1977.
- 49 J. W. Lathrop, *US Pat.*, 4 100 051, 1978.

- 50 W. A. Porter, *US Pat.*, 4 136 436, 1979.
- 51 E. Smotkin, A. J. Bard, A. Campion, M. Fox, T. Mallouk, S. E. Webber and J. M. White, *J. Phys. Chem.*, 1986, **90**, 4604–4607.
- 52 E. Smotkin, S. Cervera-March, A. Bard, A. Campion, M. Fox, T. Mallouk, S. Webber and J. White, *J. Phys. Chem.*, 1987, **91**, 6–8.
- 53 O. Khaselev and J. A. Turner, *Science*, 1998, **280**, 425–427.
- 54 S. Licht, B. Wang, S. Mukerji, T. Soga, M. Umeno and H. Tributsch, *J. Phys. Chem. B*, 2000, **104**, 8920–8924.
- 55 S. W. Boettcher, E. L. Warren, M. C. Putnam, E. A. Santori, D. Turner-Evans, M. D. Kelzenberg, M. G. Walter, J. R. McKone, B. S. Brunschwig, H. A. Atwater and N. S. Lewis, *J. Am. Chem. Soc.*, 2011, **133**, 1216–1219.
- 56 J. R. McKone, E. L. Warren, M. J. Bierman, S. W. Boettcher, B. S. Brunschwig, N. S. Lewis and H. B. Gray, *Energy Environ. Sci.*, 2011, **4**, 3573–3583.
- 57 T. J. Kempa, B. Tian, D. R. Kim, J. Hu, X. Zheng and C. M. Lieber, *Nano Lett.*, 2008, **8**, 3456–3460.
- 58 S. Y. Reece, J. A. Hamel, K. Sung, T. D. Jarvi, A. J. Esswein, J. J. H. Pijpers and D. G. Nocera, *Science*, 2011, **334**, 645–648.
- 59 M. Grätzel, *J. Photochem. Photobiol., A*, 2004, **161**, 3–14.
- 60 J. I. Basham, G. K. Mor and C. A. Grimes, *ACS Nano*, 2010, **4**, 1253–1258.
- 61 M. Shalom, J. Albero, Z. Tachan, E. Martínez-Ferrero, A. Zaban and E. Palomares, *J. Phys. Chem. Lett.*, 2010, **1**, 1134–1138.
- 62 P. Liska, K. R. Thampi, M. Grätzel, D. Brémaud, D. Rudmann, H. M. Upadhyaya and A. N. Tiwari, *Appl. Phys. Lett.*, 2006, **88**, 203103.
- 63 M. Dürr, A. Bamedi, A. Yasuda and G. Nelles, *Appl. Phys. Lett.*, 2004, **84**, 3397–3399.
- 64 J. Usagawa, S. S. Pandey, S. Hayase, M. Kono and Y. Yamaguchi, *Appl. Phys. Express*, 2009, **2**, 062203.
- 65 X.-Z. Guo, Y.-D. Zhang, D. Qin, Y.-H. Luo, D.-M. Li, Y.-T. Pang and Q.-B. Meng, *J. Power Sources*, 2010, **195**, 7684–7690.
- 66 G. D. Barber, P. G. Hoertz, S.-H. A. Lee, N. M. Abrams, J. Mikulca, T. E. Mallouk, P. Liska, S. M. Zakeeruddin, M. Grätzel, A. Ho-Baillie and M. A. Green, *J. Phys. Chem. Lett.*, 2011, **2**, 581–585.
- 67 W. J. Youngblood, S.-H. A. Lee, Y. Kobayashi, E. A. Hernandez-Pagan, P. G. Hoertz, T. A. Moore, A. L. Moore, D. Gust and T. E. Mallouk, *J. Am. Chem. Soc.*, 2009, **131**, 926–927.
- 68 D. M. Kaschak, J. T. Lean, C. C. Waraksa, G. B. Saupe, H. Usami and T. E. Mallouk, *J. Am. Chem. Soc.*, 1999, **121**, 3435–3445.
- 69 S. Fukuzumi, Y. Yamada, T. Suenobu, K. Ohkubo and H. Kotani, *Energy Environ. Sci.*, 2011, **4**, 2754–2766.
- 70 A. J. Esswein and D. G. Nocera, *Chem. Rev.*, 2007, **107**, 4022–4047.
- 71 F. Jiao and H. Frei, *Energy Environ. Sci.*, 2010, **3**, 1018–1027.
- 72 R. Brimblecombe, G. C. Dismukes, G. F. Swiegers and L. Spiccia, *Dalton Trans.*, 2009, 9374.
- 73 S. Romain, L. Vigara and A. Llobet, *Acc. Chem. Res.*, 2009, **42**, 1944–1953.
- 74 R. Nakamura and Y. Nakato, *J. Am. Chem. Soc.*, 2004, **126**, 1290–1298.
- 75 N. Sivasankar, W. W. Weare and H. Frei, *J. Am. Chem. Soc.*, 2011, **133**, 12976–12979.
- 76 R. I. Cukier and D. G. Nocera, *Annu. Rev. Phys. Chem.*, 1998, **49**, 337–369.
- 77 L. Hammarström and S. Styring, *Energy Environ. Sci.*, 2011, **4**, 2379–2388.
- 78 R. J. Debus, B. A. Barry, G. T. Babcock and L. McIntosh, *Proc. Natl. Acad. Sci. U. S. A.*, 1988, **85**, 427–430.
- 79 G. T. Babcock, B. A. Barry, R. J. Debus, C. W. Hoganson, M. Atamian, L. McIntosh, I. Sithole and C. F. Yocum, *Biochemistry*, 1989, **28**, 9557–9565.
- 80 C. J. Gagliardi, A. K. Vannucci, J. J. Concepcion, Z. Chen and T. J. Meyer, *Energy Environ. Sci.*, 2012, **5**, 7704–7717.
- 81 J. J. Concepcion, J. W. Jurss, M. K. Brennaman, P. G. Hoertz, A. O. T. Patrocínio, N. Y. Murakami Iha, J. L. Templeton and T. J. Meyer, *Acc. Chem. Res.*, 2009, **42**, 1954–1965.
- 82 M. Rodríguez, I. Romero, C. Sens and A. Llobet, *J. Mol. Catal. A: Chem.*, 2006, **251**, 215–220.
- 83 X. Sala, I. Romero, M. Rodríguez, L. Escriche and A. Llobet, *Angew. Chem., Int. Ed.*, 2009, **48**, 2842–2852.
- 84 S. W. Gersten, G. J. Samuels and T. J. Meyer, *J. Am. Chem. Soc.*, 1982, **104**, 4029–4030.
- 85 J. A. Gilbert, D. S. Eggleston, W. R. Murphy, D. A. Geselowitz, S. W. Gersten, D. J. Hodgson and T. J. Meyer, *J. Am. Chem. Soc.*, 1985, **107**, 3855–3864.
- 86 J. P. Collin and J. P. Sauvage, *Inorg. Chem.*, 1986, **25**, 135–141.
- 87 K. Nagoshi, S. Yamashita, M. Yagi and M. Kaneko, *J. Mol. Catal. A: Chem.*, 1999, **144**, 71–76.
- 88 Y. Xu, A. Fischer, L. Duan, L. Tong, E. Gabrielsson, B. Åkermark and L. Sun, *Angew. Chem., Int. Ed.*, 2010, **49**, 8934–8937.
- 89 K. Henbest, P. Douglas, M. S. Garley and A. Mills, *J. Photochem. Photobiol., A*, 1994, **80**, 299–305.
- 90 R. Zong and R. P. Thummel, *J. Am. Chem. Soc.*, 2005, **127**, 12802–12803.
- 91 H.-W. Tseng, R. Zong, J. T. Muckerman and R. Thummel, *Inorg. Chem.*, 2008, **47**, 11763–11773.
- 92 J. J. Concepcion, J. W. Jurss, J. L. Templeton and T. J. Meyer, *J. Am. Chem. Soc.*, 2008, **130**, 16462–16463.
- 93 L. Li, L. Duan, Y. Xu, M. Gorlov, A. Hagfeldt and L. Sun, *Chem. Commun.*, 2010, **46**, 7307–7309.
- 94 L. Duan, F. Bozoglian, S. Mandal, B. Stewart, T. Privalov, A. Llobet and L. Sun, *Nat. Chem.*, 2012, **4**, 418–423.
- 95 N. D. McDaniel, F. J. Coughlin, L. L. Tinker and S. Bernhard, *J. Am. Chem. Soc.*, 2008, **130**, 210–217.
- 96 J. F. Hull, D. Balcells, J. D. Blakemore, C. D. Incarvito, O. Eisenstein, G. W. Brudvig and R. H. Crabtree, *J. Am. Chem. Soc.*, 2009, **131**, 8730–8731.
- 97 J. D. Blakemore, N. D. Schley, D. Balcells, J. F. Hull, G. W. Olack, C. D. Incarvito, O. Eisenstein, G. W. Brudvig and R. H. Crabtree, *J. Am. Chem. Soc.*, 2010, **132**, 16017–16029.

- 98 G. F. Moore, J. D. Blakemore, R. L. Milot, J. F. Hull, H.-E. Song, L. Cai, C. A. Schmuttenmaer, R. H. Crabtree and G. W. Brudvig, *Energy Environ. Sci.*, 2011, **4**, 2389–2392.
- 99 F. Bozoglian, S. Romain, M. Ertem, T. K. Todorova, C. Sens, J. Mola, M. Rodríguez, I. Romero, J. Benet-Buchholz, X. Fontrodona, C. J. Cramer, L. Gagliardi and A. Llobet, *J. Am. Chem. Soc.*, 2009, **131**, 15176–15187.
- 100 Z. Deng, H.-W. Tseng, R. Zong, D. Wang and R. Thummel, *Inorg. Chem.*, 2008, **47**, 1835–1848.
- 101 Y. Xu, T. Akermark, V. Gyollai, D. Zou, L. Eriksson, L. Duan, R. Zhang, B. Åkermark and L. Sun, *Inorg. Chem.*, 2009, **48**, 2717–2719.
- 102 F. Liu, T. Cardolaccia, B. J. Hornstein, J. R. Schoonover and T. J. Meyer, *J. Am. Chem. Soc.*, 2007, **129**, 2446–2447.
- 103 T. Wada, K. Tsuge and K. Tanaka, *Inorg. Chem.*, 2001, **40**, 329–337.
- 104 J. J. Concepcion, J. W. Jurss, M. R. Norris, Z. Chen, J. L. Templeton and T. J. Meyer, *Inorg. Chem.*, 2010, **49**, 1277–1279.
- 105 L. Duan, Y. Xu, M. Gorlov, L. Tong, S. Andersson and L. Sun, *Chem.–Eur. J.*, 2010, **16**, 4659–4668.
- 106 J. Limburg, G. W. Brudvig and R. H. Crabtree, *J. Am. Chem. Soc.*, 1997, **119**, 2761–2762.
- 107 J. L. Fillol, Z. Codolà, I. Garcia-Bosch, L. Gómez, J. J. Pla and M. Costas, *Nat. Chem.*, 2011, **3**, 807–813.
- 108 J. Limburg, J. S. Vrettos, L. M. Liable-Sands, A. L. Rheingold, R. H. Crabtree and G. W. Brudvig, *Science*, 1999, **283**, 1524–1527.
- 109 Y. Naruta, M. Sasayama and T. Sasaki, *Angew. Chem., Int. Ed. Engl.*, 1994, **33**, 1839–1841.
- 110 Y. Shimazaki, T. Nagano, H. Takesue, B.-H. Ye, F. Tani and Y. Naruta, *Angew. Chem., Int. Ed.*, 2004, **43**, 98–100.
- 111 J. Chen, P. Wagner, L. Tong, G. G. Wallace, D. L. Officer and G. F. Swiegers, *Angew. Chem., Int. Ed.*, 2012, **51**, 1907–1910.
- 112 M. Wiechen, H.-M. Berends and P. Kurz, *Dalton Trans.*, 2012, **41**, 21–31.
- 113 X. Liu and F. Wang, *Coord. Chem. Rev.*, 2012, **256**, 1115–1136.
- 114 W. C. Ellis, N. D. McDaniel, S. Bernhard and T. J. Collins, *J. Am. Chem. Soc.*, 2010, **132**, 10990–10991.
- 115 C.-H. Leung, S.-M. Ng, C.-C. Ko, W.-L. Man, J. Wu, L. Chen and T.-C. Lau, *Energy Environ. Sci.*, 2012, **5**, 7903–7907.
- 116 D. Hong, J. Jung, J. Park, Y. Yamada, T. Suenobu, Y.-M. Lee, W. Nam and S. Fukuzumi, *Energy Environ. Sci.*, 2012, **5**, 7606–7616.
- 117 P. Du and R. Eisenberg, *Energy Environ. Sci.*, 2012, **5**, 6012–6021.
- 118 B. Limburg, E. Bouwman and S. Bonnet, *Coord. Chem. Rev.*, 2012, **256**, 1451–1467.
- 119 J. J. Stracke and R. G. Finke, *J. Am. Chem. Soc.*, 2011, **133**, 14872–14875.
- 120 J. A. Widegren and R. G. Finke, *J. Mol. Catal. A: Chem.*, 2003, **198**, 317–341.
- 121 N. D. Schley, J. D. Blakemore, N. K. Subbaiyan, C. D. Incarvito, F. D'Souza, R. H. Crabtree and G. W. Brudvig, *J. Am. Chem. Soc.*, 2011, **133**, 10473–10481.
- 122 W. Ruettinger, M. Yagi, K. Wolf, S. Bernasek and G. C. Dismukes, *J. Am. Chem. Soc.*, 2000, **122**, 10353–10357.
- 123 M. Yagi, K. V. Wolf, P. J. Baesjou, S. L. Bernasek and G. C. Dismukes, *Angew. Chem., Int. Ed.*, 2001, **113**, 3009–3012.
- 124 G. F. Swiegers, J. K. Clegg and R. Stranger, *Chem. Sci.*, 2011, **2**, 2254–2262.
- 125 R. Brimblecombe, D. R. J. Kolling, A. M. Bond, G. C. Dismukes, G. F. Swiegers and L. Spiccia, *Inorg. Chem.*, 2009, **48**, 7269–7279.
- 126 R. Brimblecombe, A. Koo, G. C. Dismukes, G. F. Swiegers and L. Spiccia, *J. Am. Chem. Soc.*, 2010, **132**, 2892–2894.
- 127 R. Brimblecombe, A. Koo, G. C. Dismukes, G. F. Swiegers and L. Spiccia, *ChemSusChem*, 2010, **3**, 1146–1150.
- 128 R. Hocking, R. Brimblecombe, L. Chang, A. Singh, M. Hon Cheah, C. Glover, W. H. Casey and L. Spiccia, *Nat. Chem.*, 2011, **3**, 461–466.
- 129 N. S. McCool, D. M. Robinson, J. E. Sheats and G. C. Dismukes, *J. Am. Chem. Soc.*, 2011, **133**, 11446–11449.
- 130 G. La Ganga, F. Puntoriero, S. Campagna, I. Bazzan, S. Berardi, M. Bonchio, A. Sartorel, M. Natali and F. Scandola, *Faraday Discuss.*, 2012, **155**, 177–190.
- 131 C. Streb, *Dalton Trans.*, 2012, **41**, 1651–1659.
- 132 A. Sartorel, M. Carraro, G. Scorrano, R. D. Zorzi, S. Geremia, N. D. McDaniel, S. Bernhard and M. Bonchio, *J. Am. Chem. Soc.*, 2008, **130**, 5006–5007.
- 133 Y. V. Geletii, B. Botar, P. Kögerler, D. A. Hillesheim, D. G. Musaev and C. L. Hill, *Angew. Chem., Int. Ed.*, 2008, **120**, 3960–3963.
- 134 Y. V. Geletii, Z. Huang, Y. Hou, D. G. Musaev, T. Lian and C. L. Hill, *J. Am. Chem. Soc.*, 2009, **131**, 7522–7523.
- 135 C. Besson, Z. Huang, Y. V. Geletii, S. Lense, K. I. Hardcastle, D. G. Musaev, T. Lian, A. Proust and C. L. Hill, *Chem. Commun.*, 2010, **46**, 2784–2786.
- 136 Z. Huang, Y. V. Geletii, D. Wu, C. L. Anfuso, D. G. Musaev, C. L. Hill and T. Lian, *Proc. SPIE*, 2011, **8109**, 810903.
- 137 F. M. Toma, A. Sartorel, M. Iurlo, M. Carraro, P. Parisse, C. Maccato, S. Rapino, B. R. Gonzalez, H. Amenitsch, T. Da Ros, L. Casalis, A. Goldoni, M. Marcaccio, G. Scorrano, G. Scoles, F. Paolucci, M. Prato and M. Bonchio, *Nat. Chem.*, 2010, **2**, 826–831.
- 138 M. Murakami, D. Hong, T. Suenobu, S. Yamaguchi, T. Ogura and S. Fukuzumi, *J. Am. Chem. Soc.*, 2011, **133**, 11605–11613.
- 139 Q. Yin, J. M. Tan, C. Besson, Y. V. Geletii, D. G. Musaev, A. E. Kuznetsov, Z. Luo, K. I. Hardcastle and C. L. Hill, *Science*, 2010, **328**, 342–345.
- 140 Z. Huang, Z. Luo, Y. V. Geletii, J. W. Vickers, Q. Yin, D. Wu, Y. Hou, Y. Ding, J. Song, D. G. Musaev, C. L. Hill and T. Lian, *J. Am. Chem. Soc.*, 2011, **133**, 2068–2071.
- 141 G. Zhu, Y. V. Geletii, P. Kögerler, H. Schilder, J. Song, S. Lense, C. Zhao, K. I. Hardcastle, D. G. Musaev and C. L. Hill, *Dalton Trans.*, 2012, **41**, 2084–2090.
- 142 S. Tanaka, M. Annaka and K. Sakai, *Chem. Commun.*, 2012, **48**, 1653–1655.
- 143 R. Cao, H. Ma, Y. V. Geletii, K. I. Hardcastle and C. L. Hill, *Inorg. Chem.*, 2009, **48**, 5596–5598.

- 144 L. Krishtalik, *Electrochim. Acta*, 1981, **26**, 329–337.
- 145 S. Trasatti, *Electrochim. Acta*, 1984, **29**, 1503–1512.
- 146 S. S. Dhrab, K. Sopian, M. Alghoul and M. Sulaiman, *Renewable Sustainable Energy. Rev.*, 2009, **13**, 1663–1668.
- 147 J. Kiwi and M. Grätzel, *Angew. Chem., Int. Ed. Engl.*, 1979, **18**, 624–626.
- 148 A. Harriman, G. Porter and P. Walters, *J. Chem. Soc., Faraday Trans. 2*, 1981, **77**, 2373–2383.
- 149 A. Harriman, M. C. Richoux, P. A. Christensen, S. Mosseri and P. Neta, *J. Chem. Soc., Faraday Trans. 1*, 1987, **83**, 3001–3014.
- 150 Y. Lee, J. Suntivich, K. J. May, E. E. Perry and Y. Shao-Horn, *J. Phys. Chem. Lett.*, 2012, **3**, 399–404.
- 151 Y. Kim and P. K. Dutta, *J. Phys. Chem. C*, 2007, **111**, 10575–10581.
- 152 J. Kiwi and M. Grätzel, *Angew. Chem., Int. Ed. Engl.*, 1978, **17**, 860–861.
- 153 A. Harriman, I. J. Pickering, J. M. Thomas and P. A. Christensen, *J. Chem. Soc., Faraday Trans. 1*, 1988, **84**, 2795–2806.
- 154 G. Nahor, P. Neta, P. Hambright, A. Thompson Jr and A. Harriman, *J. Phys. Chem.*, 1989, **93**, 6181–6187.
- 155 T. C. Wen and C. C. Hu, *J. Electrochem. Soc.*, 1992, **139**, 2158–2163.
- 156 M. Hara, C. C. Waraksa, J. T. Lean, B. A. Lewis and T. E. Mallouk, *J. Phys. Chem. A*, 2000, **104**, 5275–5280.
- 157 P. G. Hoertz, Y.-I. Kim, W. J. Youngblood and T. E. Mallouk, *J. Phys. Chem. B*, 2007, **111**, 6845–6856.
- 158 F. Jiao and H. Frei, *Angew. Chem., Int. Ed.*, 2009, **48**, 1841–1844.
- 159 A. J. Esswein, M. J. McMurdo, P. N. Ross, A. T. Bell and T. D. Tilley, *J. Phys. Chem. C*, 2009, **113**, 15068–15072.
- 160 J. B. Gerken, J. G. McAlpin, J. Y. C. Chen, M. L. Rigsby, W. H. Casey, R. D. Britt and S. S. Stahl, *J. Am. Chem. Soc.*, 2011, **133**, 14431–14442.
- 161 M. W. Kanan and D. G. Nocera, *Science*, 2008, **321**, 1072–1075.
- 162 Y. Surendranath, M. Dincă and D. G. Nocera, *J. Am. Chem. Soc.*, 2009, **131**, 2615–2620.
- 163 D. A. Lutterman, Y. Surendranath and D. G. Nocera, *J. Am. Chem. Soc.*, 2009, **131**, 3838–3839.
- 164 S. Zanarini, S. Vankova, S. Hernandez, V. S. Ijeri, M. Armandi, E. Garrone, B. Bonelli, B. Onida and P. Spinelli, *Chem. Commun.*, 2012, **48**, 5754–5756.
- 165 M. Morita, C. Iwakura and H. Tamura, *Electrochim. Acta*, 1977, **22**, 325–328.
- 166 V. Y. Shafirovich, N. Khannanov and A. Shilov, *J. Inorg. Biochem.*, 1981, **15**, 113–129.
- 167 F. Jiao and H. Frei, *Chem. Commun.*, 2010, **46**, 2920–2922.
- 168 V. B. R. Boppana and F. Jiao, *Chem. Commun.*, 2011, **47**, 8973–8975.
- 169 M. M. Najafpour, T. Ehrenberg, M. Wiechen and P. Kurz, *Angew. Chem., Int. Ed.*, 2010, **49**, 2233–2237.
- 170 D. Shevela, S. Koroidov, M. M. Najafpour, J. Messinger and P. Kurz, *Chem.–Eur. J.*, 2011, **17**, 5415–5423.
- 171 I. Zaharieva, M. M. Najafpour, M. Wiechen, M. Haumann, P. Kurz and H. Dau, *Energy Environ. Sci.*, 2011, **4**, 2400–2408.
- 172 M. M. Najafpour, S. Nayeri and B. Pashaei, *Dalton Trans.*, 2011, **40**, 9374–9378.
- 173 M. Najafpour, B. Pashaei and S. Nayeri, *Dalton Trans.*, 2012, **41**, 7134–7140.
- 174 I. Zaharieva, P. Chernev, M. Risch, K. Klingan, M. Kohlhoff, A. Fischer and H. Dau, *Energy Environ. Sci.*, 2012, **5**, 7081–7089.
- 175 D. M. Robinson, Y. B. Go, M. Greenblatt and G. C. Dismukes, *J. Am. Chem. Soc.*, 2010, **132**, 11467–11469.
- 176 Y. Zhao, E. A. Hernandez-Pagan, N. M. Vargas-Barbosa, J. L. Dysart and T. E. Mallouk, *J. Phys. Chem. Lett.*, 2011, **2**, 402–406.
- 177 M. Yagi, E. Tomita and T. Kuwabara, *J. Electroanal. Chem.*, 2005, **579**, 83–88.
- 178 S. Ikeda, C. Abe, T. Torimoto and B. Ohtani, *J. Photochem. Photobiol., A*, 2003, **160**, 61–67.
- 179 D.-L. Jiang, C.-K. Choi, K. Honda, W.-S. Li, T. Yuzawa and T. Aida, *J. Am. Chem. Soc.*, 2004, **126**, 12084–12089.
- 180 C. N. Kato, K. Hara, M. Kato, H. Amano, K. Sato, Y. Kataoka and W. Mori, *Materials*, 2010, **3**, 897–917.
- 181 A. S. Polo, M. K. Itokazu and N. Y. Murakami Iha, *Coord. Chem. Rev.*, 2004, **248**, 1343–1361.
- 182 B. C. O'Regan and J. R. Durrant, *Acc. Chem. Res.*, 2009, **42**, 1799–1808.
- 183 G. J. Meyer, *Inorg. Chem.*, 2005, **44**, 6852–6864.
- 184 M. J. Griffith, K. Sunahara, P. Wagner, K. Wagner, G. G. Wallace, D. L. Officer, A. Furube, R. Katoh, S. Mori and A. J. Mozer, *Chem. Commun.*, 2012, **48**, 4145–4162.
- 185 N. Damrauer, G. Cerullo, A. Yeh, T. Boussie, C. Shank and J. McCusker, *Science*, 1997, **275**, 54–57.
- 186 E. M. Kober and T. J. Meyer, *Inorg. Chem.*, 1982, **21**, 3967–3977.
- 187 J. B. Asbury, Y. Q. Wang, E. Hao, H. N. Ghosh and T. Lian, *Res. Chem. Intermed.*, 2001, **27**, 393–406.
- 188 J. B. Asbury, E. Hao, Y. Wang, H. N. Ghosh and T. Lian, *J. Phys. Chem. B*, 2001, **105**, 4545–4557.
- 189 D. P. Rillema, G. Allen, T. J. Meyer and D. Conrad, *Inorg. Chem.*, 1983, **22**, 1617–1622.
- 190 J. Nelson, *Phys. Rev. B: Condens. Matter Mater. Phys.*, 1999, **59**, 15374–15380.
- 191 P. K. Ghosh, B. S. Brunschwig, M. Chou, C. Creutz and N. Sutin, *J. Am. Chem. Soc.*, 1984, **106**, 4772–4783.
- 192 I. Gillaizeau-Gauthier, F. Odobel, M. Alebbi, R. Argazzi, E. Costa, C. A. Bignozzi, P. Qu and G. J. Meyer, *Inorg. Chem.*, 2001, **40**, 6073–6079.
- 193 E. Bae, W. Choi, J. Park, H. S. Shin, S. B. Kim and J. S. Lee, *J. Phys. Chem. B*, 2004, **108**, 14093–14101.
- 194 H. Park, E. Bae, J.-J. Lee, J. Park and W. Choi, *J. Phys. Chem. B*, 2006, **110**, 8740–8749.
- 195 K. Hanson, M. K. Brennaman, H. Luo, C. R. K. Glasson, J. J. Concepcion, W. Song and T. J. Meyer, *ACS Appl. Mater. Interfaces*, 2012, **4**, 1462–1469.
- 196 K. Hanson, M. K. Brennaman, A. Ito, H. Luo, W. Song, K. A. Parker, R. Ghosh, M. R. Norris, C. R. K. Glasson, J. J. Concepcion, R. Lopez and T. J. Meyer, *J. Phys. Chem. C*, 2012, **116**, 14837–14847.

- 197 H. D. Abruna, A. Y. Teng, G. J. Samuels and T. J. Meyer, *J. Am. Chem. Soc.*, 1979, **101**, 6745–6746.
- 198 K. Kalyanasundaram, J. Kiwi and M. Grätzel, *Helv. Chim. Acta*, 1978, **61**, 2720–2730.
- 199 K. Kalyanasundaram and M. Grätzel, *Angew. Chem., Int. Ed. Engl.*, 1979, **91**, 759–760.
- 200 D. P. Rillema, W. J. Dressick and T. J. Meyer, *J. Chem. Soc., Chem. Commun.*, 1980, 247–248.
- 201 M. Neumann-Spallart and K. Kalyanasundaram, *J. Chem. Soc., Chem. Commun.*, 1981, **9**, 437–440.
- 202 J. V. Caspar and T. J. Meyer, *Inorg. Chem.*, 1983, **22**, 2444–2453.
- 203 J. Demas and D. Taylor, *Inorg. Chem.*, 1979, **18**, 3177–3179.
- 204 M. Neumann-Spallart, K. Kalyanasundaram, C. Graetzel and M. Graetzel, *Helv. Chim. Acta*, 1980, **63**, 1111–1118.
- 205 A. Horváth, Z. Bakó, S. Papp and C. Keszei, *J. Photochem. Photobiol., A*, 1990, **52**, 271–280.
- 206 T. Lopes-Costa, P. Lopez-Cornejo, I. Villa, P. Perez-Tejeda, R. Prado-Gotor and F. Sanchez, *J. Phys. Chem. A*, 2006, **110**, 4196–4201.
- 207 D. F. Watson and G. J. Meyer, *Annu. Rev. Phys. Chem.*, 2005, **56**, 119–156.
- 208 H. Tributsch and F. Willig, *Sol. Energy Mater. Sol. Cells*, 1995, **38**, 355–366.
- 209 W. Clark and N. Sutin, *J. Am. Chem. Soc.*, 1977, **99**, 4676–4682.
- 210 C. M. Elliott and E. J. Hershenhart, *J. Am. Chem. Soc.*, 1982, **104**, 7519–7526.
- 211 A. A. Vlcek, E. S. Dodsworth, W. J. Pietro and A. B. P. Lever, *Inorg. Chem.*, 1995, **34**, 1906–1913.
- 212 R. A. Malone and D. F. Kelley, *J. Chem. Phys.*, 1991, **95**, 8970.
- 213 R. J. Crutchley and A. B. P. Lever, *Inorg. Chem.*, 1982, **21**, 2276–2282.
- 214 V. Balzani, S. Campagna, G. Denti, A. Juris, S. Serroni and M. Venturi, *Acc. Chem. Res.*, 1998, **31**, 26–34.
- 215 V. Balzani, P. Ceroni, A. Juris, M. Venturi, S. Campagna, F. Puntoriero and S. Serroni, *Coord. Chem. Rev.*, 2001, **219–221**, 545–572.
- 216 G. La Ganga, F. Nastasi, S. Campagna and F. Puntoriero, *Dalton Trans.*, 2009, 9997–9999.
- 217 F. Puntoriero, G. La Ganga, A. Sartorel, M. Carraro, G. Scorrano, M. Bonchio and S. Campagna, *Chem. Commun.*, 2010, **46**, 4725–4727.
- 218 D. Scaife, *Sol. Energy*, 1980, **25**, 41–54.
- 219 G. Sauve, M. E. Cass, G. Coia, S. J. Doig, I. Lauerma, K. E. Pomykal and N. S. Lewis, *J. Phys. Chem. B*, 2000, **104**, 6821–6836.
- 220 F. Puntoriero, A. Sartorel, M. Orlandi, G. La Ganga, S. Serroni, M. Bonchio, F. Scandola and S. Campagna, *Coord. Chem. Rev.*, 2011, **255**, 2594–2601.
- 221 G. Moore, S. Konezny, H. Song, R. Milot, J. D. Blakemore, M. L. Lee, V. S. Batista, C. A. Schmuttenmaer, R. H. Crabtree and G. W. Brudvig, *J. Phys. Chem. C*, 2012, **116**, 4892–4902.
- 222 P. A. Christensen, A. Harriman, G. Porter and P. Neta, *J. Chem. Soc., Faraday Trans. 2*, 1984, **80**, 1451–1464.
- 223 A. Harriman, G. S. Nahor, S. Mosseri and P. Neta, *J. Chem. Soc., Faraday Trans. 1*, 1988, **84**, 2821–2829.
- 224 K. Kalyanasundaram and M. Neumann-Spallart, *J. Phys. Chem.*, 1982, **86**, 5163–5169.
- 225 B. D. Sherman, S. Pillai, G. Kodis, J. Bergkamp, T. E. Mallouk, D. Gust, T. A. Moore and A. L. Moore, *Can. J. Chem.*, 2011, **89**, 152–157.
- 226 N. Kaveevivitchai, R. Chitta, R. Zong, M. El Ojaimi and R. P. Thummel, *J. Am. Chem. Soc.*, 2012, **134**, 10721–10724.
- 227 F. Li, Y. Jiang, B. Zhang, F. Huang, Y. Gao and L. Sun, *Angew. Chem., Int. Ed.*, 2012, **51**, 2417–2420.
- 228 D. L. Ashford, D. J. Stewart, C. R. Glasson, R. A. Binstead, D. P. Harrison, M. R. Norris, J. J. Concepcion, Z. Fang, J. L. Templeton and T. J. Meyer, *Inorg. Chem.*, 2012, **51**, 6428–6430.
- 229 W. Song, C. R. K. Glasson, H. Luo, K. Hanson, M. K. Brennaman, J. J. Concepcion and T. J. Meyer, *J. Phys. Chem. Lett.*, 2011, **2**, 1808–1813.
- 230 M. T. Vagnini, A. L. Smeigh, J. D. Blakemore, S. W. Eaton, N. D. Schley, F. D'Souza, R. H. Crabtree, G. W. Brudvig, D. T. Co and M. R. Wasielewski, *Proc. Natl. Acad. Sci. U. S. A.*, 2012, **109**, 15651–15656.
- 231 T. A. Moore, D. Gust, P. Mathis, J.-C. Mialocq, C. Chachaty, R. V. Bensasson, E. J. Land, D. Doizi, P. A. Liddell, W. R. Lehman, G. A. Nemeth and A. L. Moore, *Nature*, 1984, **307**, 630–632.
- 232 O. Johansson, H. Wolpher, M. Borgström, L. Hammarström, J. Bergquist, L. Sun and B. Åkermark, *Chem. Commun.*, 2004, 194–195.
- 233 J. Pan, Y. Xu, G. Benkö, Y. Feyziyev, S. Styring, L. Sun, B. Åkermark, T. Polívka and V. Sundström, *J. Phys. Chem. B*, 2004, **108**, 12904–12910.
- 234 J. D. Megiatto, A. Antoniuk-Pablant, B. D. Sherman, G. Kodis, M. Gervaldo, T. A. Moore, A. L. Moore and D. Gust, *Proc. Natl. Acad. Sci. U. S. A.*, 2012, **109**, 15578–15583.
- 235 G. F. Moore, M. Hamburger, M. Gervaldo, O. G. Poluektov, T. Rajh, D. Gust, T. A. Moore and A. L. Moore, *J. Am. Chem. Soc.*, 2008, **130**, 10466–10467.
- 236 G. F. Moore, M. Hamburger, G. Kodis, W. Michl, D. Gust, T. A. Moore and A. L. Moore, *J. Phys. Chem. B*, 2010, **114**, 14450–14457.
- 237 Y. Zhao, J. R. Swierk, J. D. Megiatto, B. Sherman, W. J. Youngblood, D. Qin, D. M. Lentz, A. L. Moore, T. A. Moore, D. Gust and T. E. Mallouk, *Proc. Natl. Acad. Sci. U. S. A.*, 2012, **109**, 15612–15616.
- 238 J. J. Concepcion, J. W. Jurss, J. L. Templeton and T. J. Meyer, *Proc. Natl. Acad. Sci. U. S. A.*, 2008, **105**, 17632–17635.
- 239 J. W. Jurss, J. C. Concepcion, M. R. Norris, J. L. Templeton and T. J. Meyer, *Inorg. Chem.*, 2010, **49**, 3980–3982.
- 240 J. J. Concepcion, J. W. Jurss, P. G. Hoertz and T. J. Meyer, *Angew. Chem., Int. Ed.*, 2009, **48**, 9473–9476.
- 241 J. R. Durrant, S. A. Haque and E. Palomares, *Coord. Chem. Rev.*, 2004, **248**, 1247–1257.
- 242 T. Berger, J. A. Anta and V. Morales-Flórez, *J. Phys. Chem. C*, 2012, **116**, 11444–11455.

- 243 J. Weidmann, T. Dittrich, E. Konstantinova, I. Lauer mann, I. Uhlendorf and F. Koch, *Sol. Energy Mater. Sol. Cells*, 1999, **56**, 153–165.
- 244 Q. Wang, Z. Zhang, S. M. Zakeeruddin and M. Grätzel, *J. Phys. Chem. C*, 2008, **112**, 7084–7092.
- 245 J. Nelson and R. E. Chandler, *Coord. Chem. Rev.*, 2004, **248**, 1181–1194.
- 246 K. D. Benkstein, N. Kopidakis, J. van de Lagemaat and A. J. Frank, *J. Phys. Chem. B*, 2003, **107**, 7759–7767.
- 247 J. Bisquert, *Phys. Chem. Chem. Phys.*, 2008, **10**, 3175–3194.
- 248 S. A. Sapp, C. M. Elliott, C. Contado, S. Caramori and C. A. Bignozzi, *J. Am. Chem. Soc.*, 2002, **124**, 11215–11222.
- 249 A. Yella, H.-W. Lee, H. N. Tsao, C. Yi, A. K. Chandiran, M. K. Nazeeruddin, E. W.-G. Diao, C.-Y. Yeh, S. M. Zakeeruddin and M. Grätzel, *Science*, 2011, **334**, 629–634.
- 250 N. D. Morris, M. Suzuki and T. E. Mallouk, *J. Phys. Chem. A*, 2004, **108**, 9115–9119.
- 251 S. A. Haque, Y. Tachibana, R. L. Willis, J. E. Moser, M. Grätzel, D. R. Klug and J. R. Durrant, *J. Phys. Chem. B*, 2000, **104**, 538–547.
- 252 J. G. Li, T. Ishigaki and X. Sun, *J. Phys. Chem. C*, 2007, **111**, 4969–4976.
- 253 J. A. Anta and V. Morales-Flórez, *J. Phys. Chem. C*, 2008, **112**, 10287–10293.
- 254 C. C. Mercado, F. J. Knorr, J. L. McHale, S. M. Usmani, A. S. Ichimura and L. V. Saraf, *J. Phys. Chem. C*, 2012, **116**, 10796–10804.
- 255 A. Solbrand, H. Lindström, H. Rensmo, A. Hagfeldt, S.-E. Lindquist and S. Södergren, *J. Phys. Chem. B*, 1997, **101**, 2514–2518.
- 256 L. Dloczik, O. Ieperuma, I. Lauer mann, L. M. Peter, E. A. Ponomarev, G. Redmond, N. J. Shaw and I. Uhlendorf, *J. Phys. Chem. B*, 1997, **101**, 10281–10289.
- 257 T. Berger, T. Lana-Villarreal, D. Monllor-Satoca and R. Gomez, *J. Phys. Chem. C*, 2007, **111**, 9936–9942.
- 258 J. Kallioinen, V. Lehtovuori, P. Myllyperkiö and J. Korppi-Tommola, *Chem. Phys. Lett.*, 2001, **340**, 217–221.
- 259 L. J. Antila, M. J. Heikkilä, V. Mäkinen, N. Humalämäki, M. Laitinen, V. Linko, P. Jalkanen, J. Toppari, V. Aumanen, M. Kemell, P. Myllyperkiö, K. Honkala, H. Häkkinen, M. Leskelä and J. E. I. Korppi-Tommola, *J. Phys. Chem. C*, 2011, **115**, 16720–16729.
- 260 S. G. Chen, S. Chappel, Y. Diamant and A. Zaban, *Chem. Mater.*, 2001, **13**, 4629–4634.
- 261 E. Palomares, J. N. Clifford, S. A. Haque, T. Lutz and J. R. Durrant, *J. Am. Chem. Soc.*, 2003, **125**, 475–482.
- 262 A. Kay and M. Grätzel, *Chem. Mater.*, 2002, **14**, 2930–2935.
- 263 J. W. Ondersma and T. W. Hamann, *J. Am. Chem. Soc.*, 2011, **133**, 8264–8271.
- 264 F. Fabregat-Santiago, J. García-Cañadas, E. Palomares, J. N. Clifford, S. A. Haque, J. R. Durrant, G. Garcia-Belmonte and J. Bisquert, *J. Appl. Phys.*, 2004, **96**, 6903–6907.
- 265 S.-H. A. Lee, Y. Zhao, E. A. Hernandez-Pagan, L. Bladell, W. J. Youngblood and T. E. Mallouk, *Faraday Discuss.*, 2012, **155**, 165–176.
- 266 Y. Ohsaki, N. Masaki, T. Kitamura, Y. Wada, T. Okamoto, T. Sekino, K. Niihara and S. Yanagida, *Phys. Chem. Chem. Phys.*, 2005, **7**, 4157–4163.
- 267 M. Adachi, Y. Murata, I. Okada and S. Yoshikawa, *J. Electrochem. Soc.*, 2003, **150**, G488–G493.
- 268 M. Adachi, Y. Murata, J. Takao, J. Jiu, M. Sakamoto and F. Wang, *J. Am. Chem. Soc.*, 2004, **126**, 14943–14949.
- 269 G. K. Mor, K. Shankar, M. Paulose, O. K. Varghese and C. A. Grimes, *Nano Lett.*, 2006, **6**, 215–218.
- 270 K. Zhu, N. R. Neale, A. Miedaner and A. J. Frank, *Nano Lett.*, 2007, **7**, 69–74.
- 271 D. Kuang, J. Brillet, P. Chen, M. Takata, S. Uchida, H. Miura, K. Sumioka, S. M. Zakeeruddin and M. Grätzel, *ACS Nano*, 2008, **2**, 1113–1116.
- 272 T.-S. Kang, A. P. Smith, B. E. Taylor and M. F. Durstock, *Nano Lett.*, 2009, **9**, 601–606.
- 273 X. Feng, K. Shankar, O. K. Varghese, M. Paulose, T. J. Latempa and C. A. Grimes, *Nano Lett.*, 2008, **8**, 3781–3786.
- 274 A. Kumar, A. R. Madaria and C. Zhou, *J. Phys. Chem. C*, 2010, **114**, 7787–7792.
- 275 J. R. Jennings, A. Ghicov, L. M. Peter, P. Schmuki and A. B. Walker, *J. Am. Chem. Soc.*, 2008, **130**, 13364–13372.
- 276 X. Feng, K. Zhu, A. Frank, C. Grimes and T. E. Mallouk, *Angew. Chem., Int. Ed.*, 2012, **124**, 2781–2784.
- 277 A. B. F. Martinson, J. W. Elam, J. Liu, M. J. Pellin, T. J. Marks and J. T. Hupp, *Nano Lett.*, 2008, **8**, 2862–2866.
- 278 N. Kopidakis, K. D. Benkstein, J. van de Lagemaat and A. J. Frank, *J. Phys. Chem. B*, 2003, **107**, 11307–11315.
- 279 A. K. Chandiran, F. Sauvage, M. Casas-Cabanas, P. Comte, S. M. Zakeeruddin and M. Graetzel, *J. Phys. Chem. C*, 2010, **114**, 15849–15856.
- 280 Y. Furubayashi, T. Hitosugi, Y. Yamamoto, K. Inaba, G. Kinoda, Y. Hirose, T. Shimada and T. Hasegawa, *Appl. Phys. Lett.*, 2005, **86**, 252101.
- 281 X. Feng, K. Shankar, M. Paulose and C. A. Grimes, *Angew. Chem., Int. Ed.*, 2009, **48**, 8095–8098.
- 282 K.-P. Wang and H. Teng, *Phys. Chem. Chem. Phys.*, 2009, **11**, 9489–9496.
- 283 H. Alarcón, M. Hedlund, E. M. J. Johansson, H. Rensmo, A. Hagfeldt and G. Boschloo, *J. Phys. Chem. C*, 2007, **111**, 13267–13274.
- 284 C. Zhang, S. Chen, L. Mo, Y. Huang, H. Tian, L. Hu, Z. Huo, S. Dai, F. Kong and X. Pan, *J. Phys. Chem. C*, 2011, **115**, 16418–16424.
- 285 X. Zhang, F. Liu, Q.-L. Huang, G. Zhou and Z.-S. Wang, *J. Phys. Chem. C*, 2011, **115**, 12665–12671.
- 286 A. Subramanian and H. Wang, *Appl. Surf. Sci.*, 2012, **258**, 6479–6484.
- 287 A. K. Chandiran, F. Sauvage, L. Etgar and M. Graetzel, *J. Phys. Chem. C*, 2011, **115**, 9232–9240.
- 288 H. Tian, L. Hu, C. Zhang, W. Liu, Y. Huang, L. Mo, L. Guo, J. Sheng and S. Dai, *J. Phys. Chem. C*, 2010, **114**, 1627–1632.
- 289 H. Tian, L. Hu, C. Zhang, L. Mo, W. Li, J. Sheng and S. Dai, *J. Mater. Chem.*, 2012, **22**, 9123–9130.
- 290 B. J. Morgan, D. O. Scanlon and G. W. Watson, *J. Mater. Chem.*, 2009, **19**, 5175–5178.

- 291 E. Dy, R. Hui, J. Zhang, Z.-S. Liu and Z. Shi, *J. Phys. Chem. C*, 2010, **114**, 13162–13167.
- 292 B. V. Bergeron, A. Marton, G. Oskam and G. J. Meyer, *J. Phys. Chem. B*, 2005, **109**, 937–943.
- 293 I. Bedja, S. Hotchandani and P. V. Kamat, *J. Phys. Chem.*, 1994, **98**, 4133–4140.
- 294 W. E. Ford, J. M. Wessels and M. A. J. Rodgers, *Langmuir*, 1996, **12**, 3449–3453.
- 295 S. Ferrere, A. Zaban and B. A. Gregg, *J. Phys. Chem. B*, 1997, **101**, 4490–4493.
- 296 J.-H. Lee, N.-G. Park and Y.-J. Shin, *Sol. Energy Mater. Sol. Cells*, 2011, **95**, 179–183.
- 297 K. Tennakone, V. P. S. Perera, I. R. M. Kottegoda and G. R. R. A. Kumara, *J. Phys. D: Appl. Phys.*, 1999, **32**, 374–379.
- 298 Z. Tebby, T. Uddin, Y. Nicolas, C. Olivier, T. Toupance, C. Labrugère and L. Hirsch, *ACS Appl. Mater. Interfaces*, 2011, **3**, 1485–1491.
- 299 S. Bhande, G. Taur, A. Shaikh, O. Joo, M.-M. Sung, R. S. Mane, A. V. Ghule and S.-H. Han, *Mater. Lett.*, 2012, **79**, 29–31.
- 300 Z. M. Jarzebski and J. P. Marton, *J. Electrochem. Soc.*, 1976, **123**, 199C–204C.
- 301 D. Jousse, C. Constantino and I. Chambouleyron, *J. Appl. Phys.*, 1983, **54**, 431–434.
- 302 A. N. M. Green, E. Palomares, S. A. Haque, J. M. Kroon and J. R. Durrant, *J. Phys. Chem. B*, 2005, **109**, 12525–12533.
- 303 X. Ai, N. A. Anderson, J. Guo and T. Lian, *J. Phys. Chem. B*, 2005, **109**, 7088–7094.
- 304 R. Jose, V. Thavasi and S. Ramakrishna, *J. Am. Ceram. Soc.*, 2009, **92**, 289–301.
- 305 A. Solbrand, K. Keis, S. Södergren, H. Lindström, S. E. Lindquist and A. Hagfeldt, *Sol. Energy Mater. Sol. Cells*, 2000, **60**, 181–193.
- 306 M. Law, L. E. Greene, J. C. Johnson, R. Saykally and P. Yang, *Nat. Mater.*, 2005, **4**, 455–459.
- 307 K. Keis, J. Lindgren, S.-E. Lindquist and A. Hagfeldt, *Langmuir*, 2000, **16**, 4688–4694.
- 308 M. Law, L. E. Greene, A. Radenovic, T. Kuykendall, J. Liphardt and P. Yang, *J. Phys. Chem. B*, 2006, **110**, 22652–22663.
- 309 V. O. Williams, N. C. Jeong, C. Prasittichai, O. K. Farha, M. J. Pellin and J. T. Hupp, *ACS Nano*, 2012, **6**, 6185–6196.
- 310 E. A. Hernandez-Pagan, N. Vargas-Barbosa, T. Wang, Y. Zhao, E. Smotkin and T. E. Mallouk, *Energy Environ. Sci.*, 2012, **5**, 7582–7589.
- 311 R. Andreatti, V. Caprio, A. Insola, R. Marotta and V. Tufano, *Water Res.*, 1998, **32**, 1492–1496.
- 312 K. C. Bower and C. M. Miller, *J. Environ. Eng.*, 2002, **128**, 131–136.
- 313 Y. Pi, M. Ernst and J. C. Schrotter, *Ozone: Sci. Eng.*, 2003, **25**, 393–397.
- 314 D. Nicosia, M. Elsener, O. Kröcher and P. Jansohn, *Top. Catal.*, 2007, **42–43**, 333–336.
- 315 L. Sigg and W. Stumm, *Colloids Surf.*, 1981, **2**, 101–117.
- 316 J. Staehelin and J. Hoigne, *Environ. Sci. Technol.*, 1982, **16**, 676–681.
- 317 N. D. Morris and T. E. Mallouk, *J. Am. Chem. Soc.*, 2002, **124**, 11114–11121.
- 318 K. Maeda, R. Abe and K. Domen, *J. Phys. Chem. C*, 2011, **115**, 3057–3064.
- 319 S. Fukuzumi, S. Kato and T. Suenobu, *Phys. Chem. Chem. Phys.*, 2011, **13**, 17960–17963.
- 320 J. Brillet, M. Cornuz, F. Le Formal, J. H. Yum, M. Grätzel and K. Sivula, *J. Mater. Res.*, 2010, **25**, 17.
- 321 K. Maeda, M. Eguchi, S.-H. A. Lee, W. J. Youngblood, H. Hata and T. E. Mallouk, *J. Phys. Chem. C*, 2009, **113**, 7962–7969.
- 322 N. I. Kovtyukhova and T. E. Mallouk, *Nanoscale*, 2011, **3**, 1541–1552.
- 323 P. G. Hoertz, Z. Chen, C. A. Kent and T. J. Meyer, *Inorg. Chem.*, 2010, **49**, 8179–8181.
- 324 A. Agiral, H. S. Soo and H. Frei, *Division of Environmental Chemistry - 242nd ACS National Meeting*, Denver, CO, 2011.